Examining tibial cartilage morphology, subchondral bone microarchitecture and *in vivo* joint loading indices in knee osteoarthritis

by

Sophie Kate Rapagna

Bachelor of Engineering (Biomed)(Hons I)

Principal Supervisor: Associate Professor Egon Perilli

Associate Supervisor: Professor Karen Reynolds

A thesis submitted to Flinders University

for the degree of

Doctor of Philosophy

College of Science and Engineering

1 October 2021

Abstract

Osteoarthritis (OA) is a debilitating disease which affects the entire synovial joint, including both the articular cartilage and underlying subchondral bone. It is multifactorial, with biomechanical factors (e.g. joint loading) playing a significant role in the initiation and the progression of the disease. However, relationships between the cartilage thickness and underlying bone microarchitecture, and how they are influenced by biomechanical factors in OA, has not yet been fully understood. The aims of this thesis were 1) to explore regional differences in, and relationships between, the tibial cartilage morphology and subchondral bone microarchitecture of human knees in OA and controls, using micro-CT imaging; and 2) to determine the association of *in vivo* joint loading indices, measured from pre-operative radiographs (alignment) and gait analysis (external joint moments), with these tissues.

The first study of this thesis investigated the influence of joint alignment in OA on tibial cartilage thickness and subchondral bone microarchitecture compared to controls (tibiae without OA). OA tibiae differed significantly from controls in cartilage thickness, subchondral bone plate thickness (SBPl.Th), trabecular bone volume fraction (BV/TV), and their medial-to-lateral ratios, depending on joint alignment. Compared to controls, cartilage thickness was significantly lower anteromedially in varus-OA, but higher posteromedially in valgus-OA. In varus-OA, the SBPl.Th and BV/TV were higher than in controls medially, whereas in valgus-OA they were higher laterally. In varus-OA the medial-to-lateral cartilage thickness ratios were significantly below controls, and SBPl.Th ratios and BV/TV ratios above controls, whereas in valgus-OA this was the opposite. This suggests structural changes in OA may reflect differences in medial-to-lateral load distribution upon the tibial plateau, due to joint alignment. Furthermore, in this study, the use of micro-CT for the analysis of cartilage thickness was validated against histology (gold standard), showing no significant differences between the two methods.

The second study investigated relationships between regional tibial cartilage thickness from micro-CT and pre-operative *in vivo* knee joint loading indices in subjects with end-stage knee OA. Significant correlations were found between cartilage thickness and joint

loading indices, positive anteromedially with the first peak knee adduction moment and external rotation moment, and negative with the mechanical axis deviation. In the lateral regions these correlations had opposite signs. Interestingly, these relationships have also the opposite sign compared to the subchondral bone microarchitecture found in a previous study from our group on the same specimens, which may suggest a complementary bone-cartilage interplay in response to loading.

Finally, in the third study, a systematic mapping of the cartilage and subchondral bone morphology of the tibial plateau (22 sub-regions) was performed in healthy knees and in OA knees. Region-specific differences and relationships between cartilage thickness and subchondral bone parameters were investigated. In controls, cartilage thickness, SBPl.Th and BV/TV were lowest in the external regions and highest in the central and anterior regions. In the varus-aligned OA group, the cartilage was thinnest anteriorly in the medial condyle, with high underlying SBPl.Th and BV/TV. In the non-varus-aligned OA group, the cartilage distribution was similar to controls, but with higher SBPl.Th and BV/TV. In both the OA and control groups, strong positive correlations existed between BV/TV and SBPl.Th. Interestingly, whereas in controls almost no relationships were found between cartilage thickness and SBPl.Th or BV/TV, in OA significant negative correlations were found, within both condyles. This suggests a cartilage and bone response in OA to habitual loading, which might be altered compared to controls. Micro-CT allows for a systematic mapping of the cartilage and subchondral bone of tibial plateaus, which revealed region-specific differences in cartilage thickness and subchondral bone microarchitecture, and region-specific relationships among them, depending on the group.

In this thesis, micro-CT was used for the non-destructive concurrent imaging of cartilage and bone microarchitecture at high spatial resolution (17 μm/pixel), which would otherwise be unattainable using clinical scans (e.g., magnetic resonance imaging or peripheral computed tomography). Joint loading indices (such as the knee adduction moment, external rotation moment and mechanical axis deviation) significantly correlated with regional cartilage thickness variations and the medial-to-lateral cartilage thickness ratios in end-stage OA, where higher regional loads corresponded to thinner regional cartilage. Here, negative relationships between cartilage thickness and underlying subchondral bone were found in OA but not in controls, suggesting a whole-joint response in OA to daily stimuli, which might be different to controls. Detectable

morphological differences between OA and non-OA joints depend on joint alignment and could become useful indicators of disease progression, warranting further exploration. Further research, however, is needed to determine whether these relationships between cartilage thickness, subchondral bone microarchitecture and joint loading indices in end-stage OA are present in earlier stages of the disease.

Declaration

I certify that this thesis does not incorporate without acknowledgement any material previously submitted for a degree or diploma in any university; and that to the best of my knowledge and belief it does not contain any material previously published or written by another person except where due reference is made in the text.

Sophie Kate Rapagna
July 25, 2021

List of publications and conferences attended during PhD Candidature

Peer-Reviewed Journal Articles (* indicates the journal article includes work presented in this thesis):

1. ***Rapagna S**, Roberts BC, Solomon LB, Reynolds KJ, Thewlis D, Perilli E. Relationships between tibial articular cartilage, *in vivo* external joint moments and static alignment in end-stage knee osteoarthritis: a micro-CT study. *Journal of Orthopaedic Research*. 2021. doi: 10.1002/jor.25140. In Press.
2. ***Rapagna S**, Roberts BC, Solomon LB, Reynolds KJ, Thewlis D, Perilli E. Tibial cartilage, subchondral bone plate and trabecular bone microarchitecture in varus- and valgus-osteoarthritis versus controls. *Journal of Orthopaedic Research*. 2021; 39(9):1988-99. doi: 10.1002/jor.24914.
3. **Rapagna S**, Berahmani S, Wyers CE, van den Bergh JPW, Reynolds KJ, Tozzi G, Janssen D, Perilli E. Quantification of human bone microarchitecture damage in press-fit femoral knee implantation using HR-pQCT and digital volume correlation. *Journal of the Mechanical Behavior of Biomedical Materials.* 2019; 97:278-87. doi: 10.1016/j.jmbbm.2019.04.054.
4. ***Rapagna S**, Roberts BC, Muratovic D, Solomon LB, Reynolds KJ, Thewlis D, Perilli E 2021. Systematic mapping of cartilage and subchondral bone in human tibial controls and osteoarthritis using micro-computed tomography. *In preparation for submission to peer-reviewed journal.*

National and International Conference Presentations:

1. **Rapagna S**, Roberts BC, Solomon LB, Reynolds KJ, Thewlis D and Perilli E (2021). Relationships between tibial cartilage thickness and subchondral bone in osteoarthritis and controls. The 12th Australasian Biomechanics Conference (ABC12), Adelaide, Australia, Dec 2021. *Podium Presentation, New Investigator Award Finalist.*

2. **Rapagna S**, Roberts BC, Solomon LB, Reynolds KJ, Thewlis D and Perilli E (2021). Relationships between cartilage thickness and subchondral bone in knee osteoarthritis and controls: a systematic mapping. Australian New Zealand Orthopaedic Research Society, 26th Annual Meeting. Online. Oct 2021, pp. 30-30. *Podium Presentation.*
3. **Rapagna S**, Roberts BC, Solomon LB, Reynolds KJ, Thewlis D and Perilli E (2020). Cartilage thickness is correlated with *in vivo* knee joint loading indices in osteoarthritic tibia. In Proceedings of the 26th Congress of the European Society of Biomechanics. Annual Congress of the European Society of Biomechanics (ESB). Webinar, Milan, Italy. Jul 2020. *Podium Presentation, European Society of Biomechanics Student Award Finalist.*

   Link to video of Official ESB Online Sessions 2020 – Student Awards: https://youtu.be/laCiIltxpww?t=2143
4. **Rapagna S**, Roberts BC, Solomon LB, Reynolds KJ, Thewlis D and Perilli E (2020). Tibia cartilage thickness is correlated with *in vivo* knee joint loading indices. The 11th Clare Valley Bone Meeting, Clare Valley, Australia, Feb 2020. *Podium Presentation.*
5. **Rapagna S**, Roberts BC, Solomon LB, Reynolds KJ, Thewlis D, Perilli E (2019). Influence of joint alignment in tibial OA vs. controls: cartilage, cortical subchondral bone plate and trabecular bone. In ANZORS Proceedings. Australian New Zealand Orthopaedic Research Society, 25th Annual Meeting. Canberra, Australia. Oct 2019, pp. 71-71. *Podium Presentation, PhD Student Award.*
6. **Rapagna S**, Roberts BC, Solomon LB, Qian H, Reynolds KJ, Thewlis D and Perilli E (2019). Tibial cartilage, subchondral bone plate and bone microarchitecture in varus- and valgus-OA vs. controls. In Proceedings of the 25th Congress of the European Society of Biomechanics (ESB). Annual Congress of the European Society of Biomechanics. Vienna, Austria. Jul 2019. *Podium Presentation.*
7. **Rapagna S**, Roberts BC, Solomon LB, Reynolds KJ, Thewlis D and Perilli E (2018). Cartilage thickness and subchondral bone microarchitecture in varus- and valgus-aligned osteoarthritic tibiae: comparison with controls. In ANZORS Proceedings. Australian & New Zealand Orthopaedic Research Society (ANZORS) 24th Annual Scientific Meeting. Perth, WA, Australia. Oct 2018, pp. 66-66. *Podium Presentation, PhD Award Finalist and The One to Watch Award.*

8. **Rapagna, S,** Berahmani S, Wyers CE, van den Bergh JP, Reynolds KJ, Tozzi G and Perilli E (2018). Quantification of bone microarchitecture damage in human femoral press-fit implantation using HR-pQCT and digital volume correlation. In ANZORS Proceedings. Australian & New Zealand Orthopaedic Research Society (ANZORS) 24th Annual Scientific Meeting. Perth, WA, Australia. Oct 2018, pp. 81-81. *Podium Presentation*
9. **Rapagna S**, Roberts BC, Solomon LB, Reynolds KJ, Thewlis D and Perilli E (2018). Comparing cartilage thickness and subchondral bone microarchitecture in varus- and valgus-aligned osteoarthritic tibiae with controls. In ABC11 Proceedings. 11th Australasian Biomechanics Conference (ABC11) Auckland, New Zealand. Dec 2018, pp. 24-24. *Podium Presentation.*
10. **Rapagna S**, Roberts BC, Solomon LB, Reynolds KJ, Thewlis D and Perilli E (2018). Tibia cartilage thickness and subchondral bone microarchitecture in varus- and valgus-aligned osteoarthritic knees: comparison with controls. 8th World Congress of Biomechanics (WCB) Dublin, Ireland. Jul 2018. *Poster Presentation*
11. **Rapagna, S**, Berahmani S, Wyers CE, van den Bergh JP, Reynolds KJ, Tozzi G and Perilli E (2018). Evaluation of bone microarchitecture damage by press-fit implantation using digital volume correlation. 8th World Congress of Biomechanics (WCB) Dublin, Ireland. Jul 2018. *Poster Presentation*

Honours and Awards

1. European Society of Biomechanics Student Award Finalist, 26th Congress of the European Society of Biomechanics, Webinar, 13th of July 2020, (one of 4 finalists, out of 62 applicants worldwide), €400 (=AUD675). Link to video of Official ESB Online Sessions 2020 – Student Awards: https://youtu.be/laCilltxpww?t=2143
2. PhD Student Award, Australian and New Zealand Orthopaedic Research Society 25th Annual Conference, Canberra, Australia 2019, AUD500
3. Travel Grant, Australian and New Zealand Orthopaedic Research Society 25th Annual Conference, Perth, Australia, 2019, AUD250
4. European Society of Biomechanics Travel Award, 25th Congress of the European Society of Biomechanics, Vienna, Austria, 2019 (20 awarded worldwide), €400 (=AUD675)
5. Research Student Conference Travel Grant, Flinders University, 2019, used to attend the 25th Congress of the European Society of Biomechanics, AUD1695
6. "Bake Your PhD" Judges and People's Choice Runner Up, Higher Degree Research Conference, Flinders University, Adelaide, South Australia, 2018, AUD100
7. "The One to Watch" Award, PhD Award Finalist, Australian and New Zealand Orthopaedic Research Society 24th Annual Conference, Perth, Australia, 2018, A pair of Zeiss Terra ED Pocket binoculars (~AUD665)
8. Travel Grant, Australian and New Zealand Orthopaedic Research Society 24th Annual Conference, Perth, Australia, 2018, AUD230
9. Commonwealth Scholarships Program for South Australia (priority industry 'Health Services and Medical Research'), 2018, AUD17,500
10. World Council of Biomechanics Student Bursary Award: Asia/Pacific, Africa, Central and South America; 8th World Congress of Biomechanics, Dublin, Ireland, 2018 (10 awarded worldwide), registration and bursary (€1,000 (=AUD1,687))
11. Research Higher Degree Student Conference Travel Grant, Flinders University 2018, used to attend the World Congress of Biomechanics, Ireland, AUD1,500

Research Training Program Scholarship, Australian Government, AUD27,000 p.a.

Acknowledgements

Firstly, thank you to Associate Professor Egon Perilli for your support and mentorship as my principal PhD supervisor. You frequently challenged me to improve my technical skills, pay attention to details and to go out of my comfort zone. The importance of celebrating the little successes is a lesson I will not forget (nor the "science" of micro-CT scanning a macchinetta).

Professor Karen Reynolds, thank you for your insightful feedback, always making time (even on short notice), and for fostering the wonderful and supportive environment that is the Medical Device Research Institute at Flinders University.

Thanks also to Dr Bryant Roberts for responding to my emails (of which there were many), sharing your knowledge and alongside with Associate Professor Dominic Thewlis, Professor Lucian Bogdan Solomon and Dr Dzenita Muratovic, providing the critical feedback and advice needed in shaping manuscripts and this thesis.

Associate Professor Kenneth Pope, for providing a welcome hobby in the form of puzzles and being a source of inspiration and mentorship.

To the PhD group, thank you for making every day at Tonsley filled with lots of laughter and fond memories, including being willing participants in cooking adventures, from gnocchi and cupcakes to life-sized skeleton cakes.

Also, to Michael, who asked for his acknowledgement to be "epic and meaningful", but really should have known better.

Finally, to my family and friends, I am forever grateful for your unconditional encouragement and humour throughout my PhD journey, and of course, for curing any stressful moment with an abundance of chocolate.

Table of Contents

List of Figures

List of Tables

Abbreviations

AL	Anterior-Lateral
AM	Anterior-Medial
BMI	Body Mass Index
BV/TV	Bone Volume Fraction
Cart.Th	Cartilage Thickness
DA	Degree of Anisotropy
DEXA	Dual X-ray Absorptiometry
ERM	External Rotation Moment
HR-pQCT	High Resolution-peripheral Quantitative Computed Tomography
IRM	Internal Rotation Moment
KAM	Knee Adduction Moment (1^{st} (KAM_1), 2^{nd} (KAM_2) peak)
KEM	Knee Extension Moment
KFM	Knee Flexion Moment
MAD	Mechanical Axis Deviation
Micro-CT	Micro-Computed Tomography
MRI	Magnetic Resonance Imaging
OA	Osteoarthritis
PL	Posterior-Lateral
PM	Posterior-Medial
pQCT	Peripheral Quantitative Computed Tomography
ROI	Region of Interest
SBP	Subchondral Bone Plate
SBPl.Po	Subchondral Bone Plate Porosity
SBPl.Th	Subchondral Bone Plate Thickness
STB	Subchondral Trabecular Bone
vBMD	Volumetric Bone Mineral Density
VOI	Volume of Interest
WS	Walking Speed

Chapter 1 **Introduction**

1.1 Motivation

Osteoarthritis (OA) is a degenerative joint disease that is most commonly reported in the knee joint (Cross *et al.*, 2014). Symptomatic knee OA affects approximately 14 million people in the United States (Deshpande *et al.*, 2016, Vina *et al.*, 2018) with knee joint replacement contributing to the majority of OA healthcare costs (Hunter *et al.*, 2019). Originally thought to be a disease of the articular cartilage, OA is now understood to affect the entire synovial joint, including both the articular cartilage and underlying subchondral bone (Radin *et al.*, 1991, Loeser *et al.*, 2012). In a healthy joint, the bone and cartilage work together to distribute and attenuate loads through the joint. However, in OA and particularly towards the later stages of the disease, the cartilage degrades, and alterations occur in the subchondral bone, eventually becoming sclerotic. This leads to symptoms such as pain, loss of joint functionality and altered kinematics, affecting quality of life (Hunter *et al.*, 2008).

OA is a multifactorial disease, with systemic risk factors including age, genetics, sex and ethnicity, and modifiable risk factors such as obesity, diet, bone metabolism and joint mechanics (Johnson *et al.*, 2014). These risk factors may lead to the initiation of OA in any of the joint tissues (Radin *et al.*, 1991). There is no known cure for knee OA, with the final treatment option being total knee replacement (Evans *et al.*, 2019). Hence, there is a need for the development of effective treatment strategies to delay and ideally prevent the progression of the disease. These may be informed by a greater understanding of the relationships between the tissues of the knee joint and risk factors of OA including local mechanical factors (joint alignment and kinematics) (Sharma *et al.*, 2001, Miyazaki *et al.*, 2002, Brouwer *et al.*, 2007).

Abnormal joint loading and malalignment during habitual loading (e.g. standing, walking) can affect the medial-to-lateral distribution of loads upon the tibial plateau (Wada *et al.*, 2001, Thorp *et al.*, 2006, Adouni *et al.*, 2014b). This can then affect the articular cartilage morphology and distribution (Andriacchi *et al.*, 2006, Eckstein *et al.*, 2008, Andriacchi *et al.*, 2009, Nakagawa *et al.*, 2015) and also the underlying subchondral bone (Wada *et al.*,

2001, Thorp *et al.*, 2006, Roberts *et al.*, 2017a, Roberts *et al.*, 2017b, Renault *et al.*, 2020, Shiraishi *et al.*, 2020), which may contribute to knee OA.

While studies have separately examined cartilage thickness, bone microarchitecture or joint loading (Wada *et al.*, 2001, Thorp *et al.*, 2006, Chaudhari *et al.*, 2008, Eckstein *et al.*, 2008, Roberts *et al.*, 2017a, Roberts *et al.*, 2017b, Roberts *et al.*, 2018), to the best of the author's knowledge, these examinations have never been performed altogether in the same patients. As cartilage and bone respond to every day mechanical loading as a single mechanical unit, they should be investigated concurrently (Ding *et al.*, 1998, Burr *et al.*, 2012).

Concurrent investigation of cartilage and bone is limited by common imaging methods. Magnetic resonance imaging (MRI) is an *in vivo* technique used for the imaging of soft tissues, but is ill suited to visualise bone. It also has a relatively low spatial resolution (e.g., 140-550 μm in-plane, with a 1500 μm slice thickness (Jerban *et al.*, 2020)), which can cause cartilage thickness to be overestimated, particularly in OA, where there are regions of thinner, denuded cartilage (Koo *et al.*, 2005, Koo *et al.*, 2009). Moreover, dual X-ray absorptiometry (DEXA) can assess bone mineral density (BMD) (Christensen *et al.*, 1982, Hulet *et al.*, 2002), but it cannot be used to assess cartilage, is limited to 2D analyses, and cannot separate the subchondral bone plate from the trabecular bone. Histology, while able to investigate cartilage and bone at high resolutions (3-5 μm in-plane), is a destructive 2D analysis and requires extensive preparation (Pritzker *et al.*, 2006, Schmitz *et al.*, 2010).

Micro-computed tomography (micro-CT), however, which has historically been used for the non-destructive characterization of 3D bone microarchitecture (e.g., 10-20 μm/pixel; Rüegsegger *et al.*, 1996, Hildebrand *et al.*, 1997b, Müller *et al.*, 1998, Perilli *et al.*, 2012), has recently been employed for the examination of human tibial articular cartilage both with contrast agents (van Tiel *et al.*, 2016, Nickmanesh *et al.*, 2018, Gatenholm *et al.*, 2019, Michalak *et al.*, 2019, Ylitalo *et al.*, 2019) and without (Delecourt *et al.*, 2016, Touraine *et al.*, 2017, Chen *et al.*, 2018). Micro-CT enables the non-destructive 3D assessment of entire excised human tibial plateaus at high resolutions, which, if combined with pre-operative joint loading indices of the subjects, would allow for the concurrent assessment of tibial cartilage and bone of these subjects. This, however, to the best of the author's knowledge, prior to this thesis, has not been done.

1.2 Aims and significance of research

The overall aim of this thesis is to quantify cartilage morphology and subchondral bone microarchitecture in human knee OA using micro-CT, accounting for *in vivo* joint loading indices. More specifically to:

1. Consider the effects of a varus and valgus knee alignment on cartilage thickness, subchondral bone plate thickness and trabecular bone volume fraction in OA and how it differs from controls.
2. Validate the human tibial cartilage thickness measured from micro-CT cross-sections (using a non-contrast agent based micro-CT imaging protocol) against histology (gold standard).
3. Investigate, in end-stage knee-OA subjects undergoing total knee replacement, relationships between external knee joint moments from pre-operative gait analysis (peak knee adduction moments, flexion/extension moments and external/internal rotation moments), joint alignment from pre-operative radiographs, and cartilage thickness of their excised tibial plateaus quantified with micro-CT.
4. Investigate region-specific relationships between cartilage thickness and subchondral bone microarchitecture in end-stage knee OA and in controls.

Understanding the relationships between joint alignment, external knee moments, cartilage morphology and bone microarchitecture may provide insights into developing and assessing OA treatments aimed at modifying joint loading. Moreover, validating a non-contrast agent micro-CT imaging protocol for the quantification of cartilage, would allow for non-destructive, *ex vivo* imaging of the human tibial plateau, for the concurrent examination of cartilage morphology and bone microarchitecture within the same scan, at higher spatial resolutions (17 μm/pixel) compared to *in vivo* imaging modalities. Finally, a detailed mapping of the cartilage morphology and bone microarchitecture in the tibial plateau could reveal morphological differences between control joints (without OA) and OA joints, which may in future become useful indicators of disease progression.

1.3 Outline of the thesis

Chapter 1: Introduction

The introduction describes the motivation, aims and significance of research of this thesis.

Chapter 2: Background

This chapter provides an overview of the knee joint, a review of the published literature on the relationship between cartilage and bone in knee OA and the influence of joint loading on these tissues. It also compares imaging modalities for the concurrent assessment of cartilage and bone.

Chapter 3: Study 1, Tibial cartilage, subchondral bone plate and bone microarchitecture in varus- and valgus-OA vs. controls

Study 1 firstly explores the effect of knee alignment on cartilage thickness, subchondral bone plate thickness and trabecular bone volume fraction in end-stage knee OA patients, comparing OA specimens with a varus or valgus knee alignment against non-OA controls (Aim 1). It secondly validates cartilage thickness measured from micro-CT against histology measurements (gold standard) (Aim 2).

Chapter 4: Study 2, Relationships between tibial articular cartilage, *in vivo* external knee joint moments and static knee alignment in end-stage knee OA: a micro-CT study

Study 2 examines relationships between cartilage thickness and pre-operative *in vivo* dynamic knee joint loading indices in end-stage knee OA subjects (Aim 3).

Chapter 5: Study 3, Systematic mapping of cartilage and subchondral bone in human tibial controls and osteoarthritis using micro-computed tomography

Study 3 presents a systematic spatial mapping (22 regions) of the cartilage and underlying bone morphological parameters, and the region-specific relationships between these, in the control and OA groups (Aims 1 and 4).

Chapter 6: Conclusions and future recommendations

The key findings, impact and significance of these findings are discussed as well as limitations of the research and recommendations for its continuation in the future.

Chapter 2 **Background**

2.1 Knee Joint

2.1.1 Function

The knee is the largest synovial joint in the body and is essential for daily activities such as walking, running, sitting-to-standing and climbing stairs (Figure 2.1) (Hirschmann *et al.*, 2015, Zhang *et al.*, 2020). It is a sliding hinge joint which supports body weight while facilitating movements such as flexion and extension, with small degrees of internal and external rotations during moderate flexion (Zhang *et al.*, 2018).

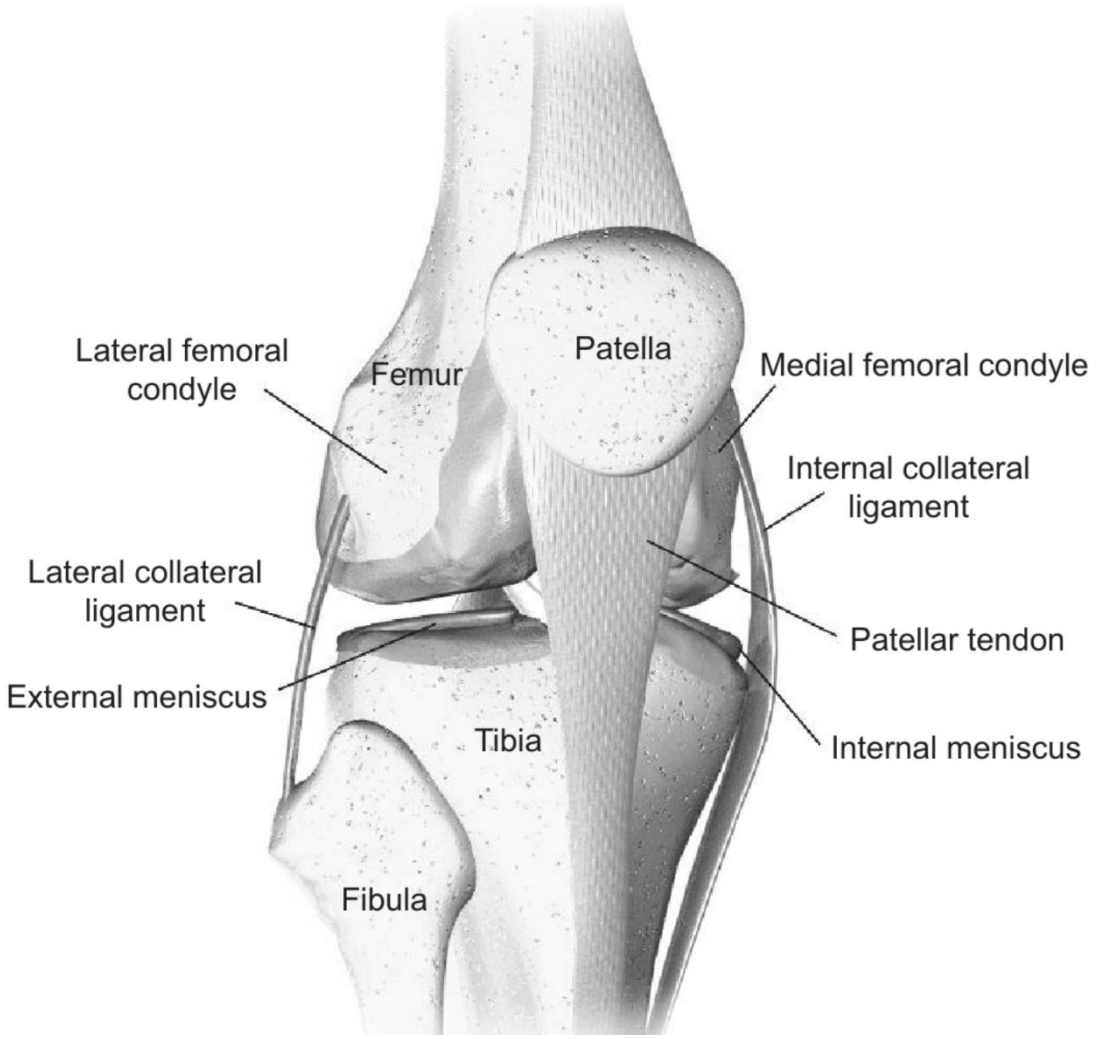

Figure 2.1: Anterior view of the knee joint. This figure has been reprinted from Elsevier Books with permission from Elsevier (Affatato, 2015).

2.1.2 Anatomy

2.1.2.1 Bones

The above movements of the knee occur due to articulations between the bones of the knee joint. The knee joint is comprised of three bones: the femur, tibia and patella (Figure 2.1). Primary articulation occurs between the femoral medial and lateral condyles and the tibial medial and lateral condyles (tibiofemoral joint). This is the largest articulation within the knee and is the weight bearing component. The patella articulates with the trochlear groove of the femur, forming the patellofemoral joint. Together, the tibia and fibula form the proximal tibiofibular joint, but this does not contribute to the movements of the knee (Figure 2.1).

2.1.2.2 Articular Cartilage

The contact point of the bones are covered by a specialised form of hyaline cartilage, known as articular cartilage, which creates smooth, frictionless articulation and assists in distributing loads onto the bones (Figure 2.2) (Fox *et al.*, 2009). Together, the bone and cartilage form the osteochondral unit (see Chapter 2.2 for more details).

2.1.2.3 Menisci

The medial and lateral menisci are crescent-shaped load-bearing fibrocartilage structures that lie flat on the tibial plateau with a concave superior surface (Figure 2.2) (Kohn *et al.*, 1995). They act as shock absorbers for daily loads (walking, running, jumping, etc) (Fox *et al.*, 2012), with the wedge-like shape of the menisci playing a role in the stability of the femorotibial joint (Ombregt, 2013). As they increase the contact area between the femoral and tibial condyles, they assist in distributing loads over the surface of the tibial plateau, preventing concentrated loads which can damage the articular cartilage (Fox *et al.*, 2012, Ombregt, 2013). Additionally, the menisci may contribute to the lubrication and nutrition of the articular cartilage (Fox *et al.*, 2012).

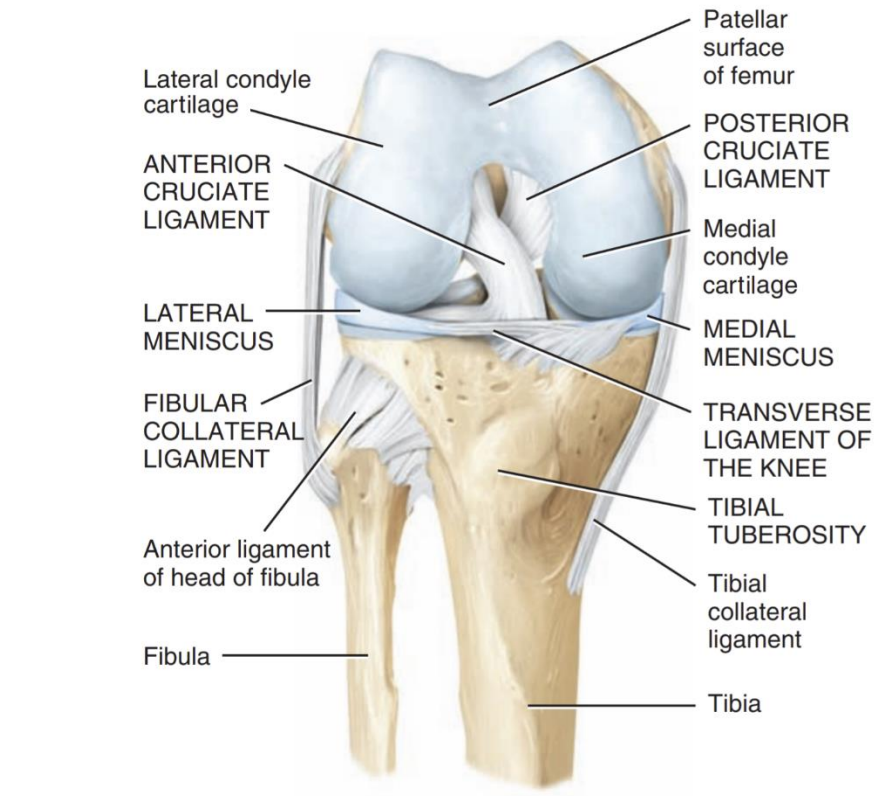

Figure 2.2: a) Inferior view of the femur displaying the femoral condyles on top of the anterior view of the tibia. b) the superior view of the tibial condyles, displaying the menisci, ligament attachment sites and articular cartilage. This figure has been reprinted with minor editing from Principles of Anatomy and Physiology with permission from John Wiley & Sons - Books (Tortora *et al.*, 2014).

2.1.2.4 Ligaments

Ligaments connect bones to bones, playing the focal role in the stability of the knee joint. The main ligaments of the knee are the anterior cruciate ligament (ACL), posterior cruciate ligament (PCL), medial collateral ligament (MCL) and lateral collateral ligament (LCL; Figure 2.2) (Abulhasan *et al.*, 2017). The ACL connects the anterior intercondylar region of the tibial plateau to the femur posteriorly at the intercondylar fossa, resisting anterior translations of the tibia (and posterior translations of the femur) (Duthon *et al.*, 2006, Abulhasan *et al.*, 2017). The PCL connects the posterior tibial plateau (in between the posterior horns of the menisci) to the femur anteriorly at the medial condyle, resisting posterior translations of the tibia and anterior translations of the femur (Gollehon *et al.*, 1987, Abulhasan *et al.*, 2017). The collateral ligaments (MCL and LCL) resist sideways translations and varus/valgus rotations with the MCL connecting the medial side of the tibia and femur, and the LCL connecting the proximal fibula to the lateral side of the femur (Gollehon *et al.*, 1987, Abulhasan *et al.*, 2017).

2.1.2.5 Muscles

The quadriceps muscle group, which includes the rectus femoris, vastus lateralis, vastus medialis and vastus intermedius, facilitates the extension (or straightening) of the knee from a bent position (Mansfield *et al.*, 2019) (Figure 2.3). The knee flexor muscles include the hamstrings muscle group (biceps femoris, semimembranosus and semitendinosus), the gracilis, sartoris, gastrocnemius, plantaris and popliteus. These flexor muscles are primarily responsible for the bending of the knee, but also play a role in the internal/external rotation and stabilisation of the knee (Figure 2.3) (Kopydlowski *et al.*, 2014, Mansfield *et al.*, 2019).

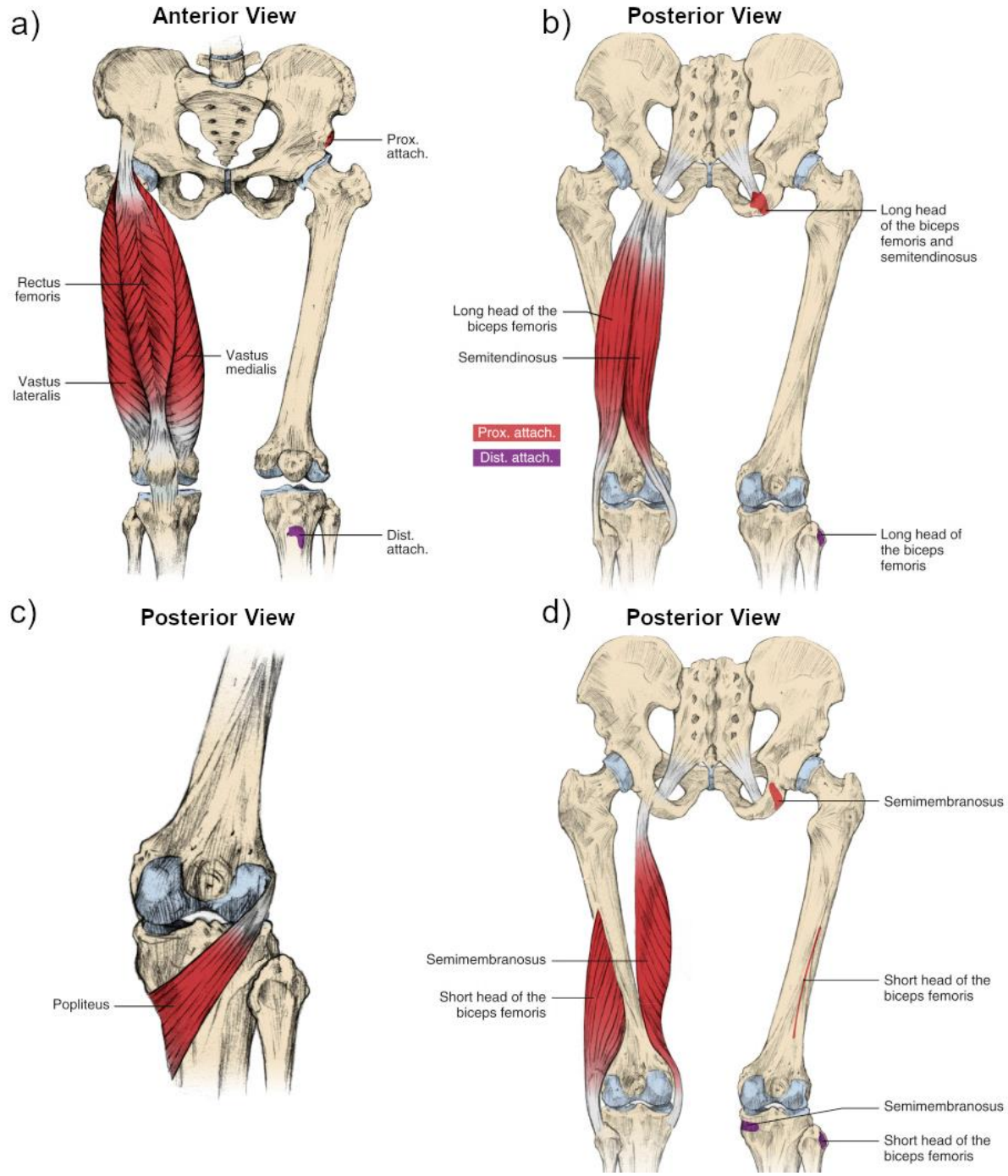

Figure 2.3: The main flexor and extensor muscles of the knee; a) the quadriceps muscles b) the popliteus, c) and d) the hamstring muscles. This figure has been reprinted with minor editing from Elsevier Books with permission from Elsevier (Mansfield et al., 2019).

2.2 The Osteochondral Unit

The osteochondral unit (OCU) is composed of articular cartilage and subchondral bone, connected through an interface of calcified cartilage (Figure 2.4) (Oláh *et al.*, 2018, Lepage *et al.*, 2019). These tissues interact with each other physiologically, biochemically and mechanically, playing a vital role in the maintenance of joint health contributing to the distribution and transfer of loads during weight bearing and joint movements (Findlay *et al.*, 2016, Goldring *et al.*, 2016, Oláh *et al.*, 2018).

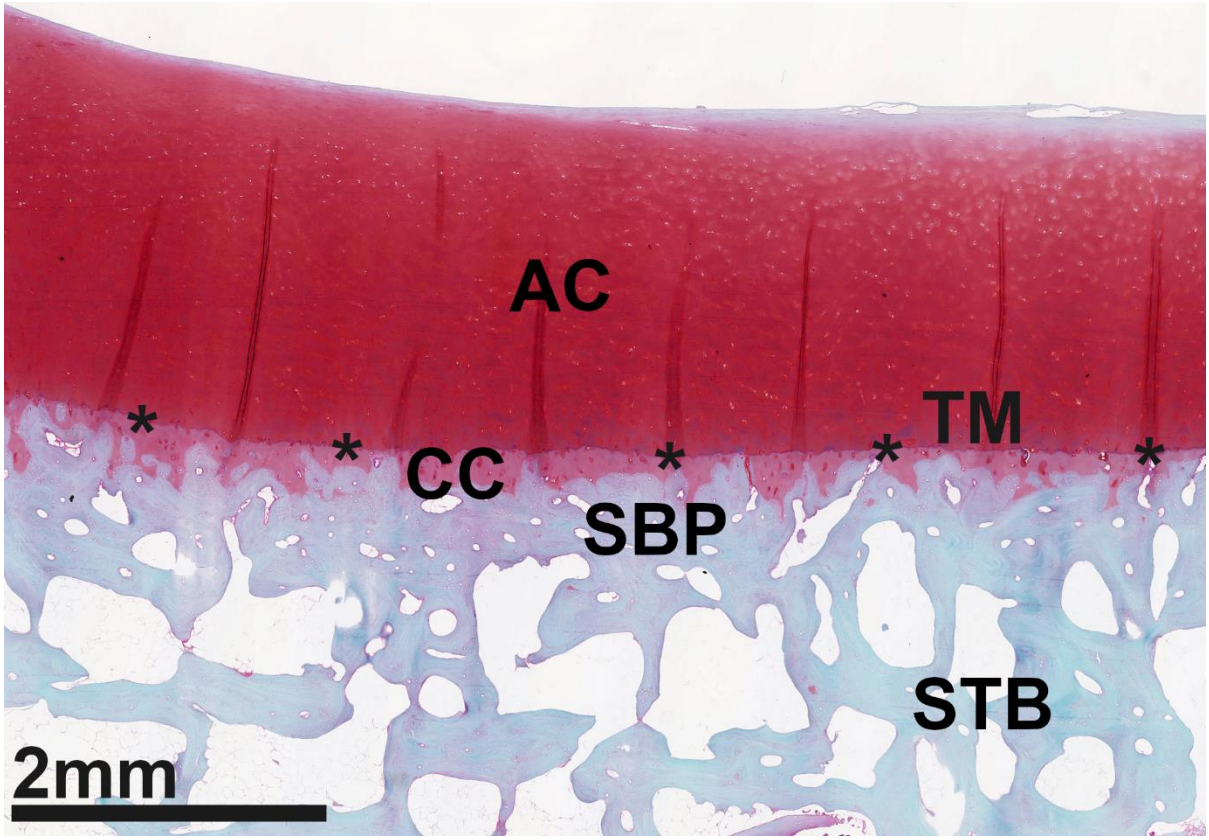

Figure 2.4: Digital image of a histology slide stained with Safranin-O/Fast Green (taken with the Nanozoomer Digital Slide Scanner) displaying articular cartilage (AC), calcified cartilage (CC), subchondral bone plate (SCP) and subchondral trabecular bone (STB). Black asterisks indicate tidemark (TM). Original magnification 40x.

2.2.1 Articular Cartilage

Articular cartilage is an avascular and aneural tissue which facilitates smooth articulation and distributes loads with minimal friction onto the bone (Figure 2.4) (Fox *et al.*, 2009). It consists of an extracellular matrix (ECM), which is primarily water (65-80% of the total weight), type II collagen, proteoglycan aggregates and sparsely distributed specialised cells (chondrocytes), which make up less than 5% of the tissue volume (Fox *et al.*, 2009, Nelson *et al.*, 2009). Proteoglycan aggregates are formed by aggregan molecules non-

covalently linked to a hyaluronic acid chain, where the aggrecan molecules are a core protein which is covalently bonded to negative charged, hydrophilic, linear chains of glycosaminoglyan side chains (Imhof *et al.*, 1999, Oláh *et al.*, 2018). Chondrocytes are metabolically active cells within the articular cartilage, responsible for the development, maintenance and repair of the ECM (Fox *et al.*, 2009). The type II collagen fibrils are highly crosslinked, entrapping the proteoglycan aggregates and other nonspecific matrix proteins (Goldring *et al.*, 2016). The orientation of these collagen fibrils, along with the proteoglycan aggregates, help determine the biomechanical properties of the articular cartilage, specifically its tensile strength and compressive resilience (Andriacchi *et al.*, 2014, Guo *et al.*, 2015).

Articular cartilage is defined by four distinct layers or zones: superficial zone, middle zone, deep zone and the calcified zone (Figure 2.5) (Fox *et al.*, 2009). Each zone plays a role in the absorption and distribution of mechanical loads. In the superficial zone (10-20% of cartilage volume), the collagen fibrils lie tightly packed, parallel to the cartilage surface, providing tensile strength and assisting the protection of underlying layers (Goldring *et al.*, 2016). This layer also contains a relatively high density of flattened chondrocytes (Fox *et al.*, 2009). The middle zone comprises 40-60% of the cartilage volume, containing obliquely aligned collagen and a low density of spherical chondrocytes, functionally providing some resistance to compression (Fox *et al.*, 2009). The deep zone (30% of the cartilage volume), containing the highest proteoglycan content and collagen fibrils aligned perpendicularly to the cartilage surface, provides the greatest resistance to compressive forces in the articular cartilage (Fox *et al.*, 2009).

When the cartilage is compressed, charged solutes and water molecules, which are attracted to the hydrophilic glycosaminoglycan chains in the proteoglycan aggregates, are extruded. The pressurisation of remaining water molecules in the ECM and perpendicular orientation of the collagen fibrils provides resistance to compression, enduring loads up to multiple times (in magnitude) a person's body weight (Fox *et al.*, 2009). When the tissue is no longer compressed, the negative charge of the proteoglycan aggregates draws the charged solutes and water back into the ECM (Fox *et al.*, 2009, Goldring *et al.*, 2016). This flow of water and synovial fluid during joint loading provides lubrication and is critical for the transport of nutrients into the caritlage (Fox *et al.*, 2009). However, nutrients may also be supplied to the deeper layers of cartilage from the underlying suchondral bone (Imhof *et al.*, 2000, Pan *et al.*, 2009, Goldring *et al.*, 2016).

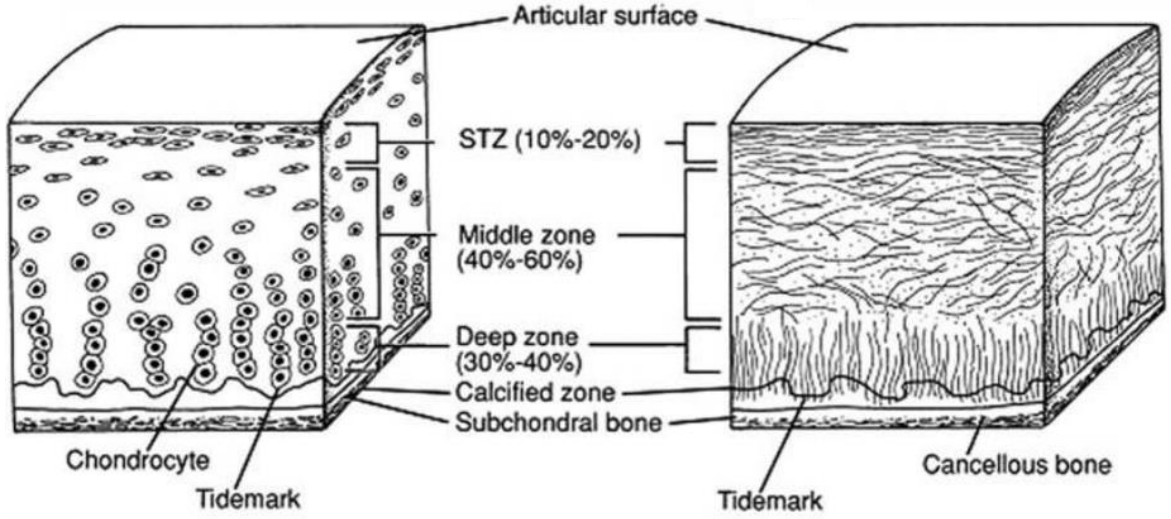

Figure 2.5: Cross-sectional diagram of non-diseased cartilage showing cellular distribution (left) and collagen fibrillar network (right). This figure has been reprinted from the Journal of the American Academy of Orthopaedic Surgeons with permission from Wolters Kluwer Health, Inc (Buckwalter et al., 1994).

2.2.2 Calcified Cartilage

The calcified cartilage is a thin (20-250 μm) intermediary layer between the articular cartilage and subchondral bone (Figure 2.4) (Zhang *et al.*, 2012). The calcified zone is separated from the deep zone by the tide mark, an approximately 5 μm thick band of mineralised cartilage which secures the collagen fibrils in the deep zone of the cartilage to the underlying subchondral bone plate (Fox *et al.*, 2009, Oláh *et al.*, 2018). Where the articular cartilage does little to attenuate the loads the joint is subjected to, the calcified cartilage plays an important role in transferring and dispersing the load across the underlying bone (Goldring *et al.*, 2016). This is assisted by the differences in material stiffness of the tissues. The articular cartilage has an elastic modulus of 1-15 MPa, compared to the approximate 0.3 GPa and 2 GPa of the calcified cartilage and subchondral bone respectively (Akizuki *et al.*, 1986, Mente *et al.*, 1994, Oláh *et al.*, 2018). During loading, the wave-like interface of the articular cartilage with the calcified cartilage assists in transforming shear stresses into compressive and tensile stresses onto the bone (Goldring *et al.*, 2016).

2.2.3 Subchondral Bone

The subchondral bone lies under the articular cartilage and plays a vital role as a mechanical shock absorber, attenuating approximately 30% of the loads through the joint compared to 1-3% that the overlying cartilage attenuates (Figure 2.4) (Oláh *et al.*, 2018).

It supports the overlying cartilage mechanically and metabolically, and maintains the joint shape (Imhof *et al.*, 2000). It consists of the subchondral bone plate (cortical endplate) and the subchondral trabecular bone (subarticular spongiosa or cancellous bone) (Li *et al.*, 2013) which exhibit different mechanical properties from each other (Choi *et al.*, 1990).

The subchondral bone plate (SBP) is a dense bony lamella that interlocks with the calcified cartilage through an undulated interface (Figure 2.4) (Oláh *et al.*, 2018). Similar to the articular cartilage/calcified cartilage interface, this undulated surface assists in transforming shear loads to compressive and tensile stresses. In a healthy tibial plateau, the SBP is thickest in the central region of the condyle (near the intercondylar tubercles), becoming thinner in concentric circles extending towards the external edges of the condyle (Figure 2.6) (Milz *et al.*, 1994). This pattern can be susceptible to changes, for example due to joint loading (Madry *et al.,* 2010, Chapter 2.3 of this thesis). The subchondral bone plate also contains pores which may be vascular and neural channels connecting into the calcified cartilage and deeper levels of articular cartilage (Berry *et al.*, 1986, Burr, 2004).

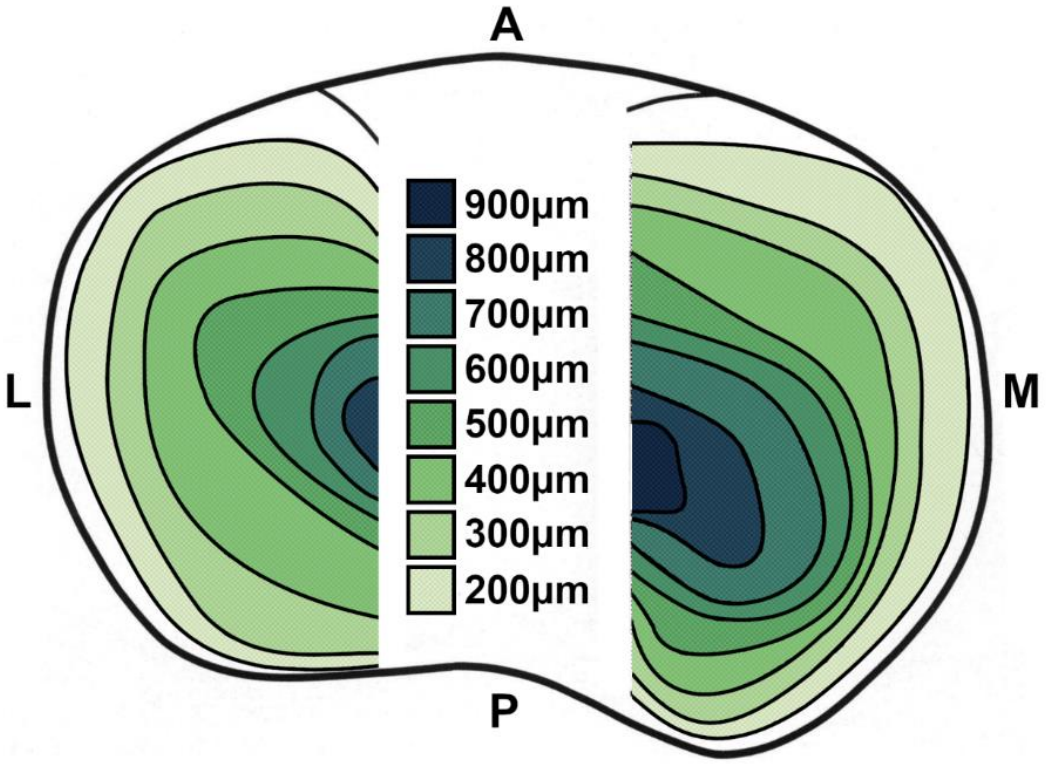

Figure 2.6: Tibial subchondral bone plate thickness distribution. This figure has been reprinted and modified from the Journal of Anatomy with permission from John Wiley & Sons – Books (Milz *et al.*, 1994).

The SBP branches out into the underlying subchondral trabecular bone (STB; Figure 2.4). Mechanically, the STB exhibits different properties to the subchondral bone plate (e.g., has a lower elastic modulus) and provides elasticity for shock absorption (Choi *et al.*, 1990, Madry *et al.*, 2010). In the tibia, the STB plays an important role in the attenuation of mechanical loads and the transmission of the loads from the joint surface to the tibial diaphysis. The STB is more porous than the SBP, having a honeycomb-like lattice appearance, and is metabolically active, containing bone marrow, sensory nerves and blood vessels (Suri *et al.*, 2012, Li *et al.*, 2013). It is a very dynamic structure where the orientation, shape and thickness of the trabeculae adapt to mechanical stimuli imposed across the joint. This bone remodelling occurs via osteoclasts and osteoblasts, causing the resorption and deposition (formation) of bone respectively (Goldring, 2012, Frost, 2001, McKinely *et al.,* 2003, Turner, 1998, Chapter 2.3 of this thesis). Hence, the trabeculae can exhibit anisotropic behaviour and consequently have different mechanical properties in different planes (Figure 2.7) (Odgaard, 1997, Odgaard *et al.*, 1997, Burr, 2004).

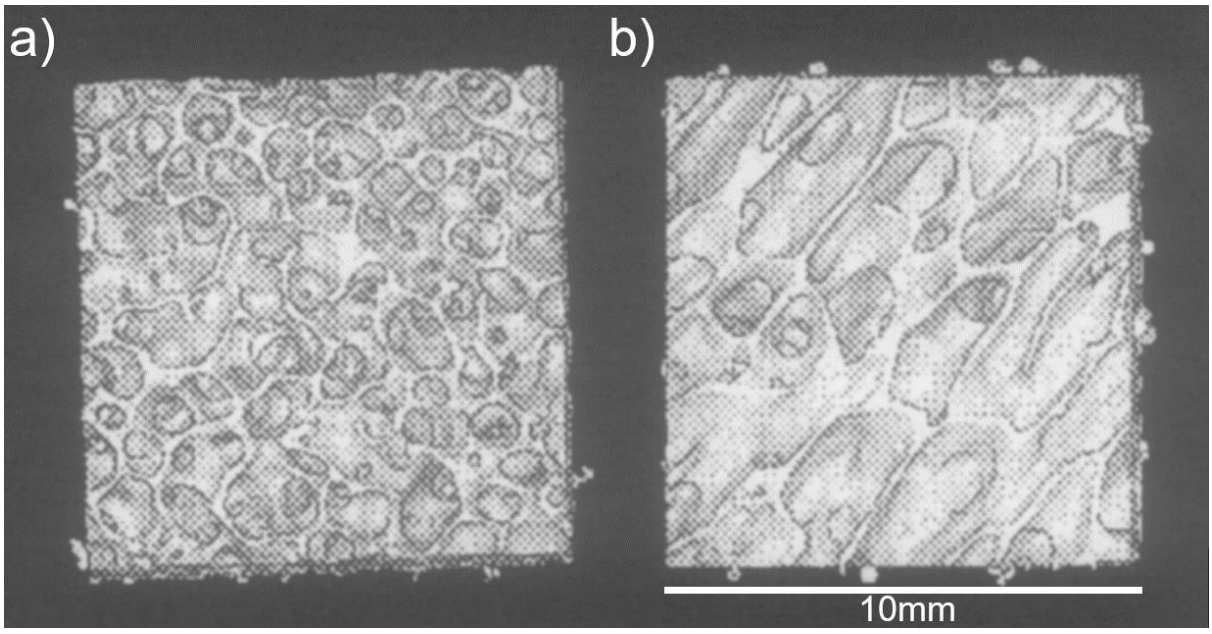

Figure 2.7 3D reconstruction of two extracted cubes of trabecular bone (10 mm width) where the arrangement of trabeculae in a) is isotropic and in b), anisotropic. This figure has been reprinted and modified from the Journal of Biomechanics with permission from Elsevier (Odgaard et al., 1997).

2.2.4 Osteochondral tissues in the various stages of OA

OA is a debilitating joint disease that can affect all articulating structures of the knee, but is most characteristically defined by the alterations of the OCU (Goldring *et al.*, 2010, Loeser *et al.*, 2012). In early OA, initial changes in the articular cartilage are marked by a reduction in proteoglycan aggregates (Figure 2.8) (Goldring *et al.*, 2016). The loss of these negatively charged molecules disrupts the regulation of fluid-flow in the cartilage, causing an excess of water to enter the ECM which swells the cartilage (Figure 2.8) (Akizuki *et al.*, 1987, Calvo *et al.*, 2004, Goldring *et al.*, 2016). The ECM degradation begins in the superficial zones of the cartilage before extending to the deeper zones as the disease progresses, with the erosion of the ECM and the development of deep fissures, cartilage delamination and denuded areas of cartilage, exposing the underlying bone (Figure 2.8) (Pritzker *et al.*, 2006, Goldring *et al.*, 2016). Underneath, the calcified cartilage expands above into the articular cartilage. There is also thought to be the penetration of sensory nerves and vascular elements through the calcified cartilage, possibly playing a role in the joint pain associated with OA (Figure 2.8) (Lane *et al.*, 1977, Burr *et al.*, 1997, Imhof *et al.*, 2000, Goldring *et al.*, 2016).

The *early stages* of OA are marked by an increase in remodelling and resorption of bone (Figure 2.8) (Burr *et al.*, 2012). Some studies report an increase in porosity of the subchondral bone plate, in addition to cortex flattening and deformation (bone attrition) and a reduced bone density (Bettica *et al.*, 2002, Reichenbach *et al.*, 2008, Goldring *et al.*, 2016).

In the *later stages* of the disease, this is followed by bone sclerosis, with reduced bone turnover, and a net increase in bone formation compared to bone resorption (Burr *et al.*, 2012). This leads to a subsequent overall thickening of the plate, formation of osteophytes at the bone surface and increases in subchondral trabecular bone volume fraction (BV/TV) and BMD compared to non-OA joints (Hannan *et al.*, 1993, Fazzalari *et al.*, 1997, Li *et al.*, 1997, Matsui *et al.*, 1997, Burr *et al.*, 2012). However, the sclerotic bone has a lower mineralisation and consequent reduced bone tissue elastic modulus, which can then lead to deformations under load (Li *et al.*, 1997, Day *et al.*, 2001, Huebner *et al.*, 2002, Goldring *et al.*, 2016). There are also reports of the formation of subchondral bone cysts (Li *et al.*, 2013) and transformation of trabeculae from rod-like structures into plate-like structures (Ding, 2010, Chen *et al.*, 2018).

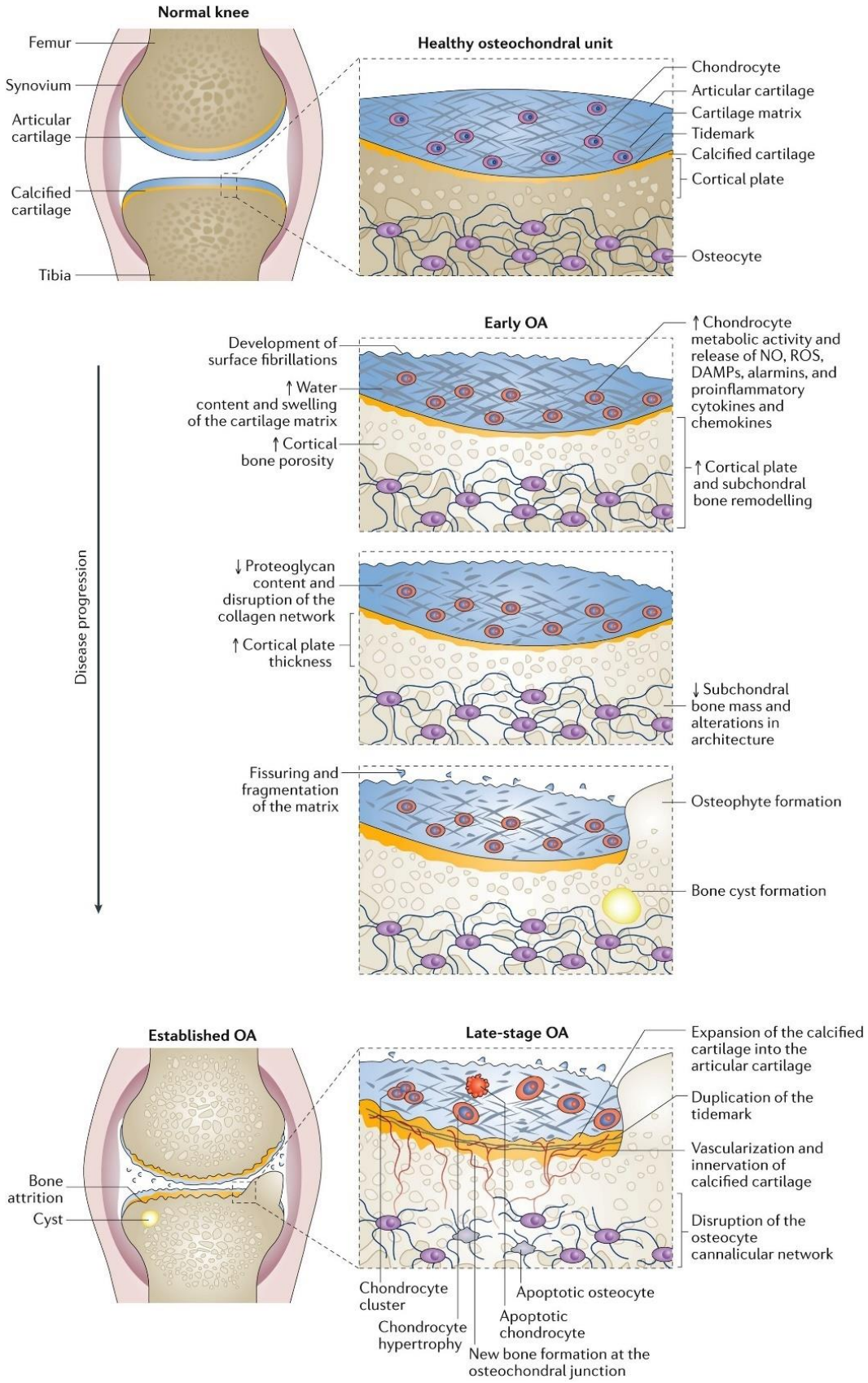

Figure 2.8: Cartilage and subchondral bone morphological changes in the progression of OA. This figure has been reprinted from Nature Reviews Rheumatology with permission from Springer Nature (Goldring *et al.*, 2016).

OA is a multifactorial disease. However, although the initiation of the disease may occur at a single-tissue (e.g. cartilage or bone) level, due to the close interactions within the OCU, OA affects all tissues in the unit which ultimately results in the degradation of cartilage and alteration of subchondral bone (Goldring *et al.*, 2016). Mechanically, OA affects the functional integrity of the unit, where any damage to the articular cartilage can substantially increase the loads transmitted to the subchondral bone in that region (Burr, 2004, Sniekers *et al.*, 2008). Moreover, adaptions of the subchondral bone can contribute to the overlying cartilage fibrillation due to the generation of local abnormal loads and shear stresses (Burr *et al.*, 2012, Li *et al.*, 2013, Bertuglia *et al.*, 2016). These disruptions then further contribute to the OA pathology in a feedback loop, progressing in joint degradation and OA severity, eventuating in the need for a total joint replacement (Burr *et al.*, 2012, Li *et al.*, 2013).

2.3 Role of Joint Loading on the Osteochondral Unit

The tibia is subject to loading during daily activities (standing, walking, etc), which also plays a role in the maintenance of joint health such as cartilage homeostasis and bone remodelling (Burr, 2004, Andriacchi *et al.*, 2009, Guilak, 2011). However, joint loading is also a risk factor of OA (Johnson *et al.*, 2014), where altered, abnormal and/or traumatic loading have been found to contribute to the onset and progression of the disease, affecting both the cartilage and the bone (Miyazaki *et al.*, 2002, Bobinac *et al.*, 2003, Griffin *et al.*, 2005, Brouwer *et al.*, 2007, Astephen *et al.*, 2008, Guilak, 2011, Burr *et al.*, 2012).

2.3.1 Mechanical alignment

In the frontal plane, the mechanical axis of the lower limb is the line connecting the centre of the femoral head to the centre of the ankle plafond (Paley, 2002). The mechanical axis deviation (MAD) is defined as the perpendicular distance from the mechanical axis to the centre of the knee joint (Paley, 2002). A varus knee alignment is defined as a medial deviation greater than 15 mm, a valgus alignment as a lateral deviation greater than 0 mm (Figure 2.9) (Paley, 2002, Roberts *et al.*, 2017b).

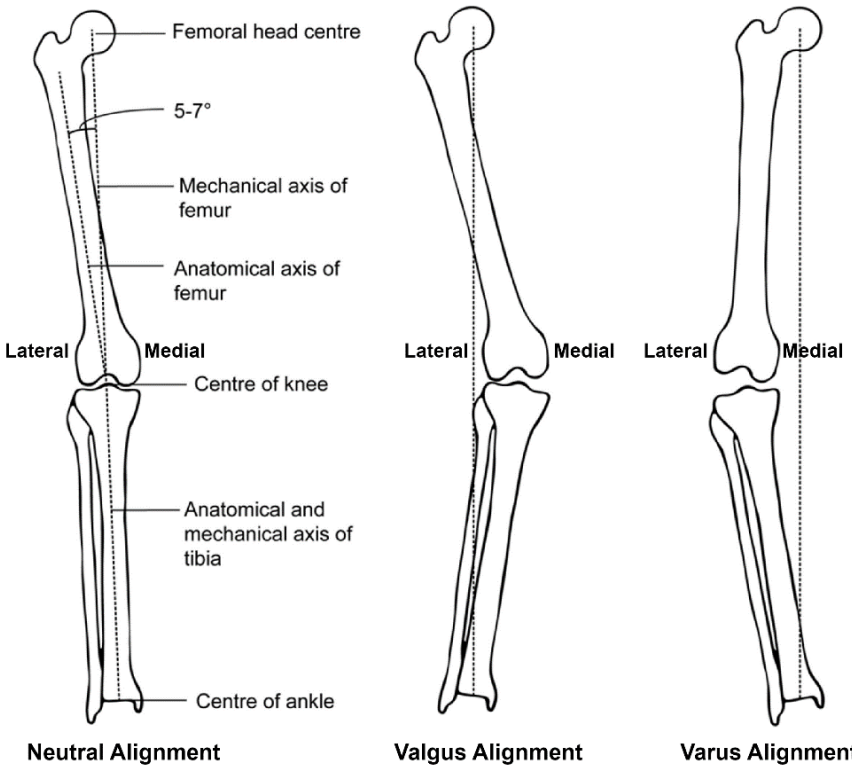

Figure 2.9: Mechanical alignment of the lower leg. This figure has been reprinted with minor modifications from Orthopaedics and Trauma with permission from Elsevier (Aweid *et al*., 2019).

These malalignments have previously been linked to altered medial-to-lateral distribution of loads upon the joint (Adouni *et al.*, 2014b, Roberts *et al.*, 2017b), increasing the risk of medial OA progression in varus-OA subjects and lateral OA progression in valgus-OA subjects (Sharma *et al.*, 2001). In a longitudinal OA study, Eckstein et al. (2008) reported the greatest loss of cartilage thickness over 5 months to occur in the central and external regions of the medial tibial condyle in varus-OA knees, and in the internal and central lateral tibial condyle in valgus-OA knees (Eckstein *et al.*, 2008). Static malalignment also affects the subchondral bone, where dual X-ray absorptiometry (DEXA) studies have shown the medial-to-lateral BMD ratio to be correlated with the mechanical axis in medial-compartment knee OA (Wada *et al.*, 2001, Hulet *et al.*, 2002, Thorp *et al.*, 2006). More recently, using micro-CT, relationships between mechanical alignment and regional subchondral bone microarchitecture in the tibial plateau in OA have also been found (Roberts *et al.*, 2017b, Roberts *et al.*, 2018, Renault *et al.*, 2020, Shiraishi *et al.*, 2020). In these studies, BV/TV was found higher in the medial condyle compared to lateral for varus-aligned OA specimens and higher in the lateral condyle for valgus-aligned OA specimens; though it is unclear how the bone microarchitecture distribution compares to non-pathological tibiae, or the overlying cartilage, in these regions.

2.3.2 External knee joint moments

The tibial plateau sustains approximately 70% of peak joint reaction forces (2-3x body weight) that occur during walking (Schipplein *et al.*, 1991, Fregly *et al.*, 2012). In a healthy joint, it has been reported that cartilage is thicker in weight-bearing regions from repetitive cyclic loading (such as walking) (Li *et al.*, 2005, Andriacchi *et al.*, 2009). Increases in loading, however, could then lead to cartilage degradation (Chaudhari *et al.*, 2008). In particular, external measures of joint loading (derived from gait analysis; Figure 2.10), including the knee adduction moment (KAM), KAM impulse and knee flexion moments (KFM), have been associated with variations in tibial cartilage thickness in OA (Erhart-Hledik *et al.*, 2015, Maly *et al.*, 2015, Edd *et al.*, 2018).

2.3.2.1 Joint load and tibial cartilage in OA

The peak KAM is a surrogate marker for *in vivo* medial-to-lateral load distribution (Schipplein *et al.*, 1991, Zhao *et al.*, 2007). In individuals with end-stage OA, higher KAMs are reported compared to those with a lower OA severity and to non-OA controls (Sharma

et al., 1998, Mündermann *et al.*, 2005). Similarly, Creaby *et al.* (2010) found the peak KAM to be associated with the severity of medial tibiofemoral cartilage defects assessed using MRI.

However, some relationships, such as those between the knee OA cartilage thickness, KFM and KAM are conflicting (Vanwanseele *et al.*, 2010, Chang *et al.*, 2015, Erhart-Hledik *et al.*, 2015, Maly *et al.*, 2015). A previous *in vivo* study reported a higher magnitude of KAM and KAM impulse being associated with a greater loss of cartilage volume in the medial tibial condyle over 12 months in medial knee OA (Maly *et al.*, 2015). However, Erhart-Hledik *et al.* (2015) and Vanwanseele *et al.* (2010) found no associations with medial or lateral tibial cartilage thickness with the KAM and KAM impulse. Moreover, Erhart-Hledik *et al.* (2015) did find an association between the medial-to-lateral tibial cartilage thickness ratio and KFM in early OA, but conflicting results exist on the influence of KFM on OA progression in longitudinal studies (Chehab *et al.*, 2014, Chang *et al.*, 2015).

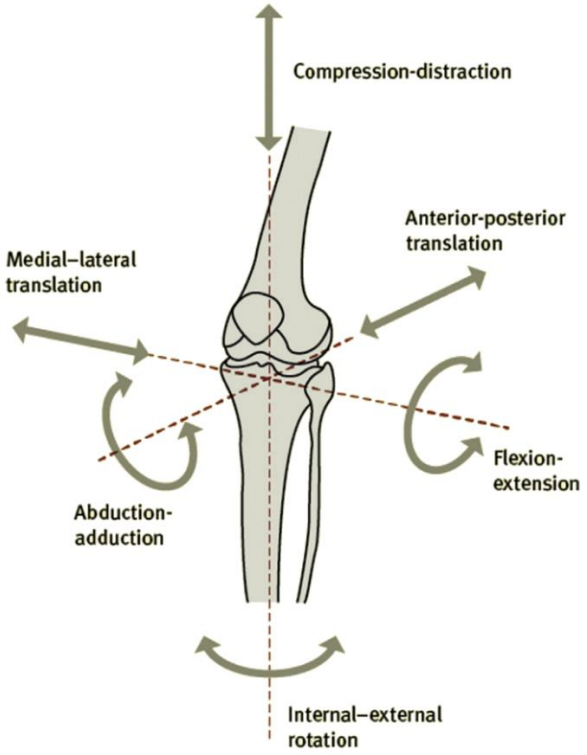

Figure 2.10: Knee joint coordinate system, illustrating motion of knee joint: motions in the sagittal plane are described by flexion/extension, motions in the frontal plane are described by abduction/adduction and, motion in the transverse plane is described by internal/external rotations. This figure has been reprinted with minor modifications from Orthopaedics and Trauma with permission from Elsevier (Shenoy et al., 2013).

2.3.2.2 Joint load and tibial subchondral bone in OA

In the subchondral bone, the medial-to-lateral BMD ratio in OA has been associated with the peak KAM (Wada *et al.*, 2001, Thorp *et al.*, 2006), the second peak KAM and KAM Impulse (Thorp *et al.*, 2006). These external knee joint moments (peak KAM, the first peak KAM, second peak KAM, KAM impulse) were also found to be significantly correlated with the medial-to-lateral subchondral trabecular bone volume fraction ratio in previous work within our group (Roberts *et al.*, 2018). Additionally, in that micro-CT study, the external rotation moment was also found to be significantly correlated (negatively) with the medial trabecular bone volume fraction and medial-to-lateral bone volume fraction ratios. It can be expected that ERM would also correlate with the articular cartilage thickness and medial-to-lateral cartilage ratio within the same regions, though to the best of the author's knowledge, this has not yet been explored.

2.4 Conventional Cartilage and Bone Imaging Methods

As described in the previous section, articular cartilage and subchondral bone respond to mechanical loads together (Ding *et al.*, 1998). Abnormal changes to one of the tissues may then lead to the abnormal remodelling or changes in the other (Mahjoub *et al.*, 2012). Thereby, the interaction of articular cartilage and the underlying subchondral bone should be investigated. This section outlines imaging techniques for the concurrent imaging of cartilage and subchondral bone of the tibia.

2.4.1 Magnetic Resonance Imaging (MRI)

Magnetic resonance imaging is an *in vivo* technique used for the imaging of soft tissues but is less suited to visualise bone. It uses a combination of a strong magnetic field and applied radio frequency (RF) to visualise hydrogen-containing tissues of the body. Briefly, the magnetic field aligns the magnetic moments of the hydrogen nuclei, and the application of a RF pulse displaces this alignment. When the RF pulse is switched off, the hydrogen nuclei realign (relax) generating a resultant radio signal that is measured to generate an image (Oldendorf, 1988, Hendee *et al.*, 2003). MRI is capable of producing excellent contrast of soft tissues and cartilage, due to the high water content in those tissues (Potter *et al.*, 1998). With the additional benefit of requiring no ionising radiation or contrast agents, it is the most commonly used imaging modality for the *in vivo* characterisation of human articular cartilage (Figure 2.11) (Cohen *et al.*, 1999, Hellio Le Graverand *et al.*, 2009, Crema *et al.*, 2011, Eckstein *et al.*, 2011, Erhart-Hledik *et al.*, 2015, Favre *et al.*, 2016, Edd *et al.*, 2018).

Figure 2.11: Coronal MRI image depicting the central medial and lateral femoral condyles (cMF and CLF respectively) and the medial and lateral tibial condyles (MT and LT respectively). The distal femur and proximal tibia are represented in the dark colour with the cartilage in the light gray colour between the two bones. This figure has been reprinted with minor modifications from Osteoarthritis and Cartilage with permission from Elsevier (Hellio Le Graverand et al., 2009).

One of the main limitations of MRI is the low spatial resolution *in vivo,* which can range, at best, from an in-plane resolution of 140x140 µm to 550x550 µm, with a 1500-3000 µm slice thickness (Eckstein *et al.*, 2008, Vanwanseele *et al.*, 2010, Erhart-Hledik *et al.*, 2015, Maly *et al.*, 2015, Jerban *et al.*, 2020, Favre *et al.*, 2021). The thickness of articular cartilage of the human tibial plateau in non-diseased joints ranges from 1.54 to 2.98mm (Shepherd *et al.*, 1999, Delecourt *et al.*, 2016), however in OA, there is a progressive thinning and degeneration of articular cartilage, which can cause its thickness to be overestimated (Koo *et al.*, 2005, Koo *et al.*, 2009). At in-plane resolutions of 0.5 mm x 0.5 mm, Koo et al. reported significant overestimations in human knee articular cartilage less than 2.5 mm thick, especially in non-weight bearing regions (Koo *et al.*, 2005, Koo *et al.*, 2009). Higher MRI resolutions have since been recommended for the quantification of cartilage, i.e. in-plane resolutions of less than 0.35mm x 0.35mm and slice thickness of 1.5 mm (10-12 min scanning time) (Eckstein *et al.*, 2006, Eckstein *et al.*, 2014). However, overestimations of cartilage thickness and underestimations of cartilage defects are still reported (Gomoll *et al.*, 2011, Campbell *et al.*, 2013). Moreover, the large slice thickness leaves MRI images susceptible to partial volume artefacts (Gold *et al.*, 2009, Liu *et al.*, 2018).

Another important limitation of MRI is the inability to directly image trabecular bone. Instead, an indirect measure of trabecular bone can be derived by the absence of measured signal compared to bone marrow (Figure 2.12) (Bolbos *et al.*, 2008, Driban *et al.*, 2012). However, at these resolutions it is difficult to resolve thin trabeculae (50–2000 µm long, ~100 µm thick (Hardisty *et al.*, 2009)) and measure 3D histomorphometry parameters (Krug *et al.*, 2005). A comparison of trabecular microarchitecture between MRI (3T, spatial resolution of 117x117x300 µm) and micro-CT (22 µm isotropic voxel size) in human bone cores (Sell *et al.*, 2005), found the apparent histomorphometry parameters measured with MRI, i.e. apparent BV/TV, trabecular thickness and trabecular number to be overestimated and trabecular separation to be underestimated compared to micro-CT, by a factor of 1.9x, 2.44x, 1.23x and 0.62x, respectively. The linear relationships between MRI and micro-CT for each parameter have reported coefficients of determination ranging from $R^2 = 0.67$ to 0.82. Similar findings were presented by Phan *et al.* (2006).

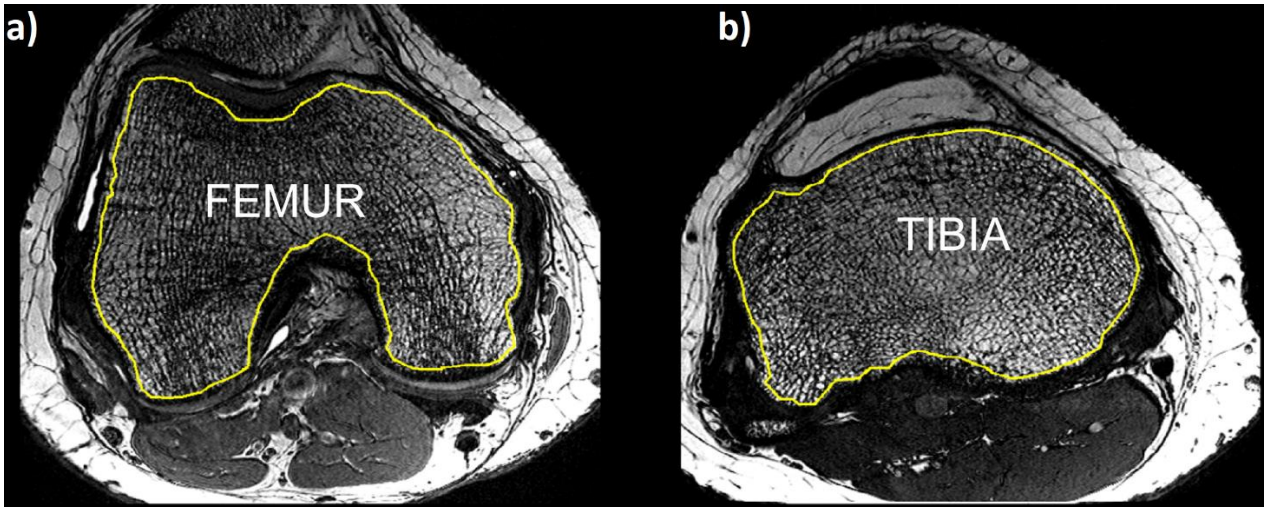

Figure 2.12: MRI transaxial images of the human knee at a spatial resolution of 195x195x1000 µm. The femur and tibia outlined in the yellow colour and within these outlines, marrow and trabecular bone are represented by light gray and dark gray/black colours respectively This figure has been reprinted with minor modifications from Osteoarthritis and Cartilage with permission from Elsevier (Bolbos *et al*., 2008).

To overcome these limitations, some studies have combined MRI for cartilage characterisation with other imaging modalities, such as DEXA (Lee *et al.*, 2013, Cao *et al.*, 2014, Teichtahl *et al.*, 2017) and high resolution peripheral quantitative computed tomography (HR-pQCT), to analyse the underlying bone. However, these are not without limitations. DEXA is an *in vivo* imaging technique using two low-dose X-ray projections to compute the bone mineral content and BMD (bone mineral content/area) (Cummings *et al.*, 2002). DEXA is low in spatial resolution (0.80 mm x 0.80 mm) (Wilson *et al.*, 2012), cannot be used to differentiate between the subchondral bone plate and trabecular bone and is limited to 2D analyses. HR-pQCT allows for *in vivo* CT imaging with a spatial resolution as high as a 60.7 µm isotropic voxel size (Kroker *et al.*, 2017). However, as discussed in Section 2.4.2, these scans are limited to patient cohorts that are physically able to fit one knee into the scanning gantry (140 mm diameter) (van den Bergh *et al.*, 2021). Moreover, being a multimodal imaging approach, the combination of MRI and HR-pQCT requires additional image processing to register the datasets (Figure 2.13).

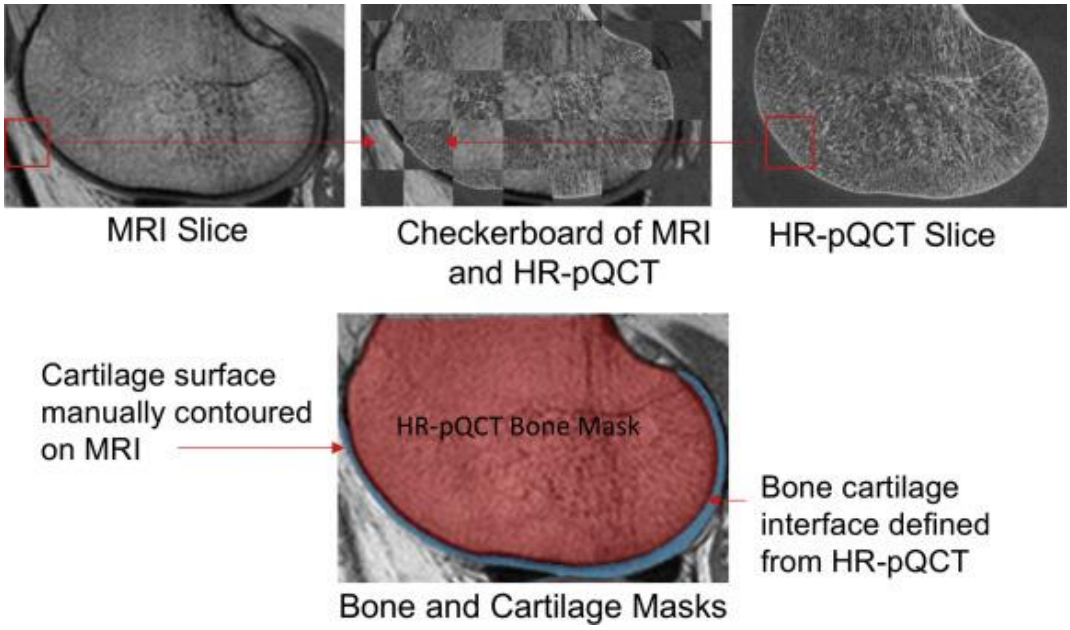

Figure 2.13: Registration of MRI and HR-pQCT datasets of the same distal femur, using a checkerboard approach (top middle) to assess if the registration was successful. This figure has been reprinted from Osteoarthritis and Cartilage with permission from Elsevier (Bhatla *et al.*, 2018).

2.4.2 High Resolution peripheral Quantitative Computed Tomography (HR-pQCT)

HR-pQCT is an *in vivo* CT imaging modality which currently has the highest achievable spatial resolution clinically (an isotropic voxel size of up to 60.7 µm) (Kroker *et al.*, 2017). This resolution is sufficient to characterise bone microarchitecture, with strong linear relationships in histomorphometric parameters with micro-CT ($R^2 > 0.89$) (Keen *et al.*, 2021) and is typically used for the *in vivo* analysis of the distal radius or distal tibia (Nishiyama *et al.*, 2013, Manske *et al.*, 2015, Mancuso *et al.*, 2020). An *ex vivo* study has demonstrated the feasibility of using contrast agents for the concurrent imaging of cartilage and bone (Michalak *et al.*, 2019). HR-pQCT has been used to scan human knees *in vivo*, but so far this has been limited to subjects with smaller knees (less than 42cm circumference) to fit into a 140 mm diameter gantry (Kroker *et al.*, 2017, van den Bergh *et al.*, 2021). HR-pQCT studies of the knee joint so far involved subjects with BMIs in the range of approximately 23.5-28 kg/m^2 (Kroker *et al.*, 2017, Bhatla *et al.*, 2018, Shiraishi *et al.*, 2020). This may not be applicable for knees of subjects with OA, where the BMI can be 32.9±4.4 kg/m^2 (average±SD) (Roberts *et al.*, 2017a), and thus presumably have a knee circumference greater than 42 cm (Bhatla *et al.*, 2018, van den Bergh *et al.*, 2021). Moreover, the HR-pQCT can only fit one leg in the gantry at a time, which requires the

person to position their other leg outside the machine for the duration of the scan; a position that might not be comfortable or physically possible for people with knee OA (Figure 2.14) (Kroker *et al.*, 2017). Although HR-pQCT is not readily available in many countries (less than 100 devices worldwide), its popularity is increasing, particularly thanks to its spatial resolution *in vivo* (van den Bergh *et al.*, 2021).

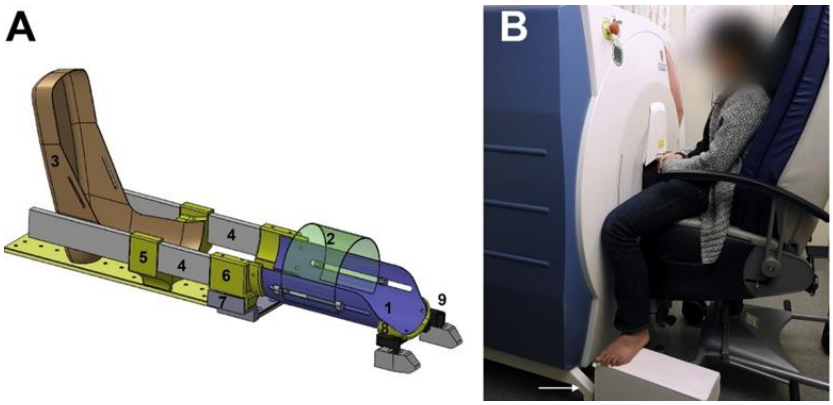

Figure 2.14: A) a custom carbon fiber rig to stabilise the subject's knee within the HR-pQCT gantry. B) the positioning of the patient during the HR-pQCT scan. This figure has been reprinted from Bone with permission from Elsevier (Kroker *et al.*, 2017).

2.4.3 Histology

Histology is the current gold-standard for *ex vivo* cartilage imaging, allowing for high resolution imaging (pixel size less than 5 µm in-plane) the quantification and analysis of the cellular content and the collagen organisation within cartilage (An *et al.*, 2003, Pritzker *et al.*, 2006, Schmitz *et al.*, 2010). It has historical use in the characterisation of OA, particularly through semi-quantitative assessment methods, such as the Osteoarthritis Research Society International (OARSI) cartilage OA histopathology grading system and Mankin system (Mankin, 1971). Using the OARSI system, OA severity is assessed based on cartilage surface and matrix integrity, cell characterisation and the presence of osteophytes. This grading system, however, only recognises subchondral bone changes in the later stages of OA, with the Mankin system not considering alterations of the subchondral bone in OA at all, which is now widely recognised to play an important role in the disease (Radin *et al.*, 1991, Loeser *et al.*, 2012).

Histology is an *ex vivo* technique and destructive, requiring physical sectioning into 3-5 µm thick slices, thereby limited to a 2D analysis. It cannot be used for longitudinal studies on the same individual (unless excised biopsies are taken at various time points) or subsequent experiments on the same specimen (e.g., mechanical testing) and is a labour intensive process, as it includes fixation, staining, sectioning and subsequent analysis at

the microscope (Ross *et al.*, 2006). The preparation and processing may also cause artefacts (e.g., affecting resultant cartilage thickness measurements) (Taqi *et al.*, 2018).

2.4.4 Micro-CT Imaging

Micro-CT has historically been used in characterising bone microarchitecture at high resolutions (Feldkamp *et al.*, 1989), initially of biopsies (max dimensions: 8 mm cubic side length) at 50 μm isotropic pixel size (Feldkamp *et al.*, 1989, Kuhn *et al.*, 1990) to more recently, entire organs (e.g. human vertebrae and tibial plateaus) at resolutions as high as 17 μm isotropic pixel size (Figure 2.15) (Perilli *et al.*, 2012, Roberts *et al.,* 2017a, Chen *et. al.,* 2018). In comparison to histology, micro-CT is non-destructive and a fast process (Müller *et al.*, 1998). It also allows for 3D analysis in comparison to 2D histomorphometry. Comparison studies between histology and micro-CT in bone biopsies from the transiliac crest and femoral head revealed high correlations (R^2= 0.71-0.96) and accuracy (mean percentage difference: 1.0 - 6.1%) (Müller *et al.*, 1998, Perilli *et al.*, 2007).

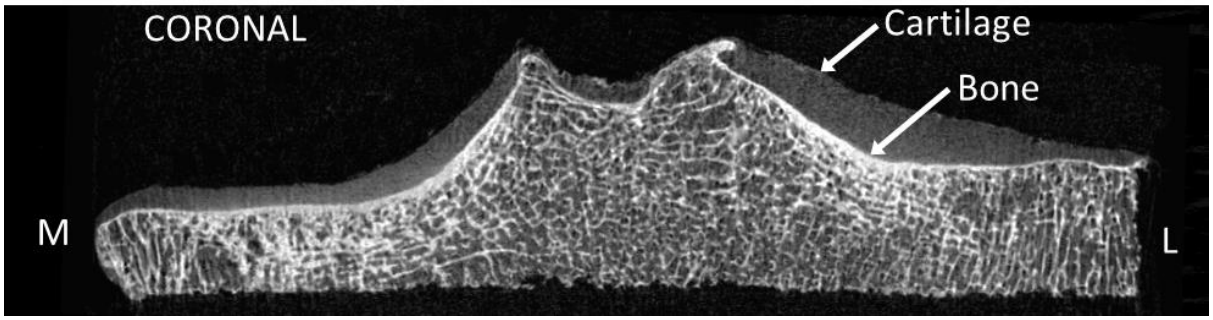

Figure 2.15: a) Micro-CT cross-section images of an entire excised right tibial plateau, at 17.4 μm isotropic voxel size (bone in bright gray colour, cartilage/marrow in dark gray).

Recently micro-CT has also been used to visualise cartilage in *ex vivo* studies (Thambyah *et al.*, 2008, Nieminen *et al.*, 2015, Delecourt *et al.*, 2016, van Tiel *et al.*, 2016, Nieminen *et al.*, 2017, Rieppo *et al.*, 2017, Touraine *et al.*, 2017, Chen *et al.*, 2018). Initially these studies used contrast agents, such as the negatively charged ioxaglate meglumine (Hexabrix™). This can be used to derive cartilage glycoaminoglycan density, as ioxaglate ions are repelled from the negatively charged glycoaminoglyans, altering the X-ray attenuation and consequent gray-level in the reconstructed scans (Palmer *et al.*, 2006). The use of contrast agents, however, can be financially expensive and take substantial amounts of time, to firstly determine the optimal contrast agent parameters (concentration and immersion time) to provide a clear delineation of articular cartilage from bone, while also having the highest sensitivity of sGAG content (Xie *et al.*, 2009).

Secondly, for large specimens (such as entire tibial plateaus), the time to stain the cartilage can be between 24 and 48h (Nieminen *et al.*, 2015, van Tiel *et al.*, 2016, Nieminen *et al.*, 2017, Gatenholm *et al.*, 2019).

Recent studies have explored alternative and quicker ways to scan cartilage with micro-CT. Mirahmadi *et al.* (2017), prior to scanning the specimen with micro-CT, coated the specimens (sections of porcine temporomandibular joint condyles) in barium sulfate, which has a high X-ray attenuation (Leng *et al.*, 2008, Landrigan *et al.*, 2011), helping to delineate the superior cartilage surface. This method was validated against subsequent histology on the same specimens.

In the images part of a previous study within our research group, aimed at characterising tibial subchondral bone (Roberts *et al.*, 2017a, Roberts *et al.*, 2017b, Roberts *et al.*, 2018), it was noted that cartilage was visible in micro-CT scans, by increasing the signal-to-noise ratio, without the use contrast agents. This suggested that gross cartilage morphology could be examined and quantified, warranting further investigation. A recent study was able to quantify cartilage thickness using similar methods (Chen *et al.*, 2018). By using these approaches, micro-CT would enable the non-destructive 3D assessment of entire excised human tibial plateaus at high spatial resolutions, for the concurrent assessment of articular cartilage and bone, without the need for coring or staining the specimen.

2.5 Challenges

The osteochondral unit plays a vital role in the maintenance of knee joint health, contributing to the distribution and transfer of loads during weight bearing and joint movements (Findlay *et al.*, 2016, Goldring *et al.*, 2016, Oláh *et al.*, 2018). In OA, the entire osteochondral unit is compromised, leading to pain and a loss of joint functionality (Hunter *et al.*, 2008). **However, while there are interactions between the cartilage and underlying bone in OA, it is not well understood what the relationships between these tissues are and if these differ 1) based on the severity of the disease, and 2) from those in healthy joints**. Additionally, it is unclear whether these relationships are location-specific or present in the entire condyles of the tibial plateau. Studies which have investigated relationships between tibial cartilage thickness and bone microarchitecture in OA are conflicting. In mild-OA, Cao et al. (2014) found no relationships between cartilage thickness (assessed via MRI) and subchondral BMD (assessed via DEXA), whereas Bolbos et. al (2018) found positive relationships using MRI. These discrepancies might be due to the imaging modalities used, which are limited in resolution, and in regard to DEXA, restricted to 2D. Liu et al. (2018) also found positive relationships between cartilage thickness and apparent BV/TV using MRI, but combined controls, mild-OA and severe-OA groups together, whereas Lindsey *et al.* (2004) found a weak negative correlation within the medial condyle in a dataset containing different severities of OA. However, a histology study, which also pooled together control and OA datasets, found the opposite (Bobinac *et al.*, 2003). Apart from spatial resolution, inconsistencies in the above findings could also be attributed to region selection and pooling together different OA severities and non-OA cohorts. The above studies were also either limited to one region of interest per condyle (Bolbos *et al.*, 2008, Cao *et al.*, 2014) or multiple regions of interest (medial and lateral) pooled together (Matsui *et al.*, 1997, Bobinac *et al.*, 2003), which might mask some relationships.

Moreover, **none of these studies have considered the effect of habitual joint loading** which also plays a substantial role in the onset and progression of OA (Miyazaki *et al.*, 2002, Griffin *et al.*, 2005, Brouwer *et al.*, 2007, Astephen *et al.*, 2008, Guilak, 2011, Johnson *et al.*, 2014). Abnormal joint loading and malalignment during habitual loading (e.g., standing and walking) can affect the medial-to-lateral distribution of loads upon the tibial plateau (Wada *et al.*, 2001, Thorp *et al.*, 2006, Adouni *et al.*, 2014b). This can then affect the articular cartilage morphology and distribution (Andriacchi *et al.*, 2006, Eckstein *et*

al., 2008, Andriacchi *et al.*, 2009, Nakagawa *et al.*, 2015) and also the underlying subchondral bone (Wada *et al.*, 2001, Thorp *et al.*, 2006, Roberts *et al.*, 2017a, Roberts *et al.*, 2017b, Renault *et al.*, 2020, Shiraishi *et al.*, 2020), which may contribute to knee OA. However, in OA, relationships between cartilage thickness and external knee moments are conflicting (Vanwanseele *et al.*, 2010, Chang *et al.*, 2015, Erhart-Hledik *et al.*, 2015, Maly *et al.*, 2015); moreover, these do not consider the external rotation moment, which has been found to significantly correlate with tibial subchondral BV/TV in OA (Roberts *et al.*, 2018) and can hence be expected to correlate with the articular cartilage.

Furthermore, while studies have separately examined tibial cartilage thickness, bone microarchitecture or joint loading indices in human subjects, to the best of the author's knowledge, **these examinations have not been performed altogether in the same cohort**, possibly as a result of limitations in imaging modalities. MRI can be used to visualise articular cartilage *in vivo,* but has a relatively low spatial resolution. This can cause cartilage thickness to be overestimated, particularly in OA where there are regions of thinner, denuded cartilage (Koo *et al.*, 2005, Koo *et al.*, 2009), and is unsuitable for resolving thin trabecular structures. Histology, while able to investigate cartilage and bone at high resolutions (<5 μm pixel size, in-plane) is destructive, limited to 2D analyses and requires extensive preparation (Pritzker *et al.*, 2006, Schmitz *et al.*, 2010). Micro-CT offers the potential for a non-destructive 3D characterisation of both cartilage and bone in entire excised human tibial plateaus at high spatial resolutions. While micro-CT imaging of cartilage typically involves the use of contrast agents, recent studies have visualised cartilage without contrast agents, though these protocols need to be validated against histology.

Taken together, there is limited understanding of the influence of joint alignment and *in vivo* loading in OA on tibial articular cartilage and bone microarchitecture within the same individuals, and how these tissues differ from non-pathological joints. Micro-CT has the potential to be used to quantify cartilage thickness and subchondral bone histomorphometry for the entire human tibial plateau, which could be combined with investigations of pre-operative gait analysis and knee alignment on the same subjects.

In this thesis, these challenges will be addressed. **Chapter 3 (Study 1)** quantifies tibia cartilage thickness, subchondral bone plate thickness and subchondral trabecular bone

volume fraction in subjects with varus- or valgus-malaligned knees diagnosed with end-stage knee OA, and compares them to controls (knees without OA). Moreover, a validation of cartilage thickness using a non-contrast agent micro-CT scanning protocol against thickness measurements from histological slides is conducted. **Chapter 4 (Study 2)** investigates relationships between pre-operative *in vivo* external knee joint moments, joint alignment and regional tibial cartilage thickness using micro-CT in subjects with end-stage knee OA. Finally, **Chapter 5 (Study 3)** describes a systematic mapping of the cartilage and subchondral bone of the tibial plateau (22 sub-regions) in healthy and OA knees, where, for each tissue, within-condyle and between-condyle (medial-to-lateral) regional differences are evaluated, alongside region-specific relationships among cartilage thickness and subchondral bone parameters.

Chapter 3
Study 1: Tibial cartilage, subchondral bone plate and trabecular bone microarchitecture in varus- and valgus-osteoarthritis versus controls

The study presented in this chapter is the subject of the following paper:

Rapagna S, Roberts BC, Solomon LB, Reynolds KJ, Thewlis D, Perilli E. Tibial cartilage, subchondral bone plate and trabecular bone microarchitecture in varus- and valgus-osteoarthritis versus controls. *Journal of Orthopaedic Research*. 2021; 39(9):1988-99 doi 10.1002/jor.24914.

Please refer to the Appendix at the end of this thesis for a detailed outline of the author's contribution to this study.

Abstract

The aim of this study was to 1) quantify tibia cartilage thickness (Cart.Th), subchondral bone plate thickness (SBPl.Th) and subchondral trabecular bone (STB) microarchitecture in subjects with varus- or valgus- malaligned knees diagnosed with end-stage knee OA and compared them to controls (non-OA); and 2) validate cartilage thickness measured from micro-CT cross-sections against histology. Tibial plateaus from 25 subjects with knee-OA (undergoing knee arthroplasty) and 15 cadavers (controls) were micro-CT scanned (17 μm/voxel). Joint alignment was classified radiographically for OA subjects (varus-aligned n = 18, valgus-aligned n = 7). Cart.Th, SBPl.Th, STB bone volume fraction (BV/TV) and their medial-to-lateral ratios were analyzed in anteromedial, anterolateral, posteromedial and posterolateral subregions. Varus-OA and valgus-OA were compared to controls.

Compared to controls (1.19–1.54 mm), Cart.Th in varus-OA was significantly lower anteromedially (0.58 mm, −59%) and higher laterally (2.19–2.47 mm, +60–63%); in valgus-OA, Cart.Th was significantly higher posteromedially (1.86 mm, +56%). Control medial-to-lateral Cart.Th ratios were around unity (0.8–1.1), in varus-OA significantly below (0.2–0.6) and in valgus-OA slightly above (1.0–1.3) controls. SBPl.Th and BV/TV were significantly higher medially in varus-OA (0.58-0.72 mm and 37–44%, respectively) and laterally in valgus-OA (0.60–0.61 mm and 32–37%), compared to controls (0.26–0.47 mm and 18–37%). In varus-OA, the medial-to-lateral SBPl.Th and BV/TV ratios were above unity (1.4–2.4) and controls (0.8–2.1); in valgus-OA they were closer to unity (0.8-1.1) and below controls. Cartilage thickness measured from micro-CT cross-section images had a strong linear relationship with the cartilage thickness measured from histology slides (R^2= 0.93), indicating that using the protocol here described is suitable for quantifying gross cartilage thickness.

Micro-CT enables the non-destructive imaging of cartilage and subchondral bone of the entire tibial plateau, without the need for contrast agents or coring. Varus- and valgus-OA tibia differ significantly from controls in Cart.Th, SBPl.Th and STB microarchitecture depending on joint alignment, suggesting structural changes in OA may reflect differences in medial-to-lateral load distribution upon the tibial plateau. Here we identified an inverse relationship between cartilage thickness and underlying subchondral bone, suggesting a whole-joint response in OA to daily stimuli.

3.1 Introduction

OA is a debilitating joint disease that can affect all articular structures, but is most characteristically defined by the degradation of cartilage and alteration of subchondral bone (Goldring *et al.*, 2010, Loeser *et al.*, 2012). The knee is the most commonly affected joint (Cross *et al.*, 2014) and, according to national joint replacement registries, is the most common joint to undergo replacement (American Joint Replacement Registry (AJRR), 2019, National Joint Registry, 2019) with a reported 38% increase in total knee arthroplasty (TKA) due to knee OA from 2006 to 2016 in Australia (Australian Institute of Health and Wealfare (AIHW), 2017). However, with TKA being the final treatment option for OA, there is a need for development of effective treatment strategies to delay and ideally prevent the progression of the disease. This may be achieved by firstly improving our understanding of relationships between independent risk factors associated with OA, such as joint mechanics and alignment (Sharma *et al.*, 2001, Miyazaki *et al.*, 2002, Brouwer *et al.*, 2007), and the joint tissues.

Knee joint malalignment has previously been linked to altered medial-to-lateral distribution of loads upon the joint (Adouni *et al.*, 2014b, Roberts *et al.*, 2017b) and has been associated with regional changes in either subchondral bone (Wada *et al.*, 2001, Thorp *et al.*, 2006, Roberts *et al.*, 2017b, Roberts *et al.*, 2018, Renault *et al.*, 2020, Shiraishi *et al.*, 2020) or cartilage (Eckstein *et al.*, 2008, Nakagawa *et al.*, 2015) in OA. In our previous study, mapping of the 3D bone microarchitecture of end-stage knee OA tibial plateaus (Roberts *et al.*, 2017b), joint alignment was suggested to be related to medial-to-lateral and within-condylar bone microarchitecture differences in OA groups. However, it is unknown whether similar variations also exist in non-pathological joints. Furthermore, those studies on bone did not consider cartilage thickness, which has also been shown to vary with joint alignment in a magnetic resonance imaging (MRI) study (Eckstein *et al.*, 2008).

Micro-CT enables the non-destructive 3D assessment of entire excised human tibial plateaus at high resolutions (Roberts *et al.*, 2017b, Chen *et al.*, 2018, Nickmanesh *et al.*, 2018, Michalak *et al.*, 2019). While historically used for the characterization of bone microarchitecture (Rüegsegger *et al.*, 1996, Hildebrand *et al.*, 1997b, Müller *et al.*, 1998, Perilli *et al.*, 2012), there is growing interest in using micro-CT for the examination of human tibial articular cartilage with contrast agents (van Tiel *et al.*, 2016, Nickmanesh *et*

al., 2018, Gatenholm *et al.*, 2019, Michalak *et al.*, 2019, Ylitalo *et al.*, 2019) and without (Delecourt *et al.*, 2016, Touraine *et al.*, 2017, Chen *et al.*, 2018). While studies have separately examined cartilage thickness, bone microarchitecture or joint alignment, to the best of the author's knowledge, these examinations have never been performed altogether in the same cohort. Moreover, comparisons with control subjects in the STB microarchitecture are conflicting and did not consider the influence of joint alignment (Ding *et al.*, 2003, Patel *et al.*, 2003). As cartilage and bone respond to every day mechanical loading as a single mechanical unit, they should be investigated concurrently (Ding *et al.*, 1998, Burr *et al.*, 2012).

Finally, as such a cartilage thickness mapping using micro-CT involves quantifying the cartilage thickness across the entire tibial plateau, including regions of thin cartilage (below 1 mm) and thick (up to 3 mm) (Shepherd *et al.*, 1999, Favre *et al.*, 2017), a validation with histology of these measurements is also required.

The aim of this preliminary study was to (1) quantify tibia cartilage thickness, cortical SBP thickness and STB bone volume fraction in subjects diagnosed with end-stage knee OA with varus- or valgus-aligned joints and compare them to control (non-OA) knees and; (2) to validate the human tibial cartilage thickness measured from micro-CT cross-sections against histology (gold standard).

3.2 Methods

3.2.1 Bone Specimens

OA group: Micro-CT scans of the human tibial plateaus generated in the previous study (Roberts *et al.*, 2017b) were used in this study. Briefly, twenty-five tibial plateaus were retrieved from end-stage knee-OA patients who underwent total knee arthroplasty surgery (Table 3.1). Approval to use these specimens for research purposes was granted by Southern Adelaide Clinical and Royal Adelaide Hospital Human Research Ethics Committees. All patients gave written informed consent.

Control group: Fifteen fresh-frozen, cadaveric tibial plateaus with no knee pathology were sourced for this purpose (Science Care, Inc. Phoenix, AZ). Approval to use these specimens was granted by the Southern Adelaide Clinical Human Research Ethics Committee.

All tibial plateaus were stored immersed (fixed) in 70% ethanol solution after retrieval.

Table 3.1: Summary of patient characteristics

Parameters	End stage knee OA subgroups		Controls	*p* value
	Varus-OA (n = 18)	Valgus-OA (n = 7)	Non-OA (n = 15)	
Age (years)	66.9 ± 7.8	70.4 ± 6.0	61.6 ± 12.9	0.295
Mass (kg)	92.5 ± 17.7	84.1 ± 16.9	83.0 ± 15.6	0.234
BMI (kg/m^2)	32.5 ± 4.8	31.5 ± 4.7		0.657
Mechanical Axis Deviation* (mm)	29.4 ± 18.7	-34.4 ± 15.6		<0.001
Mechanical Axis** (°)	173.4 ± 4.2	188.2 ± 1.7		<0.001

Values reported as average ± standard deviation; A Kruskal-Wallis test was performed to compare between the varus-OA, valgus-OA and non-OA groups for age and body mass. A Mann-Whitney U-test was used to compare between the varus-OA and valgus-OA groups for BMI, Mechanical Axis Deviation and Mechanical Axis, significance denoted by $p<0.05$. *Knee alignment determined from mechanical axis deviation (MAD), where positive deviations are indicative of a medial deviation and negative values indicate a lateral deviation (Roberts *et al.*, 2017b). **Mechanical axis (MA), defined as the medial hip-knee-ankle angle where an angle <178° was considered a varus alignment and an angle >182° was considered a valgus alignment (Sharma *et al.*, 2013).

3.2.2 Mechanical Joint Alignment from Radiographic Data

Prior to surgery, the degree of varus–valgus mechanical alignment was assessed in all patients by measure of the mechanical axis deviation (MAD), obtained on long leg weight-bearing radiographs by an experienced examiner (LBS). In the frontal plane, the mechanical axis of the lower limb is the line connecting the centre of the femoral head to the centre of the ankle plafond (Paley, 2002). The MAD was defined as the perpendicular distance from the mechanical axis to the centre of the knee joint (Paley, 2002). A varus alignment was defined as a medial deviation greater than 15 mm and a valgus alignment was defined as a lateral deviation greater than 0 mm (Paley, 2002, Roberts *et al.*, 2017b), though for operational purposes, any medial deviation (0-15 mm deviation; i.e. neutral joints, n=3) was considered varus in this study.

Micro-CT imaging

Micro-CT examination of the tibial plateaus were performed using a desktop micro-CT scanner (Skyscan 1076, Skyscan-Bruker, Belgium). Prior to scanning, the specimens were removed from the ethanol solution and individually wrapped in cling-film. Specimens were scanned in pairs, separated by a layer of polystyrene (along the resected surface) and secured in place with elastic bands, with the medial-lateral axis of each specimen

aligned with the system's rotation axis (Figure 3.1) (Roberts *et al.*, 2017b). Specimens were scanned at 17.4 μm isotropic voxel size, peak voltage 100 kVp, current 90 μA, rotation step 0.4° over 180° rotation, 590 ms exposure time and four frames averaging (Roberts *et al.*, 2017b). After scanning, the specimens were stored immersed in ethanol solution until histological processing (Section 3.2.6).

The cross-section images were then reconstructed using a filtered back-projection algorithm (NRecon software, v1.6.9.8, Skyscan-Bruker) and saved as 8-bit bitmap format images (256 gray-levels, bmp value of 0 = air, 255 = mineralized tissue). For each specimen pair, a stack of up to 4,997 consecutive cross-sections was reconstructed (corresponding to 86.9 mm length), slice thickness of one pixel (17.4 μm) producing a dataset of 70 GB (Roberts *et al.*, 2017b). The reconstructed cross-section images were then rotated in 3D such that the anatomical superior-inferior axis of each plateau was aligned with the z-axis of the image stack (Figure 3.2).

Figure 3.1: A photograph of two excised tibial plateaus, wrapped in plastic film and fixed on the carbon scanning bed of the micro-CT.

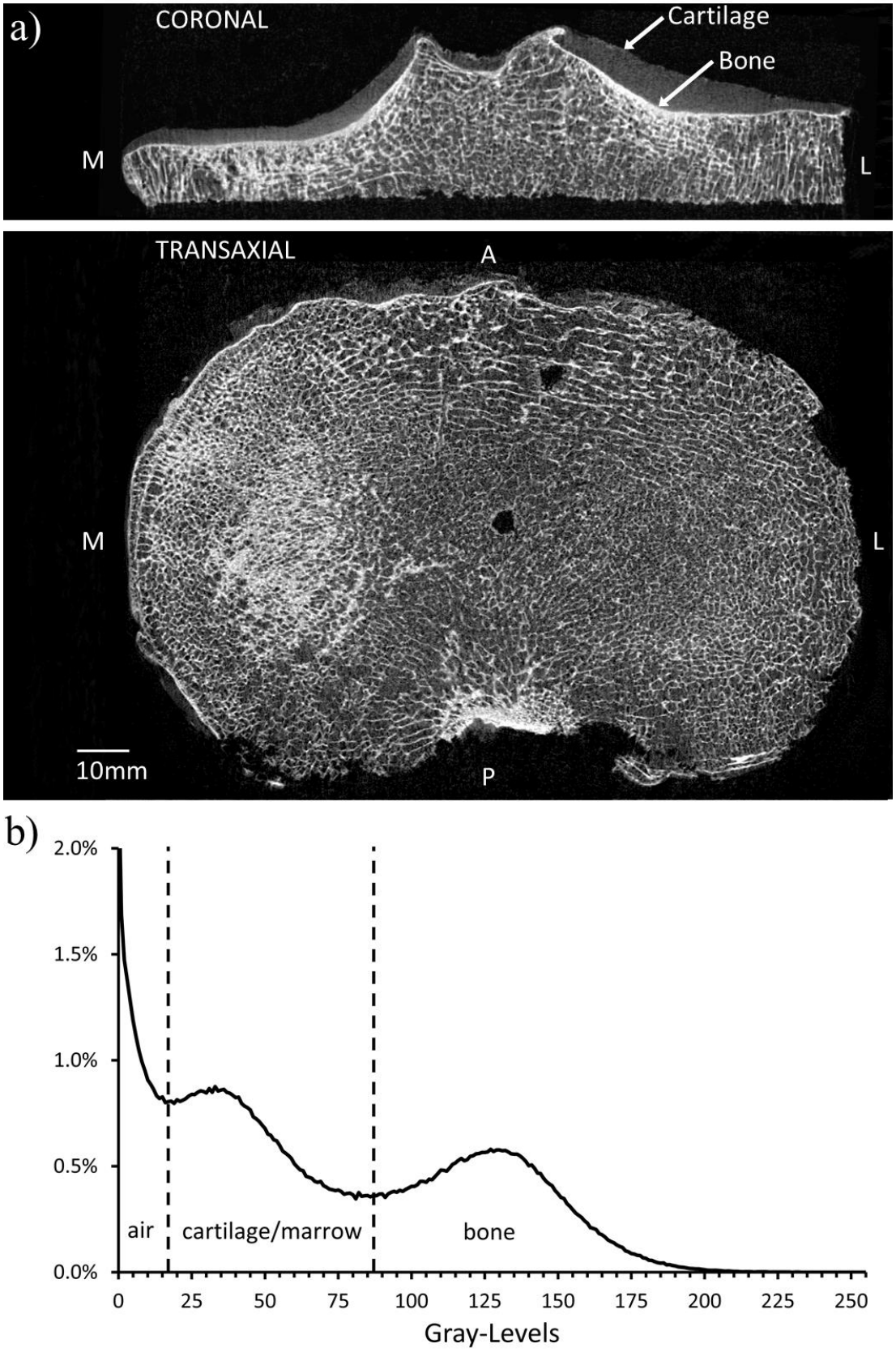

Figure 3.2: a) Micro-CT cross-section images of an entire excised right tibial plateau, at 17.4 μm isotropic voxel size (bone in bright gray colour, cartilage/marrow in dark gray). b) Example of a gray-level histogram (256 gray-levels) of a transaxial cross-section image. The threshold levels used to segment air, cartilage/marrow and bone are indicated by the dashed lines (values = 18 and 87). A: anterior, P: posterior, M: medial, L: lateral anatomical location.

3.2.3 Image segmentation: Separation of Cartilage, Subchondral Bone Plate and Subchondral Trabecular Bone

3.2.3.1 Cartilage (Cart)

A semi-automatic segmentation process was developed based on methods published in the literature (Buie *et al.*, 2007, Xie *et al.*, 2009, Gatenholm *et al.*, 2019, Ylitalo *et al.*, 2019). Firstly, on the coronal image stack of the specimen, a 3D median filter ($\sigma = 3$) was applied to minimize noise (Figure 3.3b). A "bone and marrow" mask was then created using a custom MATLAB script (2017b, The MathWorks, Inc., Massachusetts, USA) on the segmented subchondral bone plate coronal dataset (Figure 3.3d; Section 3.2.3.2). This mask extended from the superior surface of the subchondral bone plate to the resected surface of the tibial plateau, encompassing the subchondral bone and marrow. The inverse mask, containing only cartilage and air (= the image minus the "bone and marrow" mask) was then applied to the same coronal image stack (Figure 3.3f) (software CTAnalyser, Skyscan Bruker, Kontich, Belgium). Then, cartilage was segmented using a lower threshold of 18 and a higher threshold of 86 ("threshold window", excluding air and potential bone debris, respectively), as defined from the gray-level histograms over 5 representative specimens and applied consistently over all specimens (Figure 3.2; Figure 3.3g). The cartilage segmentation was verified manually every 15 slices (0.261 mm; Figure 3.3h). Then, the "shrink-wrap" plug-in of CTAnalyser was applied, to conform the boundaries of the regions of interest (ROI) to the cartilage (Figure 3.3i).

3.2.3.2 Subchondral bone plate (SBP)

The subchondral bone plate was segmented according to our previous protocol (Roberts *et al.*, 2017b). Briefly, a uniform threshold was applied to the coronal image stacks to segment the bone tissue from the background (air, marrow and cartilage). A lower threshold level (87) was defined from the gray-level histograms (256 gray-levels) over 5 representative specimens (Figure 3.1). Pixels representing bone tissue (gray-level values between 87 and 255) were segmented as solid and those representing non-bone tissue (gray-level values from 0 to 86) as background. From the coronal binarized image stacks, the SBP was then manually contoured every 15 images (0.261 mm) removing trabecular

struts adjoining the lower end of the SBP (Roberts *et al.*, 2017b). Then the "ROI shrink-wrap" plug-in was applied, to conform the ROI boundaries to the plate border.

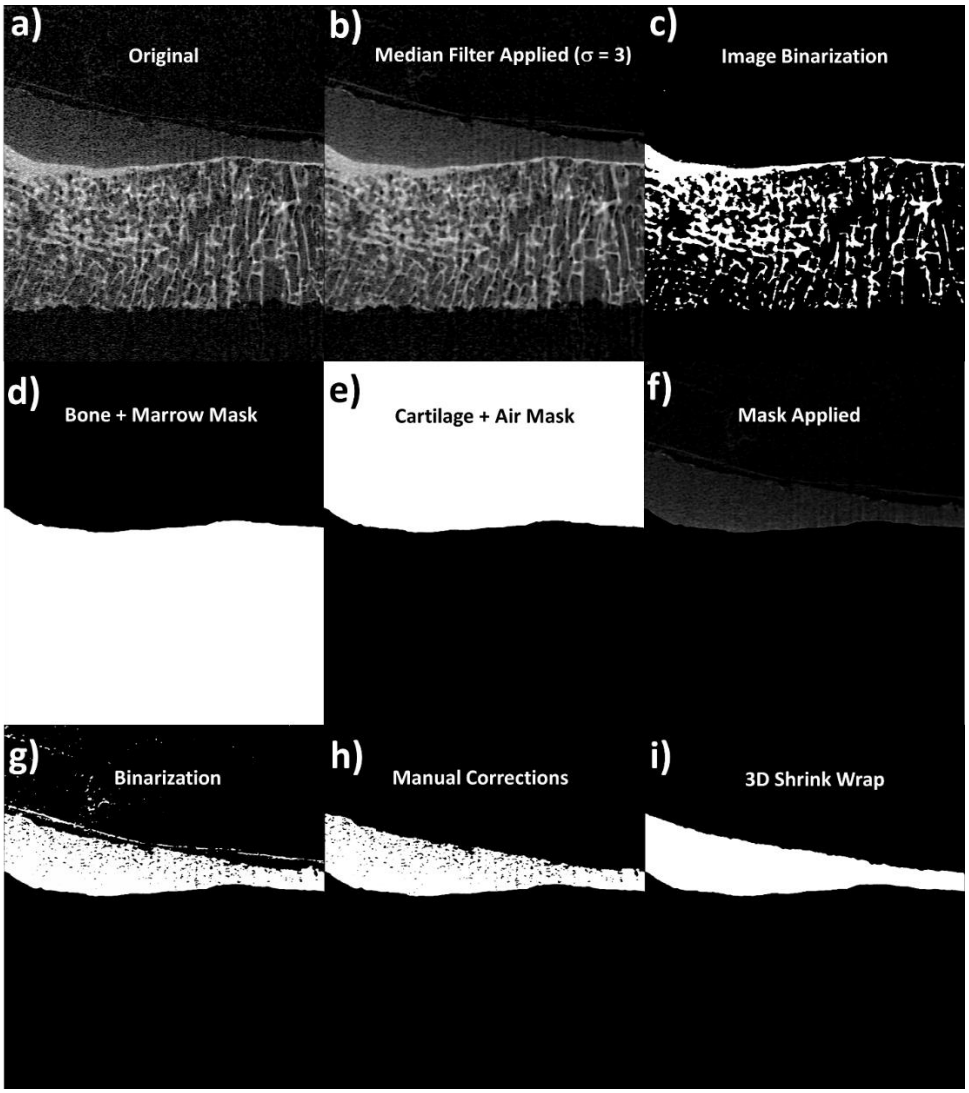

Figure 3.3: Articular cartilage segmentation from Micro-CT cross-sectional images of an excised tibial plateau, at 17.4 μm isotropic voxel size a) original micro-CT coronal cross-section image (bone in bright gray colour, cartilage/marrow in dark gray), b) coronal cross-section image with a median filter applied (σ = 3), c) coronal cross-section image binarized to segment bone (white pixels) and d) a "bone and marrow mask" encompassing all segmented bone, marrow and below, e) a "cartilage and air" mask, f) the resultant of applying the "cartilage and air" mask to the filtered cross-sectional image in b), g) image binarized to segment cartilage (white pixels), h) binarized image manually corrected to remove artefacts and i) a 3D shrink wrap was applied to conform to the edges of the cartilage surface.

3.2.3.3 Subchondral trabecular bone (STB)

The STB had its superior boundary in common with the inferior boundary of the previously saved SBP ROI, extending distally towards the growth plate. Only STB within the first 5 mm below the inferior subchondral bone plate was considered, as microarchitectural and bone mineral density differences in tibial condyles are most

prominent within this distance (Patel *et al.*, 2003, Johnston *et al.*, 2010, Roberts *et al.*, 2017a).

From the saved cartilage, SBP and STB datasets, subvolumes of interest (VOI) for morphometric analysis were then selected, as follows.

3.2.4 Volumes of interest (VOIs)

For each tibial plateau, four cylindrical VOIs (10 mm in diameter, total height of approximately 7-8 mm, depending on the specimen) were selected within regions of the tibial condyles indicated as high and low-load bearing in the literature (Adouni *et al.*, 2014b, Roberts *et al.*, 2017b), using CTAnalyser as shown previously by our group (Roberts *et al.*, 2017b). The height of the VOI varied based on the specimen, with each VOI containing the cartilage (up to 2-3 mm), the adjacent cortical SBP and STB underneath (up to 1 mm and up to 5 mm, respectively, depending on the specimen) (Figure 3.4). These cylindrical VOIs were defined in a previous study by our group (Roberts *et al.*, 2017a) and were located at the centre of the anterior or posterior halves of the medial and lateral condyles, which were defined by elliptical regions: anteromedial (AM), anterolateral (AL), posteromedial (PM) and posterolateral (PL) condyles (Figure 3.4b).

3.2.5 Morphometric analysis

From the micro-CT images, cartilage thickness (Cart.Th; mm), cortical SBP thickness (SBPl.Th; mm) and the STB bone volume fraction (BV/TV; %) were analyzed in the four cylindrical VOIs. The medial (M) and lateral (L) condyle values were also computed, as the average of the anterior and posterior VOIs within the condyles.

The average cartilage thickness was calculated by dividing the volume of the voxels identified as cartilage (in mm^3) by the circular cross-section area (in mm^2) within the cylindrical VOI (Eckstein *et al.*, 2011). This method accounts also for VOIs containing partially denuded areas of cartilage, whereas plainly using a 3D sphere-fitting thickness algorithm in these areas would overestimate the thickness over the VOI. The 3D SBPl.Th was calculated using the sphere-fitting method in the corresponding SBP VOI, as done previously (Hildebrand *et al.*, 1997a, Perilli *et al.*, 2006, Roberts *et al.*, 2017b). The STB BV/TV was calculated as the percentage voxels segmented as bone divided by the voxels constituting the examined STB VOI (Perilli *et al.*, 2012, Roberts *et al.*, 2017b).

Finally, the medial-to-lateral ratios in these parameters between cylindrical subregions within each condyle (AM:AL, AM:PL, PM:AL, PM:PL, M:L) were computed. Medial-to-

lateral ratios, for example providing insight into the distribution of bone mass (SBPl.Th, STB BV/TV) between the condyles, may also provide insights into the intra-condyle distribution of loads across the tibial plateau.

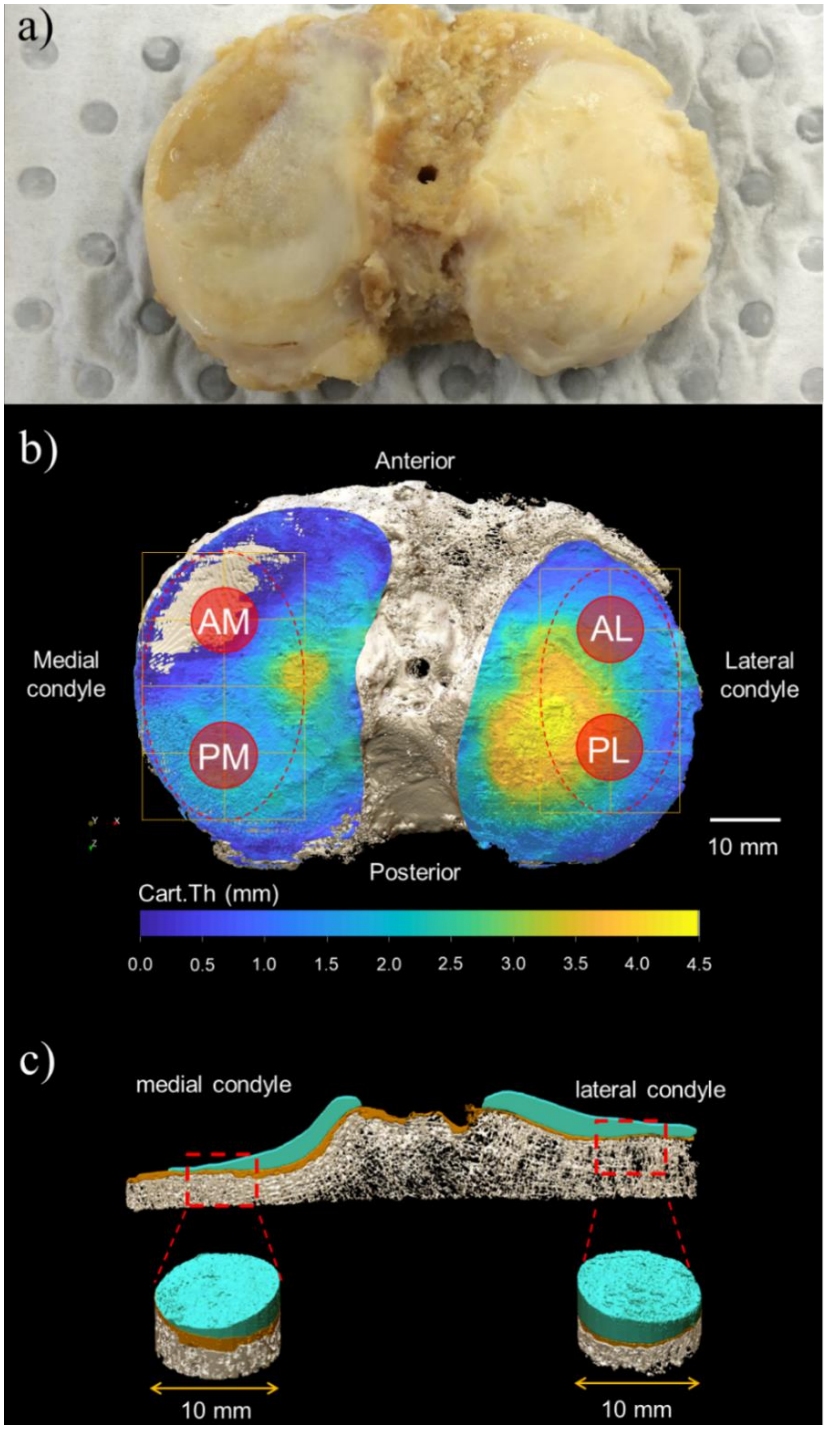

Figure 3.4: Varus-aligned OA right tibial plateau: a) Photograph. b) Micro-CT 3D rendering of the same tibial plateau (17 µm/pixel; superior view), showing cartilage thickness map and subchondral bone underneath (white colour). The red coloured circles are the 4 regions of interest investigated (10 mm diameter cylinders): antero-medial (AM), antero-lateral (AL), postero-medial (PM) and postero-lateral (PL). c) coronal view of tibial plateau, showing cartilage (blue colour), subchondral bone plate (orange colour) and subchondral trabecular bone (white colour).

3.2.6 Validation Study: Histology

After micro-CT scanning, six tibial plateaus from this study underwent histological processing to validate cartilage thickness measurements using the micro-CT scanning protocol against the gold standard (histology). This included three tibial plateaus from the OA group and three tibial plateaus from the control group.

3.2.6.1 Histology: Regions of Interest (Reference Images)

A minimum of 5 rectangles (blocks) per condyle of 15 mm x 5 mm (length x width) were defined for histological processing from superior-view photographs of each specimen (Figure 3.5). These photos were taken prior to histology and mapped to the trans-axial micro-CT cross-sections of the tibial plateau and a 3D reconstruction of the underlying bone, to assist in the systematic matching of micro-CT cross-sections with resultant histological slices (Figure 3.5). These blocks were carefully planned to include four VOIs in the AM, AL, PM, PL condyles outlined in Section 3.2.4.

3.2.6.2 Histological Processing and microscopic evaluation

After micro-CT imaging, the specimens underwent histological processing following previous protocols for Safranin-O/Fast Green staining (Schmitz *et al.*, 2010, Muratovic *et al.*, 2016, Muratovic *et al.*, 2018). The condyles of each specimen were sectioned into coronal blocks (Figure 3.5). Each block was approximately 15 x 5 x 7-10 mm (length x width x height, where height was specimen dependent). The posterolateral edge of each block was marked with India Ink to maintain block orientation during subsequent processing stages. Each block was fixed in formalin (10%), decalcified in 1% nitric acid, dehydrated in a series of ascending alcohol concentrations (75%. 85%, 90% and 100%) before being embedded in paraffin. Prior to slicing, paraffin-embedded blocks were cooled on a Tissue Tek cold plate (Tissue Tek®). Each block was then sliced coronally using a microtome (Leica RM2235, Leica Biosystems, Wetzlar, Germany) into three 4 µm thick slices spaced 100 µm apart, with the first slice starting 100 µm from the edge of the block. The slides were then stained with Safranin-O/Fast Green for clear delineation of cartilage and bone as used for the OARSI osteoarthritis cartilage histopathology assessment (Pritzker *et al.*, 2006, Schmitz *et al.*, 2010). Digital images of the entire histology slides were taken using a NanoZoomer C9600-12 scanner (Hamamatsu), with a source lens of 40x and a corresponding pixel size of 0.228 µm (Figure 3.5c).

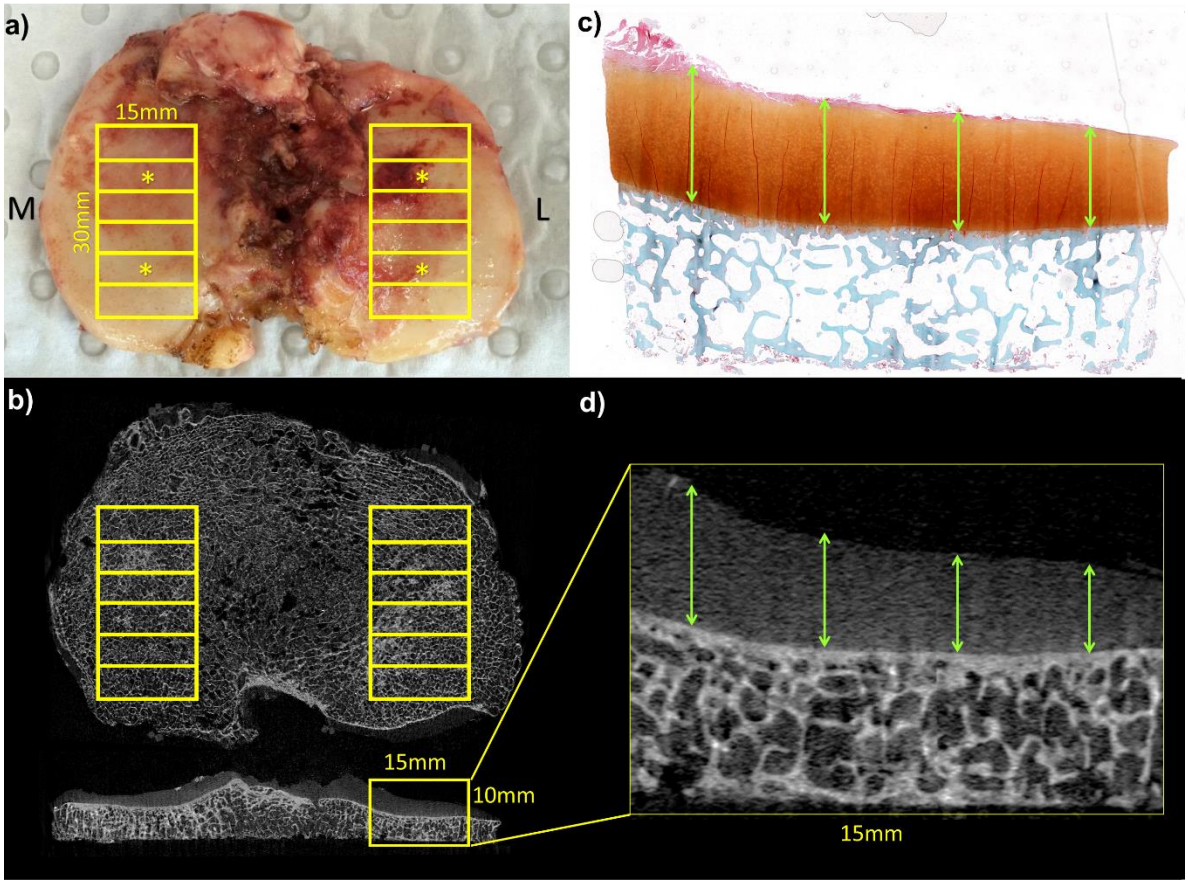

Figure 3.5: Validation study: a) A photograph of the superior view of an excised tibial plateau; b) top: transaxial and bottom: coronal view of the micro-CT cross-section image of the same tibial plateau. The asterisks indicates the blocks representative of the four regions of interest previously identified as load-bearing regions (Roberts *et al.*, 2018). The yellow rectangles indicate the blocks prepared for histological processing); c) digital image of a histology slide stained with Safranin-O/Fast Green (taken with Nanozoomer Digital Slide Scanner) with cartilage in orange colour and subchondral bone in blue colour. Original magnification 40x (0.227 µm pixel size); d) Corresponding micro-CT cross-section (17.4 µm pixel size). Green lines with arrowheads indicate where thickness measurements were taken to produce the thickness measurement.

3.2.6.3 Histology slide and Micro-CT image mapping

Coronal cross-sectional micro-CT images were mapped to the histological slides using the reference guides to find the corresponding image in the micro-CT dataset (Figure 3.5),(Perilli *et al.*, 2007). Once the first slide was matched, the next histology/micro-CT pairs were systematically found by moving to the next block (i.e. ~287 coronal micro-CT cross-sections (~5 mm). This process was repeated for all investigated regions in all specimens.

3.2.6.4 Coronal cartilage thickness measurements

The cartilage thickness for both histology and micro-CT images was assessed using the manual distance measurement tool in CT Analyzer (Perilli *et al.*, 2015) by one observer (SR). For each slide, four evenly spaced thickness measurements (from the inferior cartilage surface (cartilage/bone interface) to the superior cartilage surface (cartilage/air interface; Figure 3.5d) were taken and averaged to find the average cartilage thickness per slide.

3.2.7 Statistics

3.2.7.1 Morphometric comparisons against controls

Morphometric parameters (Cart.Th, SBPl.Th, BV/TV) in the 4 tibial regions (AM, AL, PM and PL) and their regional ratios for the varus-OA and valgus-OA group, were compared to controls using a Kruskal-Wallis test, which if significant, was followed by post-hoc Mann-Whitney U-tests. To account for multiple testing, the false discovery rate (FDR) was controlled (FDR = 0.05) using a Benjamini-Hochberg adjustment (Benjamini *et al.*, 1995). Non-parametric tests were used in this study, rather than parametric tests, due to the small sample size of the valgus-OA group (n=7) and because the assumption of homogeneity of variance (Levene's test) and assumption of normality (Shapiro-Wilk's test) were not met in some comparisons. Statistical analysis was performed using SPSS Statistics 25 (IBM Corp., Armonk, NY).

3.2.7.2 Validation of micro-CT versus histology cartilage thickness measurements

To assess the correspondence in measurements between the two techniques, a linear regression "micro-CT Cart.Th vs. histology Cart.Th" analysis was performed, using the average cartilage thickness measurements of the micro-CT coronal cross-section (Figure 3.5d) and the corresponding ones from the histology slide (Figure 3.5c). This was done for 10 slides per specimen, for the 6 specimens (60 measurements total). Comparisons between cartilage thickness measured from micro-CT and histology were then performed, for the slides corresponding to the anteromedial, anterolateral, posteromedial, posterolateral, medial and lateral regions (Figure 3.5a), as well as for their medial-to-lateral ratios, using a Wilcoxon signed rank test with Bonferroni adjustment

for multiple testing. Statistical significance was defined as $p<0.05$ and was performed using SPSS Statistics 25 (IBM Corp., Armonk, NY).

3.3 Results

Age and body mass were not significantly different between varus-OA, valgus-OA and controls groups. Body mass index (BMI) did not significantly differ between varus-OA and valgus-OA groups, whereas knee alignment did (Table 3.1).

Figure 3.6 displays representative tibial plateaus from each group (control, varus-OA and valgus-OA), with photograph (top) and the 3D-distribution of cartilage thickness (middle) and of subchondral trabecular bone obtained by micro-CT (bottom), whereas coronal cross-sections for appreciation of also the subchondral bone plate thickness are shown in Figure 3.7.

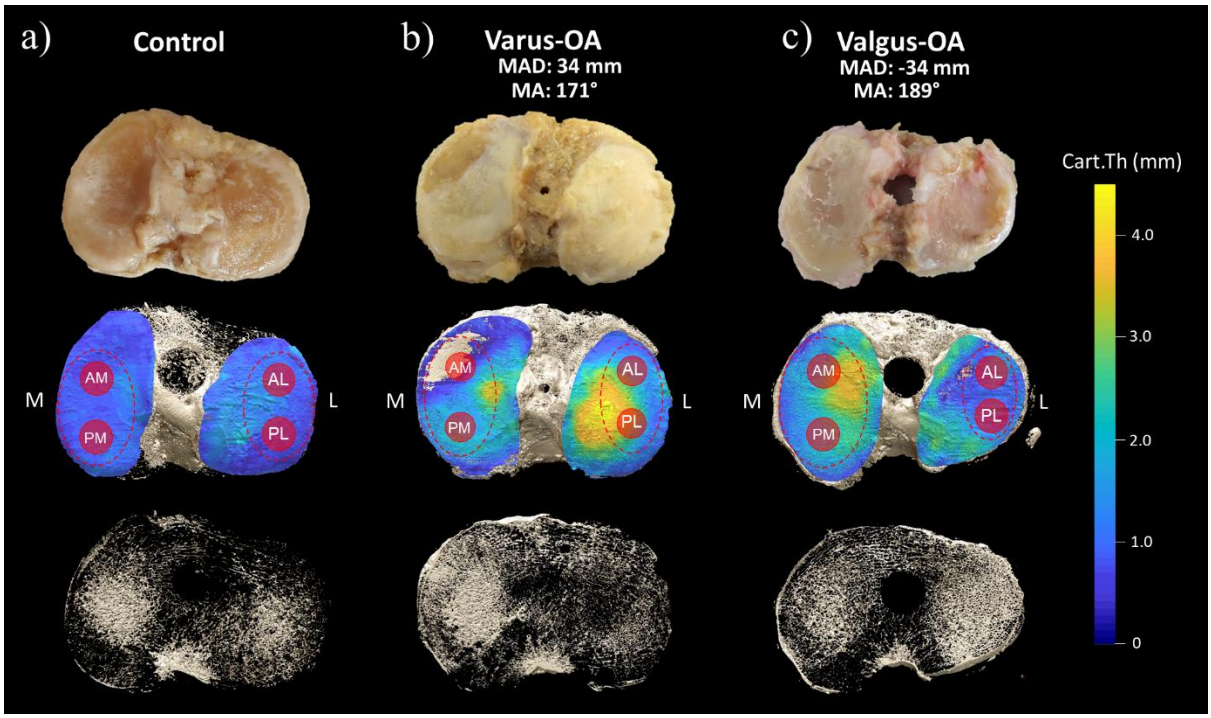

Figure 3.6: Top row: Photographs of three representative excised right tibial plateaus, belonging to the a) control, b) varus-OA and c) valgus-OA group. Middle row: Micro-CT 3D rendering of the tibial plateaus showing cartilage thickness (Cart.Th) map. Noting the rather uniform distribution of cartilage thickness in control, compared to a more heterogeneous distribution in varus-OA and valgus-OA, depending on the joint alignment. Bottom row: Micro-CT 3D rendering of a slice of underlying subchondral trabecular bone (white colour) for each specimen. MAD: mechanical axis deviation (mm), MA: mechanical axis (°).

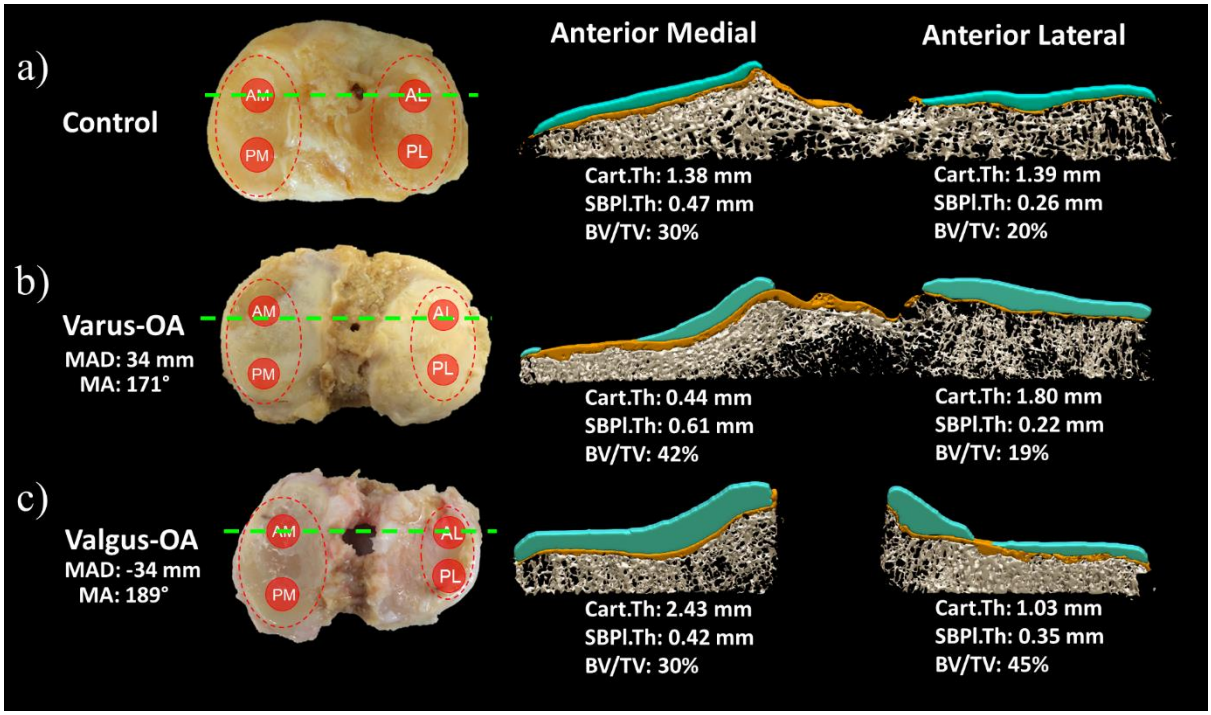

Figure 3.7: Left column: Photographs of three representative excised tibial plateaus belonging to the a) control, b) varus-OA and c) valgus-OA group. Right column: Micro-CT 3D rendering of a coronal slice (1.31 mm thick) taken from the anterior region of each tibial plateau (see dashed green line in left column), showing cartilage in blue colour, the subchondral bone plate in orange colour and subchondral trabecular bone in white colour. MAD: mechanical axis deviation (mm), MA: mechanical axis (°).

3.3.1 Cartilage

For the control group, the distribution of cartilage appears mostly uniform across the plateau (Figure 3.6a), with an average thickness of approximately 1.4 mm in all 4 VOIs (1.19 – 1.54 mm; Figure 3.8a, Table 3.2). In varus-OA the average Cart.Th range was 0.58 – 2.47 mm and for valgus-OA 1.20 – 1.86 mm, depending on the region. Compared to controls (Figure 3.6a), varus-OA exhibited a significantly thinner average Cart.Th in the AM ROI (0.58 mm, -59%, $p<0.001$, Figure 3.6b, Figure 3.7b, Figure 3.8a, Table 3.2) and thicker in the lateral regions (2.19 mm (AL) to 2.47 mm (PL); up to +63%, $p<0.001$). For valgus-OA, whereas average Cart.Th was not different to controls laterally, it was significantly thicker medially, ranging from 1.71 mm (AM) to 1.86 mm (PM) (+56% in PM ROI, $p<0.001$).

In controls the medial-to-lateral Cart.Th ratios were close to unity (range: 0.8-1.1, Figure 3.8b, Table 3.2), in varus-OA they were all well below unity and below the values of controls (0.2-0.6, $p<0.025$); whereas in valgus-OA, they were similar to or higher than in controls (1.0-1.3).

3.3.2 Subchondral bone plate

For the controls, the average SBPl.Th range was 0.26 - 0.47 mm, for varus-OA 0.39 - 0.72 mm and for valgus-OA 0.43 - 0.61 mm (Figure 3.7b, Figure 3.8c, Table 3.2), depending on the region. SBPl.Th was significantly higher medially in varus-OA compared to controls (up to +107%, Figure 3.7b, Figure 3.8c, $p<0.001$), whereas it was significantly higher laterally in valgus-OA (up to +135%, $p<0.001$ in PM region, and $p=0.005$ in PL region).
In varus-OA, the medial-to-lateral SBPl.Th ratios (range 1.4-2.0) were above unity and higher than in controls (0.8-1.8, Figure 3.8d, Table 3.2); in valgus-OA (0.8-1.0) they were closer to unity and lower than controls.

3.3.3 Subchondral trabecular bone

Average BV/TV ranged between 18% and 37% in controls, between 20% and 44% in varus-OA and between 23% and 37% in valgus, depending on the region (Figure 3.7, Figure 3.8e, Table 3.2). The BV/TV in varus-OA was significantly higher medially (BV/TV= 44% AM ($p=0.022$) and 37% PM ($p=0.007$)) compared to controls (BV/TV= 37% AM and 24% PM, Figure 3.7, Figure 3.8e, Table 3.2), whereas in valgus-OA the BV/TV was significantly higher anterolaterally (BV/TV= 32% ($p=0.004$)) compared to controls (BV/TV= 18%).
Correspondingly, in varus-OA, the medial-to-lateral BV/TV ratios were above unity (1.6-2.4) and higher than controls (0.9-2.1, Figure 3.8f, Table 3.2). In valgus-OA, they were closer to unity and lower (0.8-1.1; AM:AL ($p=0.004$) and PM:AL ($p=0.006$)) than in controls.

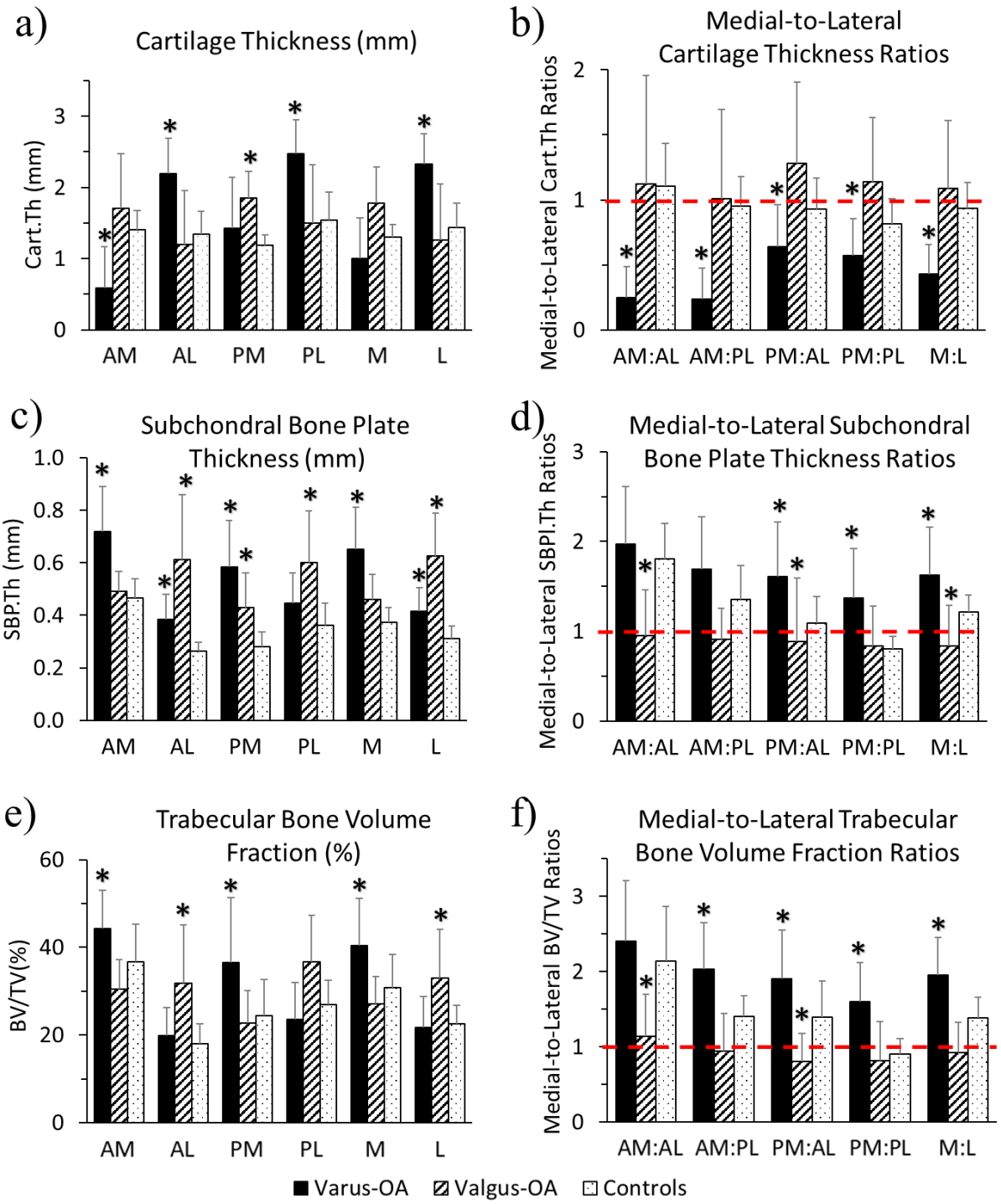

Figure 3.8: a) Cart.Th, b) medial-to lateral Cart.Th ratios, c) SBPl.Th, d) medial-to-lateral SBPl.Th ratios, e) BV/TV, f) medial-to-lateral BV/TV ratios; average values and standard deviation (error bars) for the three groups examined (varus-OA n=18, valgus-OA n=7, controls n=15): dashed horizontal line indicates unity. A Kruskal-Wallis test followed by a Mann-Whitney U-test was performed to compare the varus-OA and valgus-OA groups against the control group; *Significant difference compared to control (Benjamini-Hochberg adjusted, false-discovery rate = 0.05). A: anterior, P: posterior, M: medial, L: lateral anatomical location.

Table 3.2: Mean ± standard deviation (SD) and Median [minimum, maximum] of subregional cartilage thickness, subchondral bone plate thickness and subchondral trabecular bone volume fraction and their medial-to-lateral ratios

	Varus-OA		Valgus-OA		Controls	
			Cartilage Thickness (mm)			
VOI	**Mean ±SD**	**Median [min,max]**	**Mean ±SD**	**Median [min,max]**	**Mean ±SD**	**Median [min,max]**
AM	0.58 ±0.58	0.40 [0.00,1.87]	1.71 ±0.76	1.94 [0.16,2.43]	1.41 ±0.27	1.38 [0.89,1.92]
AL	2.19 ±0.49	2.23 [1.34,3.56]	1.20 ±0.76	1.62 [0.06,1.90]	1.34 ±0.32	1.25 [0.85,1.99]
PM	1.42 ±0.72	1.75 [0.10,2.23]	1.86 ±0.37	1.92 [1.29,2.43]	1.19 ±0.14	1.23 [0.98,1.41]
PL	2.47 ±0.47	2.50 [1.84,3.24]	1.50 ±0.83	1.76 [0.00,2.28]	1.54 ±0.40	1.55 [0.95,2.39]
M	1.00 ±0.57	1.11 [0.05,1.93]	1.78 ±0.51	1.93 [0.94,2.43]	1.30 ±0.18	1.33 [0.97,1.60]
L	2.33 ±0.42	2.30 [1.66,3.35]	1.26 ±0.79	1.52 [0.03,1.95]	1.44 ±0.33	1.38 [1.06,2.19]
Ratio			**Medial-to-Lateral Ratios**			
AM:AL	0.25 ±0.24	0.20 [0.00,0.80]	1.12 ±0.85	1.10 [0.10,2.40]	1.10 ±0.33	0.99 [0.67,1.70]
AM:PL	0.24 ±0.23	0.20 [0.00,0.70]	1.00 ±0.67	0.90 [0.10,1.80]	0.95 ±0.22	0.94 [0.50,1.41]
PM:AL	0.63 ±0.33	0.70 [0.00,1.20]	1.28 ±0.65	1.10 [0.70,2.40]	0.93 ±0.23	0.90 [0.64,1.44]
PM:PL	0.58 ±0.29	0.70 [0.00,0.90]	1.12 ±0.50	0.80 [0.70,1.80]	0.82 ±0.19	0.85 [0.47,1.14]
M:L	0.43 ±0.23	0.44 [0.02,0.76]	1.09 ±0.52	1.05 [0.51,1.80]	0.94 ±0.20	0.90 [0.56,1.23]
VOI			**Subchondral Bone Plate Thickness (mm)**			
AM	0.72 ±0.17	0.68 [0.47,1.13]	0.49 ±0.08	0.48 [0.41,0.60]	0.47 ±0.07	0.45 [0.35,0.59]
AL	0.39 ±0.10	0.37 [0.22,0.61]	0.61 ±0.25	0.63 [0.29,0.97]	0.26 ±0.03	0.26 [0.20,0.31]
PM	0.58 ±0.18	0.60 [0.22,0.89]	0.43 ±0.13	0.41 [0.32,0.71]	0.28 ±0.05	0.28 [0.19,0.39]
PL	0.45 ±0.12	0.40 [0.32,0.70]	0.60 ±0.20	0.58 [0.38,0.91]	0.36 ±0.09	0.38 [0.22,0.49]
M	0.65 ±0.16	0.63 [0.37,1.01]	0.46 ±0.10	0.42 [0.37,0.64]	0.37 ±0.05	0.38 [0.28,0.47]
L	0.42 ±0.09	0.39 [0.29,0.56]	0.61 ±0.16	0.62 [0.37,0.77]	0.31 ±0.05	0.31 [0.25,0.39]
Ratio			**Medial-to-Lateral Ratios**			
AM:AL	1.97 ±0.65	1.95 [0.90,3.30]	0.96 ±0.48	0.70 [0.53,1.90]	1.81 ±0.39	1.70 [1.30,2.50]
AM:PL	1.69 ±0.58	1.65 [0.80,3.00]	0.93 ±0.36	0.90 [0.50,1.40]	1.35 ±0.38	1.30 [0.90,2.10]
PM:AL	1.61 ±0.60	1.70 [0.60,2.60]	0.88 ±0.70	0.60 [0.40,2.40]	1.09 ±0.29	1.00 [0.70,1.90]
PM:PL	1.38 ±0.55	1.20 [0.60,2.50]	0.83 ±0.45	0.70 [0.40,1.60]	0.80 ±0.16	0.80 [0.50,1.00]
M:L	1.64 ±0.53	1.60 [0.90,2.80]	0.82 ±0.45	0.70 [0.50,1.70]	1.21 ±0.20	1.20 [1.00,1.60]
VOI			**Subchondral Trabecular Bone Volume Fraction (%)**			
AM	44.3 ±8.80	43.0 [33.0,62.1]	30.4 ±6.83	30.5 [20.5,42.9]	36.6 ±8.71	36.5 [22.7,58.3]
AL	19.8 ±6.45	18.2 [11.6,36.5]	31.8 ±13.4	28.3 [18.7,54.0]	18.0 ±4.54	16.6 [9.85,24.8]
PM	36.5 ±14.8	31.5 [14.7,67.4]	22.8 ±7.32	21.3 [14.5,31.5]	24.5 ±8.22	24.4 [14.3,45.5]
PL	23.6 ±8.36	21.4 [12.9,46.5]	36.6 ±10.6	40.3 [19.9,49.1]	27.0 ±5.53	25.5 [17.6,36.8]
M	40.4 ±10.8	36.6 [25.9,64.8]	27.1 ±6.25	26.1 [20.2,37.2]	30.8 ±7.53	30.1 [21.1,45.5]
L	21.7 ±7.18	19.6 [13.3,41.5]	32.9 ±11.2	31.5 [18.7,51.6]	22.5 ±4.35	21.9 [13.7,29.2]
Ratio			**Medial-to-Lateral Ratios**			
AM:AL	2.41 ±0.80	2.19 [1.37,4.66]	1.14 ±0.56	1.08 [0.38,1.97]	2.14 ±0.72	1.92 [1.43,3.54]
AM:PL	2.03 ±0.62	1.72 [1.33,3.33]	0.94 ±0.50	0.75 [0.42,1.61]	1.41 ±0.27	1.41 [0.94,1.83]
PM:AL	1.91 ±0.64	1.89 [0.77,3.07]	0.80 ±0.38	0.78 [0.37,1.45]	1.40 ±0.48	1.23 [0.95,2.73]
PM:PL	1.60 ±0.52	1.58 [0.68,2.69]	0.81 ±0.52	0.56 [0.39,1.58]	0.90 ±0.20	0.89 [0.55,1.27]
M:L	1.95 ±0.50	1.99 [1.09,2.84]	0.93 ±0.39	0.89 [0.39,1.49]	1.38 ±0.27	1.36 [1.06,1.93]

3.3.4 Validation study: cartilage thickness measurement comparison (micro-CT vs. histology)

A strong linear relationship was found for cartilage thickness measured by micro-CT and by histology (Figure 3.9), with a high coefficient of determination (R^2= 0.926, p<0.001, Figure 3.9). No statistically significant differences were observed among the techniques in the selected load bearing regions of interest and the medial-to lateral ratios among these regions (Figure 3.9).

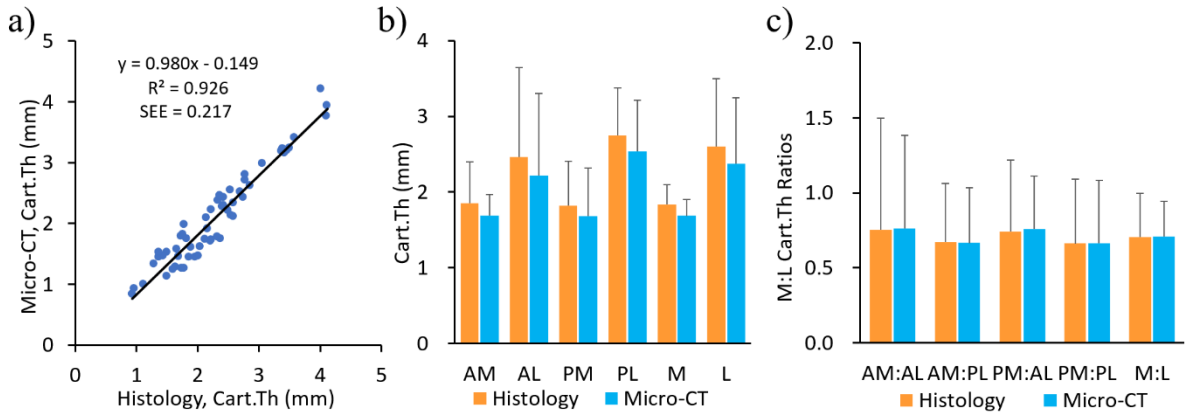

Figure 3.9: Validation study: a) scatterplot and line of best-fit for cartilage thickness measured by histology and micro-CT containing the cartilage thickness from 10 slides per tibial plateau; R2 = the coefficient of determination, SEE: Standard error of the estimate; b) and c) bar graphs indicating the average cartilage thickness and standard deviation (error bars) of cartilage thickness as measured by histology (orange colour) and micro-CT (blue colour) for b) cartilage thickness per region and c) medial-to-lateral cartilage thickness ratios.

3.4 Discussion

In this preliminary study, tibial cartilage morphology and subchondral bone microarchitecture of subjects diagnosed with end-stage knee OA were compared against non-OA knees using high-resolution micro-CT imaging, while accounting for joint alignment. Differences in cartilage thickness, underlying cortical plate thickness and subchondral trabecular bone volume fraction between OA and control joints were found when grouping the OA cohort by joint alignment. Medially, the varus-OA group had significantly lower Cart.Th compared to the controls (up to 59% lower) and significantly higher SBPl.Th and BV/TV underneath (up to 107% and 49% higher, respectively). Conversely, the valgus-OA group, laterally, had slightly thinner cartilage and significantly thicker SBP and BV/TV (up to 135% and 76%, respectively) compared to controls. Accordingly, in the varus-OA group, the medial-to-lateral Cart.Th ratios were lower and the medial-to-lateral BV/TV (Figure 3.8f) and SBPl.Th ratios (Figure 3.8d) higher compared to controls; the opposite was seen in the valgus-OA group. Moreover, micro-

CT and histology were found to not significantly differ in cartilage thickness measurements.

Knee joint malalignment has been previously linked to altered medial-to-lateral distribution of loads (Adouni *et al.*, 2014b), with joint contact forces higher medially than laterally in varus-alignments and the opposite for valgus-alignments. As cartilage is an avascular tissue with limited capacity for regeneration and repair (Fox *et al.*, 2009), whereas bone can adapt to everyday mechanical loading (Turner, 1998), our findings might reflect the medial-to-lateral joint loading ratio that the joint has been subjected to in daily life (Adouni *et al.*, 2014b). In the present study, in the OA groups, regions of lower cartilage thickness (Figure 3.8a) corresponded to regions of thicker cortical SBP (Figure 3.8c) and higher BV/TV (Figure 3.8e) underneath. Conversely, regions of thicker cartilage corresponded to regions of thinner cortical SBP and lower BV/TV. This suggests an interplay between cartilage and bone in OA, with an inverse relationship between cartilage thickness and bone volume. This is consistent with current literature on OA, with the response of the joint as a whole to daily stimuli, involving both cartilage and bone (Bobinac *et al.*, 2003, Burr *et al.*, 2012). However, whereas the present M:L cartilage thickness ratios (Figure 3.8b) are consistent with previous MRI studies in OA, those studies did not consider the bone (Eckstein *et al.*, 2008). Similarly, while the M:L BV/TV and SBPl.Th ratios are consistent with bone mineral density studies using dual X-ray absorptiometry (DEXA) (Christensen *et al.*, 1982, Hulet *et al.*, 2002), DEXA cannot be used to assess cartilage, it is limited to 2D analyses and cannot separate the subchondral bone plate from the underlying trabecular bone. This study combines subregional assessment of the cartilage morphology and bone microarchitecture using high-resolution micro-CT in tibial plateaus from OA patients and controls, accounting for joint alignment.

Somewhat surprisingly, cartilage was thicker in some regions of the OA groups compared to controls (i.e. thicker laterally in varus-OA specimens and thicker medially in valgus-OA, Figure 3.6 and Figure 3.8a). A previous *in vivo* MRI study has reported regions of thicker cartilage in the femorotibial compartment of knee OA patients (with a Kellgren Lawrence grade of 2 (mild)) compared to controls (Hellio Le Graverand *et al.*, 2009). The authors of that study speculated the thickening to be due to cartilage swelling in earlier stages of OA. We suggest that in the present study the regions of thicker cartilage in the malaligned OA specimens (laterally for varus-OA, medially for valgus-OA) may have been

subjected to less local everyday loading than in controls and hence, the cartilage has eroded less compared to a non-OA joint.

The significant regional differences between OA and non-OA tibiae reported in this study may have been masked ("averaged out") in previous studies (Chen *et al.*, 2018), that did not consider joint alignment. Such "averaging out" becomes evident when combining the present varus-OA and valgus-OA groups (i.e. no subdivision based on joint alignment) and comparing them to controls (Figure 3.10). While we have more varus-OA specimens (n=18) than valgus-OA (n=7), this distribution follows that of the alignment of knee OA subjects of the general population (Niu *et al.*, 2009). As such, the pattern in cartilage thickness, SBPl.Th and BV/TV of the combined OA group follows that of the varus-OA group, but to a lesser degree. For example, Cart.Th in AM for the varus-OA group was significantly thinner than in the control group by 59%; when combining the OA groups, this difference shrinks to only 35%, becoming not statistically significant. Similarly, the SBPl.Th differences diminish in the combined OA group compared to controls, although maintaining statistical significances, whereas the medial-to-lateral SBPl.Th ratios show almost no differences from the controls anymore. Additionally, the BV/TV differences diminish (vanish) when comparing the combined OA group to controls. This is also the case for the medial-to-lateral ratios of Cart.Th and BV/TV (Figure 3.10b, d, f), where the opposite distributions of Cart.Th, SBPl.Th and BV/TV across the medial and lateral condyles for the varus-OA and valgus-OA groups shown in Figure 3.6, Figure 3.7 and Figure 3.8 almost vanish. Not taking account of joint alignment may then explain why, for example, in a recent micro-CT study in OA and non-OA tibial plateaus, no significant differences in cartilage thickness and BV/TV in the lateral regions were found between the two groups (Chen *et al.*, 2018), whereas differences found in the medial regions were similar to our varus-OA group, but to a lesser degree. However, in that study, the patient cohort was 30 kg lighter compared to ours in body mass (60.3 ± 7.4 kg (OA group; no reported BMI) vs. 90 ± 17.6 kg (OA group)), which could also, in part, explain possible differences in findings between studies.

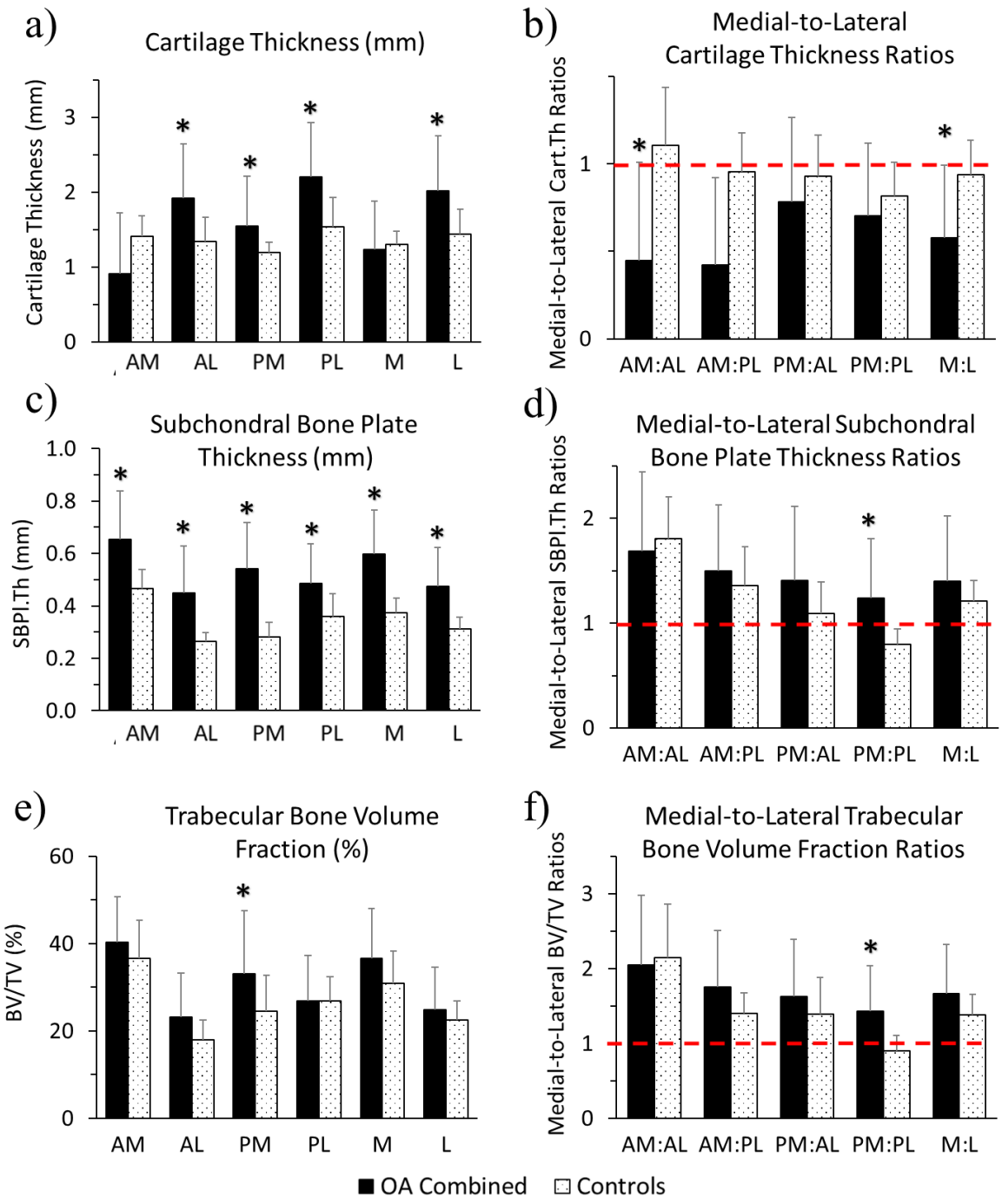

Figure 3.10: Same graphs as in Figure 3.8, but not accounting for joint alignment in OA (varus-OA and valgus-OA combined) a) Cart.Th, b) medial-to-lateral Cart.Th ratios, c) SBPl.Th, d) medial-to-lateral SBPl.Th ratios, e) BV/TV, f) medial-to-lateral BV/TV ratios; average values and standard deviation (error bars) for the two groups examined (OA n = 25, controls n=15): dashed horizontal line indicates unity. A Mann-Whitney U-test was used to compare between the OA-combined group and the control-group for each parameter; *Significant difference compared to control (Benjamini-Hochberg adjusted, false-discovery rate = 0.05). A: anterior, P: posterior, M: medial, L: lateral anatomical location.

A limitation of this study is that we did not have joint alignment nor BMI data for our cadaveric non-OA tibial plateaus. The OA knees in this study were mostly varus-aligned or valgus-aligned. This is in agreement with data reported in the literature (Niu *et al.*, 2009), where in a study of over 5,000 OA and non-OA knees, OA joints ranged from extremely varus to extremely valgus, whereas non-OA joints were found to be mainly neutral-, if not slightly varus-aligned (Niu *et al.*, 2009). Our OA cohort is reflective of that reported OA-distribution and it can be assumed that the alignment of the cadaveric controls also follows that of the reported general population. Furthermore, literature reports about control knees having on average a neutral to slightly varus alignment are consistent with our medial-to-lateral ratios of subchondral bone plate thickness ratios and trabecular BV/TV, where the pattern of controls is similar to that of varus-OA but to a lesser severity (Figure 3.8d and f). This possibly reflects similar joint loading in daily life, although to a lesser extent in people without knee OA.

Our controls had a cartilage thickness across all regions of 1.2-1.5 mm and medial-to-lateral thickness ratios of approximately 1, indicating a rather uniform distribution among the medial and lateral VOIs. This thickness is slightly lower than for non-OA tibial plateaus reported in some literature (1.7 - 2.5 mm on average) (Delecourt *et al.*, 2016, Chen *et al.*, 2018). This could be due to the region selection (Delecourt *et al.*, 2016, Chen *et al.*, 2018), where both studies included regions close to the tibial plateau midline, whereas our anterior and posterior regions were further from the midline (closer to the anterior or posterior aspect, as these were the centre of the anterior and posterior halves of the condyle, respectively) and hence at least partially covered by the meniscus. Regions covered by the menisci (i.e. further from the midline of the tibia) have been reported to contain thinner cartilage (Koo *et al.*, 2007, Favre *et al.*, 2017). Indeed, our cartilage thickness values in controls are comparable to those reported by Delecourt et al, with "2D measurements" of 1.7 mm in their more peripheral regions (Delecourt *et al.*, 2016). Another study reported tibial cartilage thickness of 1 - 4 mm in non-OA knees (Favre *et al.*, 2017), however, that study was performed in a younger cohort (39.7±12.5 years vs. 61.6±12.9 years in the present study) and used clinical MRI, which has been found to overestimate cartilage thickness if under 2 mm (Koo *et al.*, 2005).

In this preliminary study, cartilage and bone morphometric parameters (Cart.Th, SBPl.Th, BV/TV) in the 4 tibial regions (AM, AL, PM and PL) and their regional ratios for the varus-OA and valgus-OA group were compared against the control group. However, one could

have chosen a different approach to the comparison, that is, considering all possible combinations between groups and variables and including also within-group comparisons. This was not our goal and for such an approach, our sample size would have been likely underpowered. This may be the goal for further studies.

Outcome of the validation study (micro-CT vs. histology):

Our micro-CT analysis of articular cartilage did not use any contrast agents. Instead, cartilage was visualized by maximizing the signal-to-noise ratio (i.e. by increasing the exposure time and frame averaging and decreasing the rotation step). Cartilage thickness measured from micro-CT cross-sections using this protocol had a strong linear relationship with the cartilage thickness measured from histology slides. Moreover, the cartilage thickness measurements in four anatomical regions and their medial-to-lateral ratios did not significantly differ among techniques. Hence, using the protocol here described, the gross cartilage thickness can be quantified on entire tibial plateaus using micro-CT, without the need for extensive preparation or staining. Moreover, this can be performed concurrently with the more commonly assessed bone microarchitecture, on the same specimens.

A limitation of the here used micro-CT method is that it cannot be used to derive proteoglycan content. Future studies might use contrast agents, such as Hexabrix, to derive proteoglycan content in the cartilage (Gatenholm *et al.*, 2019). Furthermore, as our imaging method requires excised tibial plateaus, we were restricted to analyzing end-stage OA. However, monitoring the progression of OA *in vivo* may be possible by using a combination of MRI and high-resolution peripheral quantitative CT (HR-pQCT), or contrast-enhanced HR-pQCT (Michalak *et al.*, 2019) in future. The use of *in vivo* HR-pQCT could also allow for analysis of bone microarchitecture more distal to the first 5 mm of the tibial plateau investigated in this study as there may be value in looking deeper into the joint (near the epiphyseal line) where sclerosis may not occur (Burnett *et al.*, 2017).

3.5 Conclusion

Micro-CT enables the non-destructive assessment of gross cartilage morphology and bone microarchitecture. In this preliminary study, OA and non-OA tibias were found to differ significantly in Cart.Th, SBPl.Th and STB microarchitecture depending on joint alignment, suggesting that joint structural changes in OA may reflect differences in medial-to-lateral load distribution upon the tibial plateau. The inverse relationship

between the cartilage thickness, the underlying subchondral bone plate thickness and subchondral trabecular bone volume suggests the response of the joint as a whole to daily stimuli involving both cartilage and bone. Moreover, cartilage thickness measurements using a non-contrast agent based micro-CT scanning protocol were validated against histology, allowing for the micro-CT assessment of cartilage thickness without the need for staining. Detectable morphological differences between OA and non-OA joints depend on joint alignment and could become useful indicators of disease progression, warranting further exploration.

Chapter 4
Study 2: Relationships between tibial articular cartilage, *in vivo* external knee joint moments and static knee alignment in end-stage knee osteoarthritis: a micro-CT study

In the previous chapter (Study 1), the articular cartilage thickness, subchondral bone plate thickness and subchondral trabecular BV/TV in varus-OA and valgus-OA knees were compared to controls. This chapter extends on the previous chapter, by investigating the relationships between joint loading indices (external knee moments from pre-operative gait analysis and static knee alignment) and cartilage thickness in the 25 knee OA specimens of the previous chapter.

The study presented in this chapter is the subject of the following paper:

Rapagna S, Roberts BC, Solomon LB, Reynolds KJ, Thewlis D, Perilli E. Relationships between tibial articular cartilage, *in vivo* external joint moments and static alignment in end-stage knee osteoarthritis: a micro-CT study. *Journal of Orthopaedic Research*. 2021. In Press. doi: 10.1002/jor.25140.

Please refer to the Appendix at the end of this thesis for a detailed outline of the author's contribution to this study.

Abstract

Biomechanical factors (e.g. joint loading) have a significant role in the progression of osteoarthritis (OA). However, some relationships between *in vivo* joint loading indices and tibial cartilage thickness are conflicting. This study investigated relationships between pre-operative *in vivo* external knee joint moments, joint alignment and regional tibial cartilage thickness using micro-CT in subjects with end-stage knee OA. Tibial plateaus from 25 patients that underwent knee replacement for OA were micro-CT scanned (17 μm/voxel). Prior to surgery, subjects underwent gait analysis to calculate external knee moments. The mechanical axis deviation (MAD) was obtained from pre-operative radiographs. Cartilage thickness (Cart.Th) was analyzed from micro-CT images, in anteromedial, anterolateral, posteromedial and posterolateral subregions of interest. Medial-to-lateral Cart.Th ratios were also explored. Relationships between Cart.Th and joint loading indices were examined using Pearson's correlations. Significant correlations were found between Cart.Th and joint loading indices, positive anteromedially with the first peak knee adduction moment ($r= 0.55$, $p<0.01$) and external rotation moment (ERM; $r= 0.52$, $p<0.01$), and negative with MAD ($r= -0.76$, $p<0.001$). In the lateral regions, these correlations had opposite signs. The medial-to-lateral Cart.Th ratio correlated strongly with ERM ($r= 0.63$, $p=0.001$) and MAD ($r= -0.75$, $p<0.001$). Joint loading indices correlated with regional cartilage thickness values and their medial-to-lateral ratios in end-stage knee OA subjects, with higher regional loads corresponding to thinner cartilage. These relationships have the opposite sign compared to the subchondral bone microarchitecture found in a previous study by our group on the same specimens, which may suggest a complementary bone-cartilage interplay in response to loading.

4.1 Introduction

OA is a degenerative joint disease that is most commonly reported in the knee joint (Cross *et al.*, 2014) with an estimated 303.1 million cases of knee and hip OA globally (Safiri *et al.*, 2020). The highest age-standardized prevalence is in the United States, followed by North Africa, the Middle East and Australasia (Safiri *et al.*, 2020). The disease has economic burdens, with knee joint replacement contributing to the majority of OA healthcare costs (Hunter *et al.*, 2019). While the mechanisms behind this multifactorial disease are not well understood, biomechanical factors (e.g. joint loading) have been found to play a significant role in the onset and progression of the disease (Miyazaki *et al.*, 2002, Griffin *et al.*, 2005, Brouwer *et al.*, 2007, Astephen *et al.*, 2008, Guilak, 2011).

Abnormal joint loading, which may be chronic over- or under-loading, and malalignment during habitual loading (e.g. standing, walking) can affect the medial-to-lateral distribution of loads upon the tibial plateau (Wada *et al.*, 2001, Thorp *et al.*, 2006, Adouni *et al.*, 2014b). This can then affect the articular cartilage morphology and distribution, which may contribute to knee OA (Chapter 3; Rapagna et al., 2021a, Andriacchi et al., 2006, Eckstein et al., 2008, Andriacchi et al., 2009). In particular, external measures of joint loading (derived from gait analysis), including the knee adduction moment (KAM), KAM impulse and knee flexion moments (KFM), have been associated with variations in tibial cartilage thickness in OA (Erhart-Hledik *et al.*, 2015, Maly *et al.*, 2015, Edd *et al.*, 2018).

However, some relationships, such as those between the knee OA cartilage thickness, KFM and KAM are conflicting (Vanwanseele *et al.*, 2010, Chang *et al.*, 2015, Erhart-Hledik *et al.*, 2015, Maly *et al.*, 2015). Although these discrepancies can be attributed to gait analysis protocols (e.g. inverse dynamic calculations and marker placement) (Thewlis *et al.*, 2008, Camomilla *et al.*, 2017) and range of patient cohorts (e.g, varus to valgus knee alignment), they could also be attributed to the use of magnetic resonance imaging (MRI) for *in vivo* cartilage imaging. MRI has a relatively low spatial resolution (0.140 – 0.310 mm in plane, with a 1.5 mm slice thickness), which can cause cartilage thickness to be overestimated, particularly in OA where there are regions of thinner, denuded cartilage (Koo *et al.*, 2005, Koo *et al.*, 2009). However, high resolution cartilage thickness measurements, such as those obtained by micro-computed tomography (micro-CT), have not yet been combined with *in vivo* knee joint loading in OA subjects in the scientific

literature. Micro-CT enables the non-destructive 3D assessment of entire excised human tibial plateaus at high resolutions, with growing interest in the examination of human articular cartilage (Chen *et al.*, 2018, Gatenholm *et al.*, 2019, Rapagna *et al.*, 2021a).

Using micro-CT, our group has previously shown associations between joint moments and the regional subchondral bone microarchitecture in end stage knee OA (Roberts *et al.*, 2018). Among these, relationships also with the external rotation moment (ERM) were found, which in general are underreported in the literature. As there is a whole joint response in OA (Bobinac *et al.*, 2003, Burr *et al.*, 2012), it can be expected that relationships with joint moments may also be reflected in the overlying cartilage.

The aim of this study was to investigate in people with end-stage knee OA, relationships between knee joint external moments (peak knee adduction moments, flexion/extension moments and external/internal rotation moments from pre-operative gait analysis), joint alignment (pre-operative radiographs) and cartilage thickness of their excised tibial plateaus quantified with 3D micro-CT. We hypothesize, based on the literature and a previous study from our group on the tibial subchondral bone (Roberts *et al.*, 2018), that the frontal plane loading indices (static alignment (Eckstein *et al.*, 2008, Roberts *et al.*, 2018), peak knee adduction moments and impulse (Maly *et al.*, 2015, Edd *et al.*, 2018, Roberts *et al.*, 2018)), which are indicators of medial joint loading, and the ERM (transverse plane) (Roberts *et al.*, 2018), will be most strongly associated with measurements of the medial tibial condyle cartilage thickness.

4.2 Methods

4.2.1 Participants

Micro-CT scans generated in the previous study (Chapter 3; Rapagna *et al.*, 2021a, Roberts *et al.*, 2018) were used in this study. Briefly, 25 subjects diagnosed with end-stage knee OA (68±7 years; 90±18 kg) were recruited for this study (Table 4.1). Subjects underwent gait analysis within one week prior to their total knee arthroplasty surgery (Roberts *et al.,* 2018), with their excised tibial plateau retrieved for micro-CT scanning (stored immersed in 70% ethanol solution). Approval for this study was granted by the Southern Adelaide Clinical and Royal Adelaide Hospital Human Research Ethics Committees (HREC/13/SAC/402). All patients gave written informed consent.

Table 4.1: Summary of patient characteristics and gait parameters (prior to knee arthroplasty) (n = 25)

Age (years)	68 ± 7
Sex (male:female)	11:14
Affected limb (right:left)	13:12
Height (m)	1.67 ± 0.09
Body mass (kg)	90.2 ± 17.6
BMI (kg/m^2)	32.2 ± 4.7
Knee moments (Nm/kg)	
knee flexion moment, KFM	0.35 ± 0.23
knee extension moment, KEM	-0.11 ± 0.29
First peak adduction moment, KAM1	-0.40 ± 0.23
Second peak adduction moment, KAM2	-0.39 ± 0.22
Knee adduction moment impulse	27.0 ± 14.2
External rotation moment, ERM	0.022 ± 0.023
Internal rotation moment, IRM	-0.085 ± 0.079
Walking Speed (m/s)	0.70 ± 0.25
Static alignment	
Mechanical axis deviation (mm)	9.2 ± 34.8

Average ± standard deviation

4.2.2 Gait Analysis

Subjects completed, without footwear and at a self-selected walking speed, three successful trials along a 10 m walkway (Roberts *et al.*, 2018). Three-dimensional (3D) kinematics and ground reaction force data were captured using 12 VICON MX-F20 cameras (Vicon Metrics, Oxford, UK) and four floor embedded force platforms (2 _ 9281B, Kistler Instrument Corporation, Switzerland; 2 _ AMTI BP400600, Advanced Mechanical Technology Inc., USA) at 100 and 400 Hz, respectively. Forty retro-reflective markers were placed over anatomical landmarks defining the joints of the lower limbs. A lower limb kinematic model (described by Thewlis *et al.* (2015)) was generated in Visual3D (V5, C-Motion Inc., USA). Model pose was reconstructed using inverse kinematics (Lu *et al.*, 1999). External joint moments were calculated using a recursive Newton-Euler method (Doriot *et al.*, 2004). The knee moments were calculated relative to the tibial coordinate system and normalized to body mass (Nm/kg) and time (101 points representing 0-100% of the stance phase). The mean of the three successful trials was computed and used for analysis.

The moments investigated in this study were the first peak KAM (KAM1), second peak KAM (KAM2), peak KAM (either KAM1 or KAM2), peak KFM, terminal stance peak knee

extension moment (KEM), ERM and the internal rotation moment (IRM). The KAM impulse (area under the adduction moment curve) was computed using the trapezoidal method across the entire stance phase.

4.2.3 Mechanical Joint Alignment from Radiographic Data

The mechanical axis deviation (MAD) for each subject was obtained from pre-operative long leg weight-bearing radiographs, assessed by an experienced examiner (LBS). The MAD was defined as the perpendicular distance from the knee joint and the mechanical axis (the line connecting the centre of the femoral head to the ankle plafond) (Paley, 2002). A varus alignment was defined as a medial deviation greater than 15 mm, valgus alignment as a lateral deviation greater than 0 mm and a neutral alignment between the two (Paley, 2002, Roberts et al., 2017b, Chapter 3; Rapagna et al., 2021a).

4.2.4 Micro-CT Imaging

The excised tibial plateaus were imaged using a desktop micro-CT scanner (Skyscan 1076, Skyscan-Bruker, Kontich, Belgium). Prior to being scanned, specimens were removed from the ethanol solution and individually wrapped in cling-film. The excised plateaus were scanned in pairs, separated by a layer of polystyrene along the resected surface (secured in place with elastic bands). The medial-lateral axis of each specimen aligned with the micro-CT system's rotation axis (Chapter 3; Rapagna *et al*., 2021a, Roberts *et al.,* 2017b). Specimens were scanned at 17.4 μm isotropic voxel size using a 100 kVp peak voltage, 90 μA current, rotation step 0.4° over 180° rotation, 590 ms exposure time, four frames averaging and 0.5 mm thick aluminium filter for beam hardening artefact reduction.

A filtered back-projection algorithm was used to reconstruct the cross-section images (NRecon software, v1.6.9.8, Skyscan-Bruker), which were then saved in an 8-bit bitmap format (256 gray-levels, bmp value of 0 = air, 255 = mineralized tissue). For each specimen pair, a stack of up to 4,997 consecutive cross-sections was reconstructed (corresponding to 86.9 mm length) with a slice thickness of one pixel (17.4 μm) and resulting dataset of 70 GB (Roberts *et al.*, 2017b). The reconstructed cross-section images were then rotated in 3D, such that the anatomical superior-inferior axis of each plateau was aligned with the z-axis of the image stack (Chapter 3; Rapagna *et al*., 2021a, Roberts *et al*., 2017b).

4.2.5 Cartilage segmentation

Non-calcified cartilage was segmented from each tibial plateau using a semi-automatic process described previously (Chapter 3; Rapagna *et al*., 2021a) and based on methods outlined in the literature (Buie *et al.*, 2007, Xie *et al.*, 2009, Gatenholm *et al.*, 2019, Ylitalo *et al.*, 2019). Briefly, segmentation was performed on the coronal image stack of the specimen (Figure 4.1b). After minimizing noise (3D medial filter; $\sigma = 3$), the bone and marrow were segmented, using a custom MATLAB script (2017b, The MathWorks, Inc., Massachusetts, USA) to create a mask ("bone and marrow") extending form the superior surface of the subchondral bone plate to the lower end of the tibial plateau. The inverse mask, containing only cartilage and air (= the image minus the "bone and marrow" mask) was then applied to the same coronal image stack (software CTAnalyser, Skyscan Bruker, Kontich, Belgium). Then, the cartilage was segmented using a lower threshold of 18 and a higher threshold of 86 ("threshold window", excluding air and potential bone debris, respectively), as defined from the gray-level histograms over five representative specimens and applied consistently over all specimens (Chapter 3; Rapagna *et al.*, 2021a). A sensitivity analysis on the threshold window was conducted on 5 tibial plateaus, based on methods outlined by Hara *et al.* (2002) (Figure 4.2). The cartilage segmentation was verified manually every 15 slices (0.261 mm). Then, the "shrink-wrap" plug-in of CTAnalyser was applied, to conform the boundaries of the regions of interest (ROI) to the cartilage.

4.2.6 Volumes of interest (VOIs)

For each tibial plateau, four cylindrical VOIs (10 mm in diameter) were selected within regions of the tibial condyles indicated as high and low-load bearing in the literature (Adouni *et al.*, 2014b, Roberts *et al.*, 2017b) using CTAnalyser as shown previously by our group (Chapter 3; Rapagna *et al*., 2021a, Roberts *et al*., 2017b). These cylindrical VOIs were located at the centre of the anterior or posterior halves of the medial and lateral condyles, which were defined by elliptical regions: anteromedial (AM), anterolateral (AL), posteromedial (PM) and posterolateral (PL) condyles (Roberts *et al.*, 2017a) (Figure 4.1). The medial (M) and lateral (L) regions were computed as the average cartilage thickness of the anterior and posterior VOIs within each condyle (Roberts *et al.*, 2018).

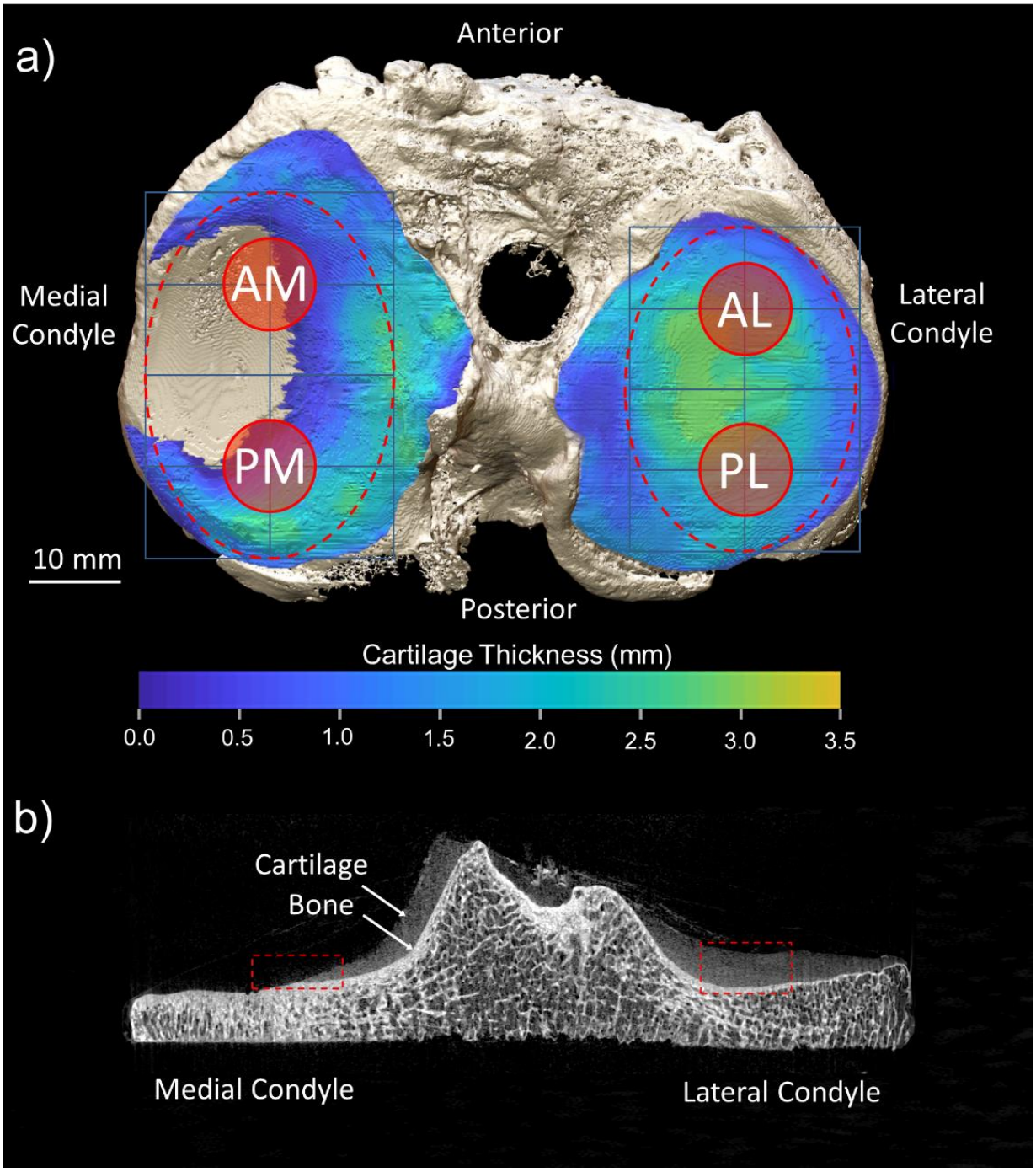

Figure 4.1: a) Micro-CT 3D rendering of and osteoarthritic right tibial plateau (17.4 µm/pixel; superior view), showing cartilage thickness map and subchondral bone underneath (white colour). The red coloured circles are the 4 regions of interest investigated (10 mm diameter cylinders): anteromedial (AM), anterolateral (AL), posteromedial (PM) and posterolateral (PL); b) Micro-CT coronal cross-section of the same tibial plateau at 17.4 µm isotropic voxel size, showing cartilage and marrow in dark gray and bone in bright gray colour, with the region of interest indicated by the red dashed lines.

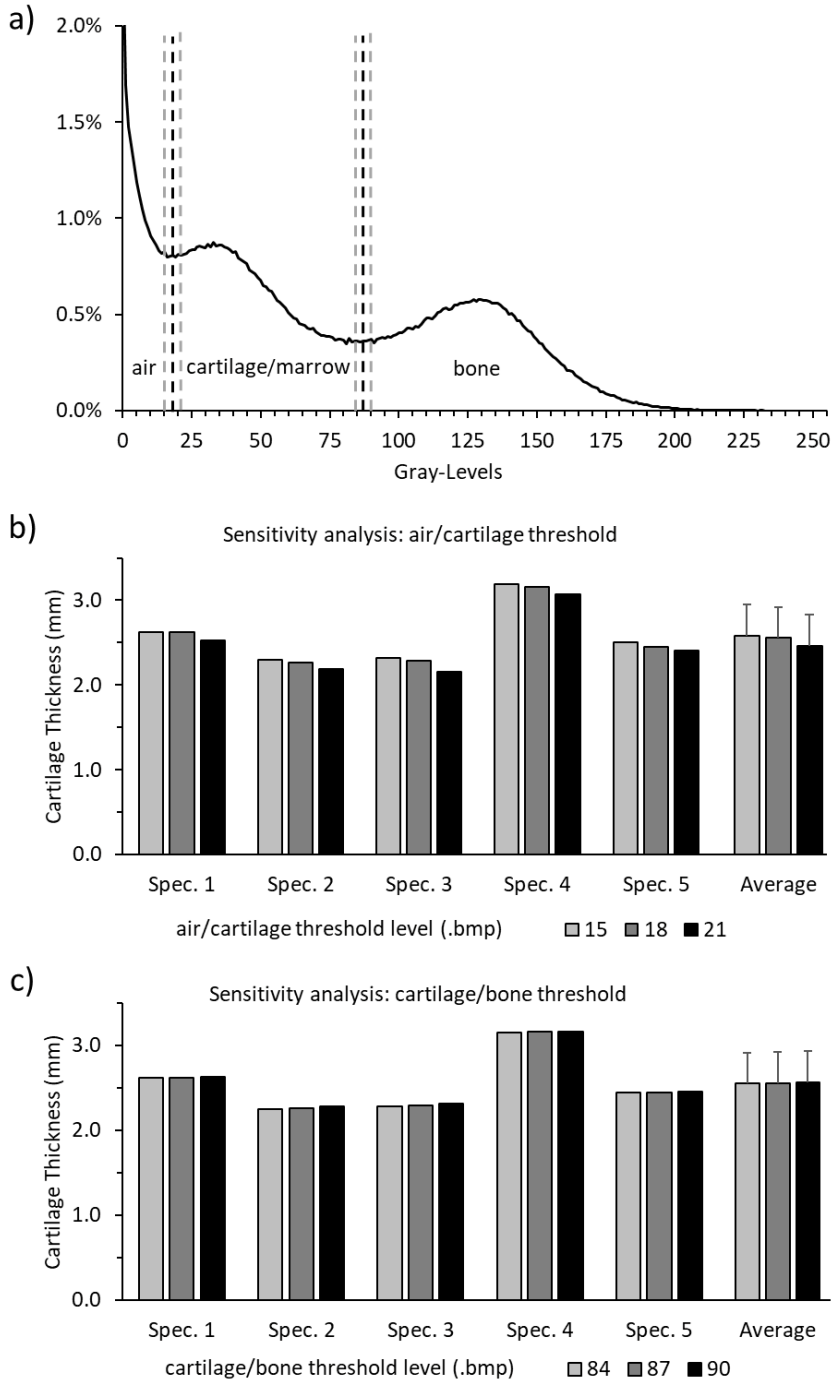

Figure 4.2: Sensitivity analysis. a) Example of a gray-level histogram (256 gray-levels) of a transaxial cross-section image15. The chosen threshold levels used to segment air, cartilage/marrow and bone are indicated by the dashed black lines (values = 18 and 87). The gray dashed lines indicate ±1.2% (±3 gray-level values) used for the sensitivity analysis. b) the cartilage thickness was calculated, when using the chosen "air/cartilage" threshold (18; dark gray colour) and for a threshold 1.2% lower (15; light gray colour) and 1.2% higher (21; black colour). c) the cartilage thickness was calculated when using the chosen "cartilage/bone" threshold (87; dark gray colour) and for a threshold 1.2% lower (84; light gray colour) and 1.2% higher (90; black colour). Overall, variations by 1.2% of the threshold values (+/- 3 gray levels) results in negligible changes of 0.010 mm (0.39%) for the cartilage/bone threshold and 0.09 mm (3.4%) for the air/cartilage threshold, which is several times smaller than the differences detected in this study.

4.2.7 Morphometric Analysis

The average cartilage thickness (Cart.Th, mm) was calculated in the VOIs as the total volume of voxels identified as non-calcified cartilage (mm^3) divided by the cross-section area of the cylindrical VOI (mm^2) (Chapter 3; Rapagna *et al*., 2021a, Eckstein *et al*., 2011). This thickness calculation accounts for VOIs containing partially denuded (0 mm thick) areas of cartilage, which might otherwise cause overestimations of cartilage thickness when using a 3D sphere-fitting thickness algorithm. Finally, the medial-to-lateral Cart.Th ratios between the subregions within each condyle (AM:AL, AM:PL, PM:AL, PM:PL and M:L) were computed.

4.2.8 Statistical analysis:

After testing data for normality (Shapiro-Wilks test), differences in Cart.Th and medial-to-lateral Cart.Th ratios among the subregions (AM, PM, AL, PL) and between M and L were assessed using two independent repeated measures ANOVA, which, if significant, were followed by post-hoc paired t-tests with Bonferroni adjustment for multiple comparisons. Relationships between Cart.Th in the subregions and their medial-to-lateral ratios with the joint moments and MAD were examined using Pearson's correlations, with subsequent Benjamini-Hochberg adjustment (false discovery rate = 0.05), to control for multiple testing (Benjamini *et al.*, 1995).

After assessing the above relationships, multiple linear regression was performed to control for potentially confounding variables that influence the medial joint reaction force and medial-to-lateral load distribution. The ERM, KAM1 and walking speed (WS) were input as covariates in the model, as they have been previously identified to influence the medial-to-lateral distribution of loads on the tibial plateau and the medial condyle forces (Schipplein *et al.*, 1991, Kutzner *et al.*, 2013, Adouni *et al.*, 2014b, Roberts *et al.*, 2018). Joint loading indices which were significantly associated with Cart.Th and/or medial-to-lateral Cart.Th ratios (MAD, KFM, KAM2 and KAM Impulse) were then forward entered into the multiple regression models, to predict variations in AM Cart.Th and M:L Cart.Th ratio (i.e. the cartilage parameters with the strongest correlations). The peak KAM was not entered into the models due to multicollinearity with KAM1 (tolerance value below 0.1 (Hair *et al.*, 2014)). Statistical significance was defined as $p < 0.05$ and was performed using SPSS Statistics 25 (IBM Corp., Armonk, NY).

4.3 Results

4.3.1 Regional tibial cartilage thickness and medial-to-lateral ratios

Significant differences were found among the four identified regions in this tibial OA cohort. The lowest average cartilage thickness was found anteromedially (Figure 4.3a), which was significantly thinner than the anterolateral, posteromedial and posterolateral regions. The highest average cartilage thickness was found posterolaterally. The average medial-to-lateral cartilage thickness ratios were below unity, ranging from 0.41±0.49 (AM:PL Cart.Th ratio) to 0.79±0.48 (PM:AL Cart.Th ratio), with statistical significances shown in Figure 4.3b.

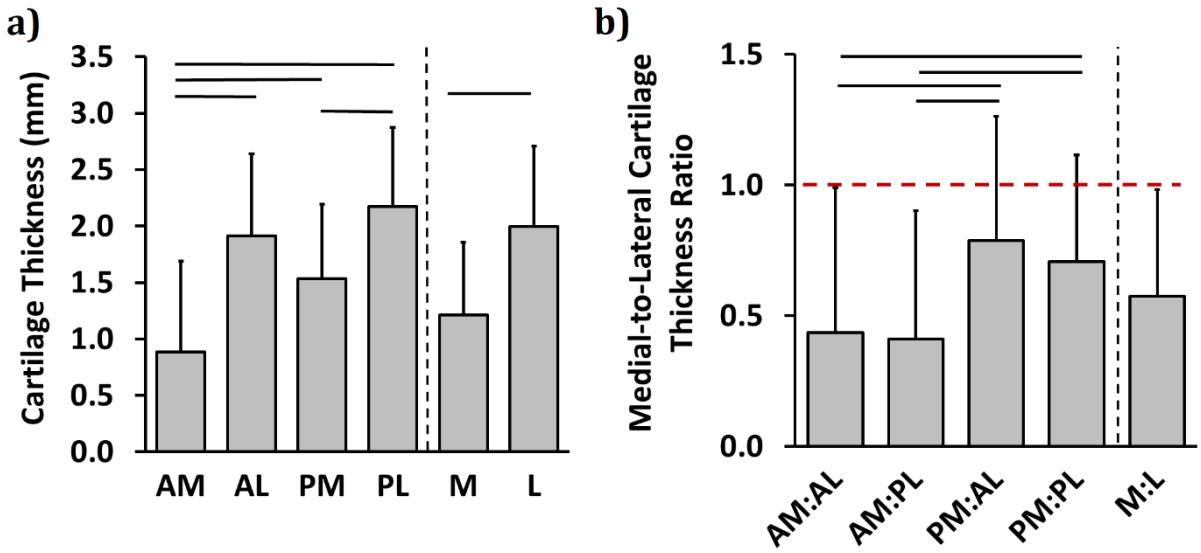

Figure 4.3: Bar plots reporting values of a) 3D average cartilage thickness (error bars indicating standard deviation) in the four subregions of interest within the proximal tibial plateau for all OA patients (n = 25) and b) their medial-to-lateral cartilage thickness ratios. AM: anteromedial, AL: anterolateral, PM: posteromedial, PL: posterolateral, M: medial, L: lateral ($p < 0.05$, paired t-test Bonferroni adjustment). Horizontal dashed line indicates unity in the medial-to-lateral cartilage thickness ratios.

4.3.2 Relationships between tibial cartilage thickness and knee joint loading indices

Significant associations were found between cartilage thickness and joint loading indices. MAD had the strongest correlations with cartilage thickness compared to the other joint loading indices, the strongest being "AM Cart.Th vs. MAD" ($r = -0.76$, $p<0.0001$, Figure 4.4 and Figure 4.5a). In the anteromedial and medial regions, cartilage thickness correlated positively with KAM1, ERM and KAM, and negatively with MAD and KAM Impulse (Figure 4.4). In the lateral regions, the associations between cartilage thickness and loading

indices had opposite signs to those found medially (Figure 4.4). The KFM was significantly related with cartilage thickness in the lateral region. No significant associations were found for the other investigated joint loading parameters (KEM and IRM) with regional cartilage thickness.

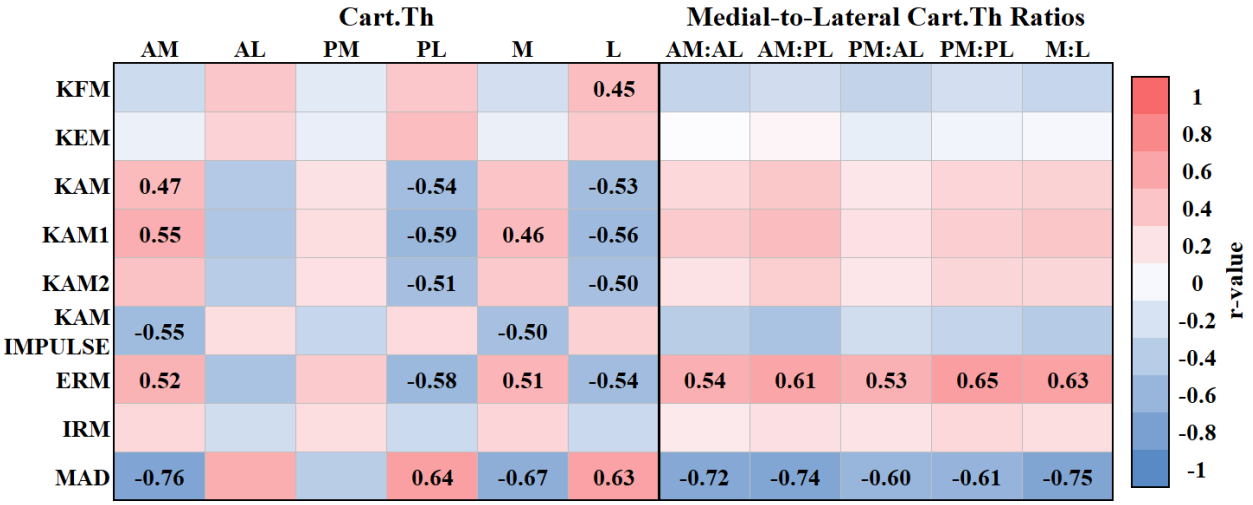

Figure 4.4: Heatmap of Pearson's correlation coefficients (r-values) for "knee joint loading indices vs. subregional cartilage thickness (Cart.Th) and subregional medial-to-lateral Cart.Th ratios". The reported r-values are significant (Benjamini-Hochberg adjusted, false discovery rate = 0.05). AM: anteromedial, AL: anterolateral, PM: posteromedial, PL: posterolateral, KFM: knee flexion moment, KEM: knee extension moment, KAM: knee adduction moment, ERM: external rotation moment, IRM: internal rotation moment, MAD: mechanical axis deviation.

4.3.3 Relationships between tibial cartilage thickness ratios and knee joint loading indices

When considering the medial-to-lateral cartilage thickness ratios, strong negative associations were found with MAD (Figure 4.4 and Figure 4.5c) and positive associations with ERM (Figure 4.4 and Figure 4.5b). The strongest associations were found between the M:L Cart.Th ratio and MAD ($r = -0.75$, $p<0.001$) and between the PM:PL Cart.Th ratio and ERM ($r = 0.65$, $p=0.001$). No significant associations were found between the remaining joint loading indices and medial-to-lateral cartilage thickness ratios.

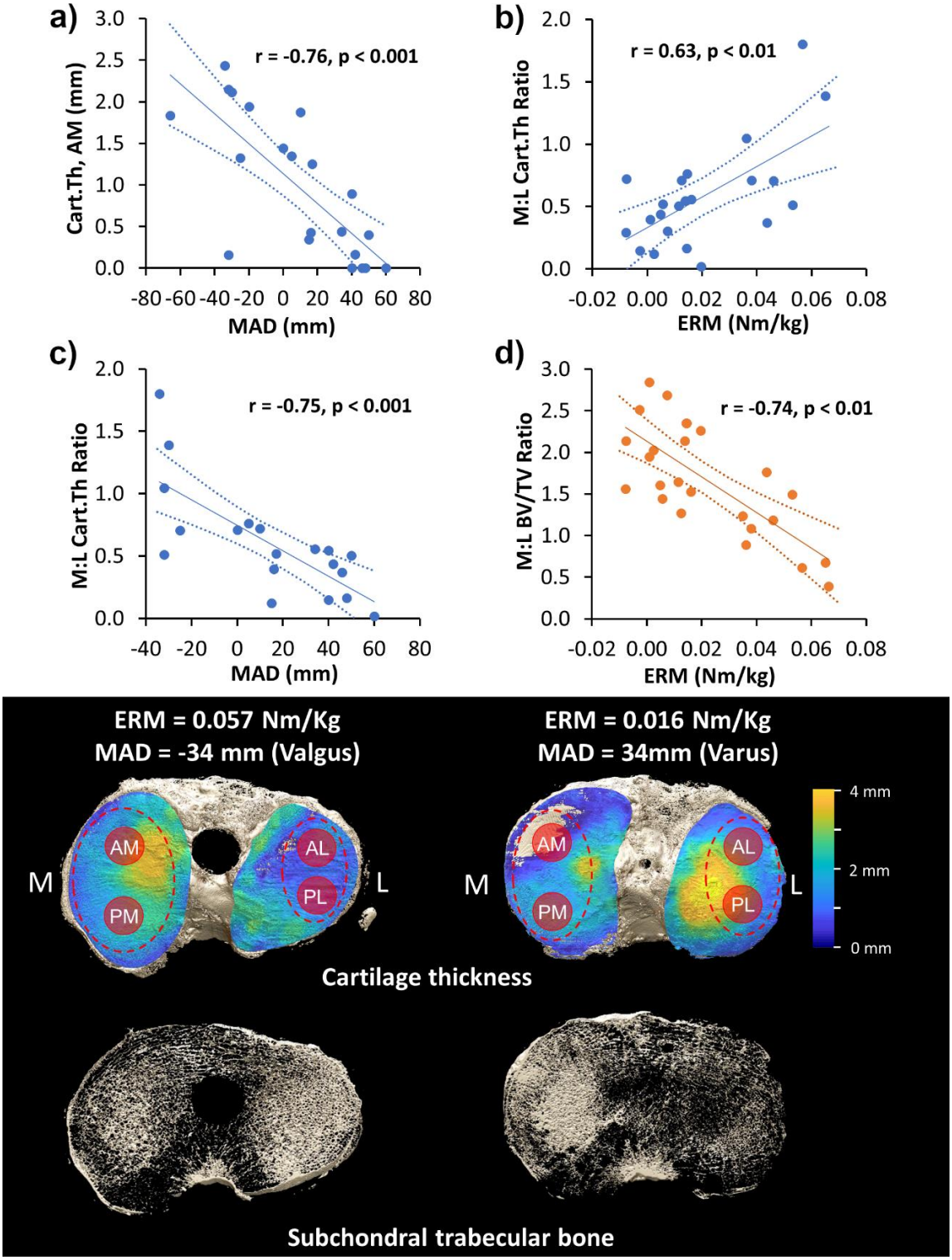

Figure 4.5: Top: Scatter plot with line of best fit (solid line) and 95% confidence interval (dashed lines) for Pearson's Correlation a) "AM Cart.Th vs MAD", b) "M:L Cart.Th vs ERM", c) "M:L Cart.Th vs MAD" and d) "M:L BV/TV vs ERM". The scatterplot in d) has been reprinted from Osteoarthritis and Cartilage with permission from Elsevier (Roberts et al. 2018). Bottom: Micro-CT 3D rendering of representative osteoarthritic tibial plateaus showing cartilage thickness map and micro-CT 3D rendering of a slice of underlying subchondral trabecular bone (white colour) for each specimen. AM: anteromedial, AL: anterolateral, PM: posteromedial, PL: posterolateral, L: lateral, M: medial, BV/TV: bone volume fraction, Cart.Th: cartilage thickness, ERM: external rotation moment, MAD: mechanical axis deviation.

4.3.4 Stepwise multilinear regression analysis

Joint loading indices which were significantly associated with cartilage thickness and/or medial-to-lateral cartilage thickness ratios (MAD, KFM, KAM2 and KAM Impulse) were forward entered into regression models for the prediction of AM Cart.Th and M:L Cart.Th ratio, with ERM, KAM1 and WS as covariates. The MAD explained an additional 19-20% of the variation in the AM Cart.Th model (final model: ERM, KAM1, WS, MAD; adjusted R^2 = 0.557, p=0.009) and an additional 23-24% of the variation in the M:L Cart.Th ratio model (final model: ERM, KAM1, WS, MAD; adjusted R^2 = 0.615, p=0.004) compared to these regression models without MAD (Table 4.2). The KFM, KAM2 and KAM Impulse did not significantly improve the models.

Table 4.2**:** Summary of multiple linear regression analysis, for prediction of AM Cart.Th and M:L Cart.Th ratio

Dependent Var.	Model	Unadj. R^2	Adj. R^2	ΔR^2	P-value
AM Cart.Th	ERM, KAM1	0.380	0.315		0.011
	ERM, KAM1, MAD	0.580	0.509	0.199*	0.009
	ERM, KAM1, WS	0.457	0.367		0.01
	ERM, KAM1, WS, MAD	0.642	0.557	0.185*	0.009
M:L Cart.Th	ERM, KAM1	0.406	0.336		0.012
	ERM, KAM1, MAD	0.649	0.583	0.243*	0.004
	ERM, KAM1, WS	0.468	0.368		0.016
	ERM, KAM1, WS, MAD	0.696	0.615	0.228*	0.004

The mechanical axis deviation (MAD), which was the joint loading index most strongly associated with the dependent variables, was forward entered into the regression models. Variables that influence the medial-to-lateral (ERM, KAM1) and/or medial condyle forces (WS, ERM, KAM1) were input as covariates. *Significant F-change, indicating MAD significantly improves prediction.

4.4 Discussion

This study investigated regional associations of tibial cartilage thickness in end-stage knee OA subjects with external knee joint moments and knee alignment. Joint loading indices (KAM, ERM and MAD) significantly correlated with regional cartilage thickness measurements, particularly in the regions with the thinnest (AM) and thickest (PL) cartilage, with ERM and MAD correlating with the medial-to-lateral cartilage thickness ratios. Joint loading indices combined further explained the variation of AM Cart.Th and M:L Cart.Th ratio.

The cartilage thickness in the anteromedial region was significantly associated with MAD and most of the external knee joint moments investigated (KAM Impulse, KAM1, ERM and peak KAM). The strongest correlation was between AM Cart.Th and MAD (r = -0.76), where to a variation from a valgus to varus knee alignment corresponded a thinner cartilage thickness anteromedially (Figure 4.5a). Similarly, all medial-to-lateral cartilage thickness ratios were negatively and significantly associated with MAD (r = -0.60 to -0.75; Figure 4.4, Figure 4.5c). This supports previous studies that have linked knee joint malalignment with altered medial-to-lateral distribution of loads upon the joint (Adouni *et al.*, 2014b, Roberts *et al.*, 2017b, Han *et al.*, 2020).

Positive correlations were found in the AM region between cartilage thickness, KAM1 and the peak KAM, but not so in the PM region. As a larger KAM magnitude could be indicative of higher medial joint loading compared to lateral (Zhao *et al.*, 2007), this could suggest the thinning of cartilage medially to be due to higher medial habitual loads compared to lateral in knee OA, or to some areas of cartilage being exposed to loads they are unaccustomed to. This is consistent with Creaby *et al.* (2010) who found the peak KAM to be associated with the severity of medial tibiofemoral cartilage defects assessed using MRI. Moreover, in our study the KAM impulse was negatively associated with cartilage thickness in the AM (r = -0.55) and M (r = -0.50) regions. This supports previous *in vivo* reports of a higher magnitude KAM impulse being associated with a greater loss of cartilage volume in the medial tibial condyle over 12 months in medial knee OA (Bennell *et al.*, 2011, Maly *et al.*, 2015).

Interestingly, the ERM was correlated with all medial-to-lateral Cart.Th ratios (r = 0.53 to 0.65), in addition to the regional cartilage thickness in PL (r=-0.58), L (r=-0.54), AM (r=0.52) and M (r=0.51) (Figure 4.4, Figure 4.5). To the best of the authors' knowledge, relationships between ERM and cartilage thickness have not yet been reported in knee OA. In our previous study (Roberts *et al.*, 2018), the underlying subchondral trabecular bone and the medial-to-lateral bone volume fraction (BV/TV) ratios were significantly associated with the ERM, particularly for AM BV/TV (r = -0.74) and the M:L BV/TV ratio (r = -0.74). However, the relationships between gait parameters and cartilage thickness found in the present study have the opposite sign compared to those of the same gait parameters and the underlying subchondral bone BV/TV, on the same specimens (Figure 4.5d). As altered rotation mechanics lead to shifts in the tibiofemoral contact regions (Andriacchi *et al.*, 2004, Hatfield *et al.*, 2011), reductions in ERM may indicate increased

stress concentrations in the AM region, resulting in the wearing down of cartilage and increase of underlying subchondral bone in that region.

In a previous study by our group focussing on subchondral bone in the same specimens, in multiple linear regression models it was found that ERM significantly improved predictions of AM BV/TV and the M:L BV/TV ratio when controlling for MAD, KAM1 and WS (Roberts *et al.*, 2018). However, in this study, for predictions of the overlying AM cartilage thickness and the M:L cartilage thickness ratio, the ERM did not significantly improve the model. Instead, the MAD, which was most strongly associated with AM cartilage thickness (r = -0.76) and the M:L ratio (r = -0.75), explained additional variations in the multiple linear regression models when controlling for ERM, KAM1 and walking speed. Hence, whereas the addition of the ERM improves the prediction of the underlying BV/TV, addition of the MAD improves the prediction of cartilage thickness in end-stage tibial OA.

As hypothesized, the AM and M cartilage thickness correlated well with KAM1, ERM and MAD. However, a surprising finding was that the PL and L regions had similar, if not stronger, correlations with KAM, KAM1 and ERM compared to the AM and M regions, with the opposite sign. Conversely, two previous studies (using MRI for quantifying cartilage thickness) found no relationship between tibial lateral cartilage thickness in late-OA and KAM (Vanwanseele *et al.*, 2010, Erhart-Hledik *et al.*, 2015). This may be because the present study included specimens with a wide range of mechanical axis deviation (ranging from varus to valgus), revealing a correlation over a broader range of specimens, whereas Erhart-Hledik et *al.* (2015) investigated patients with medial-OA (typically varus-aligned). Vanwanseele et *al.* (2010), while including both medial- and lateral-OA in their study, had a small sample size (n=6) with a smaller range of cartilage thickness (1.83±0.33 mm) compared to this study (1.62±0.86 mm).

A characteristic of this study is the spatial resolution used (isotropic voxel size of 17 μm) on entire human tibial plateaus. Micro-CT enables scanning of *ex vivo* human tibial plateaus at high spatial resolution, in comparison to previous studies on cartilage using MRI, which can range from 140x140x1500 μm to 310x310x1500 μm (Eckstein *et al.*, 2008, Vanwanseele *et al.*, 2010, Erhart-Hledik *et al.*, 2015, Maly *et al.*, 2015). This higher resolution may also explain significant correlations between cartilage thickness and gait parameters in OA found in this study, that were not found in other studies (such as with medial and lateral cartilage thickness and ERM and KAM).

It is worth mentioning that in this study, when examining the relationships between articular cartilage thickness and gait parameters, there were specimens with denuded areas of cartilage (regional cartilage thickness = 0 mm for some specimens). The tibial plateaus were collected from patients with end-stage knee OA. As such, particularly in the anterior medial region, there were areas of little to no cartilage. Once there is no cartilage left, any additional loading or progression of OA, cannot further reduce the cartilage. This resulted in some 0 mm values in the regional cartilage thickness data for some specimens, which in some cases weakened the statistical correlations between cartilage thickness and the joint moments. Similarly, as cartilage is unlikely to grow back naturally, if the patient had modified their gait pattern over time, reducing the load on an area of the tibial plateau, this would unlikely be reflected in the cartilage thickness, particularly in end-stage OA (i.e. the cartilage would unlikely increase in thickness, with reduced load). Conversely, in regions where cartilage degrades, the underlying bone may adapt to loading, increasing its density. In the same specimens, this could explain why in most instances, joint moments had similar or stronger correlations with the underlying trabecular BV/TV (found in a previous study by our group, focusing on bone (Roberts *et al.*, 2018)) than with cartilage thickness found here. E.g. ERM was strongly positively correlated with BV/TV in the AM region (r = -0.74) but less so, although negatively, with cartilage thickness (r = 0.52). Similarly for the medial-to-lateral ratios, the KAM, KAM1, KAM2, KAM Impulse and IRM were significantly correlated with medial-to-lateral BV/TV ratios (previous study), but not with medial-to-lateral cartilage thickness ratios here.

In a recent study conducted by our group in a young healthy cohort, whole joint loading (ERM, KFM and KAM2) explained 60% of the variation of PM:PL volumetric bone mineral density (vBMD) measured *in vivo* (Thewlis *et al.*, 2021). The same gait parameters correlated with the cartilage thicknesss and/or with the medial-to-lateral cartilage thickness ratios in the present study. Hence, the vBMD measured with pQCT *in vivo*, could be a useful marker in monitoring the progression of OA and the effects of treatments aimed at altering joint loading. Future studies may also monitor the progression of OA *in vivo* at high resolutions using contrast-enhanced HR-pQCT (Michalak *et al.*, 2019), through the analysis of underlying subchondral bone microarchitecture, joint space width and articular cartilage. Where the role of the KAM in OA has been documented in the literature, further investigation on the role of ERM on knee morphology during the progression of OA is needed.

4.5 Conclusion

In knees of people with end-stage knee OA, joint loading indices (such as KAM, ERM and MAD) significantly correlated with regional cartilage thickness variations and the medial-to-lateral cartilage thickness ratios. Interestingly, these relationships have the opposite sign compared to those for the underlying subchondral bone microarchitecture found in a previous study by our group on the same specimens; taken together, this may suggest a whole joint response to loading. These findings may contribute to improve understanding of OA and development of targeted treatment options.

Chapter 5
Study 3: Systematic mapping of cartilage and subchondral bone in human tibial controls and osteoarthritis using micro-computed tomography

Chapters 3 and 4 (Studies 1 and 2, respectively) highlighted that in knee OA, tibial plateau regions with thinner cartilage had a corresponding higher amount of BV/TV underneath, compared to other regions within the tibial plateau. Moreover, relationships between cartilage thickness and external knee joint moments had the opposite sign compared to those between subchondral bone microarchitecture and same knee joint moments found in a previous study by our group on the same specimens, suggesting a complementary bone-cartilage interplay in response to loading. However, these relationships between cartilage and bone have not yet been explored systematically.
In this chapter, a dense mapping (22 ROIs per tibia) of the tibial cartilage and underlying subchondral bone morphometric parameters in OA and control subjects will be performed, and region-specific relationships between these parameters investigated.

The study presented in this chapter is in preparation for submission as a manuscript to a peer-reviewed journal:

Rapagna S, Roberts BC, Muratovic D, Solomon LB, Reynolds KJ, Thewlis D, Perilli E. Systematic mapping of cartilage and subchondral bone in human tibial controls and osteoarthritis using micro-computed tomography. 2021. *In Preparation.*
Please refer to the Appendix at the end of this thesis for a detailed outline of the author's contribution to this study.

5.1 Abstract

Tibial cartilage and bone act as a functional unit, responding to daily stimuli together. Nevertheless, relationships between the cartilage thickness and underlying bone microarchitecture, and whether they differ between osteoarthritic (OA) and healthy joints, has not yet been fully understood. In this study, a systematic mapping of the cartilage and subchondral bone of the tibial plateau (22 sub-regions) was performed in OA knees and in controls. 26 osteoarthritic tibial plateaus (from knee arthroplasty; n=16 varus-aligned OA and n=7 non-varus-aligned OA) and 15 cadaveric tibial plateaus without OA (controls) were micro-CT scanned (17 µm/voxel). Cartilage thickness (Cart.Th), subchondral bone plate thickness (SBPl.Th), porosity (SBPl.Po) and subchondral trabecular bone volume fraction (BV/TV) were analyzed in 22 sub-regions across the tibial condyles. For each tissue, within-condyle and between-condyle (medial-to-lateral) regional differences were evaluated in each group. Region-specific relationships between cartilage thickness and subchondral bone parameters were investigated. In controls, Cart.Th, SBPl.Th and BV/TV were lowest in the external regions and highest in the central and anterior regions. In the varus-aligned OA group, however, the cartilage was thinnest anteriorly in the medial condyle with high underlying SBPl.Th and BV/TV. In the non-varus-aligned OA group, the cartilage distribution was similar to controls, but with higher underlying SBPl.Th and BV/TV. Interestingly, whereas in controls almost no relationships were found between cartilage thickness and the underlying subchondral bone, significant negative correlations were found (Cart.Th vs SBPl.Th, Carth.Th vs. BV/TV) in the OA group. Micro-CT allows for a systematic mapping of the cartilage and subchondral bone of entire tibial plateaus, which revealed region-specific differences within and between condyles, and region-specific relationships among these tissues.

5.2 Introduction

Knee OA is a degenerative disease affecting approximately 654 million individuals worldwide (Cui *et al.*, 2020) with consequent physiological and economic burdens (Gupta *et al.*, 2005, Litwic *et al.*, 2013, Chen *et al.*, 2020, Gwynne-Jones *et al.*, 2020). The disease affects the entire synovial joint, including the articular cartilage and underlying subchondral bone (Radin *et al.*, 1986, Goldring *et al.*, 2010, Loeser *et al.*, 2012). Cartilage and bone are thought to form a functional unit, responding to daily stimuli together (Ding *et al.*, 1998, Imhof *et al.*, 2000). However, the region-specific relationships between the cartilage thickness and the underlying bone microarchitecture, and whether these may differ between osteoarthritic and healthy tibial plateaus, has not yet been fully investigated.

In the literature, relationships between tibial cartilage thickness and subchondral bone assessed using magnetic resonance imaging (MRI) and dual energy X-ray absorptiometry (DEXA) are conflicting (Bolbos *et al.*, 2008, Cao *et al.*, 2014, Liu *et al.*, 2018). Cao et al. (2014) found no relationships between cartilage thickness and subchondral bone mineral density in OA. However, Bolbos et al. (2008) found positive correlations between cartilage thickness and apparent BV/TV in mild-OA. Liu et al. (2018) also found positive correlations, but in a dataset combining controls and OA; whereas Lindsey *et al.* (2004) found a slight negative correlation in the medial condyle in OA. These discrepancies may be attributed to use of DEXA for bone analysis (limited to bone and 2D measurements) and MRI for cartilage and bone microarchitecture analysis (which may not be appropriate due to the low spatial resolution). Indeed, in histology studies on tibiae, BV/TV was found to significantly increase with the grade of cartilage degeneration (assessed using Mankin's score (Mankin *et al.*, 1971)) (Matsui *et al.*, 1997, Bobinac *et al.*, 2003). Moreover, the above studies were either limited to one region of interest per condyle (Lindsey *et al.*, 2004, Bolbos *et al.*, 2008, Cao *et al.*, 2014), multiple regions of interest (medial and lateral) pooled together for analysis (Matsui *et al.*, 1997, Bobinac *et al.*, 2003) and/or various stages of OA (Lindsey *et al.*, 2004) and control datasets grouped together (Bobinac *et al.*, 2003, Liu *et al.*, 2018), which might mask some relationships. Investigating region-specific relationships using high resolution imaging, from a dense mapping of the tibial plateau instead, might provide new insights into the pathological changes that occur in OA.

Micro-CT is capable of such detailed analysis (see Chapter 3; Rapagna *et al.*, 2021a). Previously, in the tibial plateau in late-stage OA (11 regions per condyle), using micro-CT (Roberts *et al.*, 2017b), our group showed regional heterogeneity in the subchondral bone microarchitecture, with region-specific associations between cortical bone plate and the underlying trabecular bone. However, it is unknown if these correlations are a feature of OA, or if these exists also in controls. Moreover, that systematic mapping study did not consider cartilage. In recent years, however, micro-CT has increasingly been used for the concurrent 3D analysis of the cartilage and bone of entire human tibial plateaus at high spatial resolutions (Chen *et al.*, 2018, Gatenholm *et al.*, 2019, Rapagna *et al.*, 2021a). Gatenholm *et al.* (2019) found BV/TV to be lower in OA condyles with intact cartilage compared to those with deep cartilage defects, but did not consider controls. Other studies investigated differences among condyles in selected regions (Chen *et al.*, 2018, Rapagna *et al.*, 2021a), but a systematic mapping of the entire plateau using a dense grid, investigating region-specific correlations between the cartilage and bone, has not yet been performed.

The aims of this study were: 1) to perform, in micro-CT scans of entire human tibial plateaus from controls and OA, a systematic spatial mapping (22 regions) of the cartilage thickness and underlying subchondral bone morphology; and 2) to map the region-specific relationships in these parameters in control and OA groups.

5.3 Methods

5.3.1 Bone Specimens

Micro-CT scans in this study were used from our previous studies (Table 5.1) (Chapter 3; Rapagna *et al*., 2021a, Roberts *et al*., 2017b).

5.3.1.1 Control specimens

Briefly, 15 fresh-frozen cadaveric tibial plateaus (age: 61.6 ± 12.9 years; mass: 83.0 ± 15.6 kg) with no knee pathology were used as controls in this study (Science care, Inc.) (Chapter 3; Rapagna *et al.,* 2020a). After retrieval the tibial plateaus were stored fully submerged in 70% ethanol solution. Approval to use these specimens for research purposes was granted by the Southern Adelaide Clinical Human Research Ethics Committee.

5.3.1.2 OA specimens

26 osteoarthritic tibial plateaus were retrieved from patients (age: 68.1 ± 7.3 years, mass: 88.9 ± 18.4 kg, BMI: 31.8 ± 5.1 kg/m^2) with end-stage knee OA undergoing total knee replacement surgery (Chapter 3; Rapagna *et al.,* 2021a, Roberts *et al.,* 2017b). After retrieval, the tibial plateaus were stored fully submerged in 70% ethanol solution.

Approval to use these specimens for research purposes was granted by the Southern Adelaide Clinical and Royal Adelaide Hospital Human Research Ethics Committees. All patients gave written informed consent.

5.3.1.3 Mechanical axis deviation

In the OA group, the mechanical axis deviation (MAD) was measured from preoperative long leg weight-bearing radiographs by an experienced examiner (LBS). The MAD was defined as the perpendicular distance from the mechanical axis to the centre of the knee joint (Paley, 2002). A varus alignment was defined as a medial deviation greater than 15 mm, neutral alignment as 0-15mm deviation and a valgus alignment was defined as a lateral deviation greater than 0 mm (Paley, 2002, Roberts *et al.*, 2017b).

The OA tibial plateaus were subdivided into the varus-OA group (n=16, age: 66.9 ± 7.5 years, mass: 89.1 ± 20.0 kg, BMI: 31.5 ± 5.7 kg/m^2) and the non-varus-OA group (valgus-OA (n=7) and neutral specimens (n=3), age: 70.0 ± 6.9 years, mass: 88.6 ± 16.6 kg, BMI: 32.3 ± 4.2 kg/m^2).

Table 5.1: Summary of subject characteristics

Parameters	Controls	End stage knee OA subgroups		*p* value
	Non-OA (n = 15)	Varus-OA (n = 16)	Non-Varus-OA (n = 10)	
Age	61.6 ± 12.9 years	66.9 ± 7.3 years	70.0 ± 6.9 years	0.295
Mass	83.0 ± 15.6 kg	89.1 ± 20.0 kg	88.6 ± 16.6 kg	0.234
BMI		31.5 ± 5.7 kg/m^2	32.3 ± 4.2 kg/m^2	0.657
Knee		34.5 ± 17.2 mm	-22.4 ± 22.6 mm	<0.001

Values reported as average ± standard deviation; a Kruskal-Wallis test was performed to compare between the varus-OA, non-varus-OA and control groups for age and body mass. A Mann-Whitney U-test was used to compare between the varus-OA and non-varus-OA groups for BMI and knee alignment, significance denoted by p<0.05. *Knee alignment determined from mechanical axis deviation (MAD), where positive deviations are indicative of a medial deviation and negative values indicate a lateral deviation.

5.3.2 Micro-CT Imaging

The excised tibial plateaus then underwent micro-CT imaging in pairs using a desktop micro-CT scanner (Skyscan 1076, Skyscan-Bruker, Kontich, Belgium) as described previously (Chapters 3, 4; Rapagna *et al.*, 2021a, Rapagna *et al.,* 2021b, Roberts *et al.,* 2017b). Briefly, excised tibial plateaus were removed from the ethanol solution and wrapped separately in plastic cling film. The tibial plateaus were scanned in pairs, separated by a layer of polystyrene along their resected surfaces and secured to the scanning bed using elastic bands. The medial-to-lateral axis of the specimens were aligned to the rotation axis of the micro-CT system.

Specimens were scanned at 17.4 μm isotropic voxel size using a peak voltage of 100 kVp, 90 μA current, 0.4° over 180° rotation step, 590 ms exposure time and four frames averaging. A filtered back-projection algorithm was used to reconstruct the cross-section images (NRecon software, v1.6.9.8, Skyscan-Bruker) which were saved in 8-bmp format with 256 gray-levels (bmp value of 0 = air; 255 = mineralized tissue). The reconstructed dataset was 70 GB, consisting of a stack of up to 4,997 consecutive cross-section images (86.9 mm in length) with a slice thickness of one pixel (17.4 μm) (Roberts *et al.*, 2017b). These cross-section images were then rotated in 3D to align the anatomical superior-inferior axis of each plateau with the z-axis of the image stack (Chapters 3, 4; Rapagna *et al.*, 2021a, Rapagna *et al.,* 2021b, Roberts *et al.,* 2017b).

After scanning, the specimens were unwrapped (clingwrap removed) and stored immersed in 70% ethanol solution.

5.3.3 Cartilage

Cartilage segmentation was performed semi-automatically on the coronal image stacks of the specimens as described previously (Chapters 3, 4; Rapagna *et al.*, 2021a, Rapagna *et al.,* 2021b), derived from methods published in the literature (Buie *et al.*, 2007, Xie *et al.*, 2009, Gatenholm *et al.*, 2019, Ylitalo *et al.*, 2019).

A “bone and marrow” mask was first created using a custom MATLAB script (2017b, The MathWorks, Inc., Massachusetts, USA) on the segmented subchondral bone plate coronal dataset (Section 5.3.4). This mask extended from the superior surface of the subchondral bone plate to the resected surface of the tibial plateau, encompassing the subchondral bone and marrow. The inverse mask, containing only non-calcified cartilage and air, was then applied to the coronal image stack (software CTAnalyser, Skyscan Bruker, Kontich,

Belgium). The cartilage was then segmented using a threshold window determined from the gray-level histograms over five specimens and applied consistently over all specimens. I.e. a threshold window of 18 ("air/cartilage" threshold) to 87 ("cartilage/bone" threshold) which excluded air and any bone debris respectively. The cartilage segmentation was manually verified every 15 slices (0.261 mm) and the "shrink-wrap" plug-in of CTAnalyser was applied to conform the boundaries of the region of interest (ROI) to the cartilage.

5.3.4 Subchondral bone plate

The subchondral bone plate was segmented according to as previous protocol by our group (Roberts *et al.*, 2017b). The bone tissue was segmented from the background (air, marrow and cartilage) by applying a uniform threshold (lower threshold level of 87 defined from the gray-level histograms over 5 representative specimens) across all specimens. This created a stack of coronal binarized images, where pixels representing bone tissue (gray-level values between 87 and 255) were segmented as solid, and those representing non-bone tissue (gray-levels 0 to 86) as background. Manually, the inferior surface of the subchondral bone plate was contoured every 15 images (0.261 mm) to remove any trabecular struts adjoining to the SBP. The "ROI shrink-wrap" plug-in was then applied to conform the ROI boundaries to the plate border.

5.3.5 Trabecular bone

The STB was defined from the inferior boundary of the previously saved SBP ROI extended down towards the growth plate for approximately 5 mm. The first 5 mm of the STB was investigated, as microarchitectural and bone mineral density differences in tibial condyles are most prominent within this distance (Patel *et al.*, 2003, Johnston *et al.*, 2010, Roberts *et al.*, 2017a).

From the saved cartilage, SBP and STB datasets, sub-volumes of interest (VOI) for morphometric analysis were then selected, as follows.

5.3.6 Regions of interest

For each tibial plateau, 22 cubic volumes of interest (VOIs; 5 mm in width and length, total height of approximately 7-8 mm, depending on the specimen) were selected per tibial plateau (11 VOIs per condyle). The location of each VOI was determined by a grid template normalised to an ellipse defining each condyle (Roberts *et al.*, 2017b) (Figure

5.1). This standardized approach ensured the same anatomical location for each region across specimens.

The height of the VOI varied based on the specimen, with each VOI containing the cartilage (up to 2-4 mm), the adjacent cortical SBP, and STB underneath (approximately ~5 mm) depending on the specimen to satisfy the continuum assumption for 3D morphometric analysis of trabecular bone (Harrigan *et al.*, 1984, Tassani *et al.*, 2013).

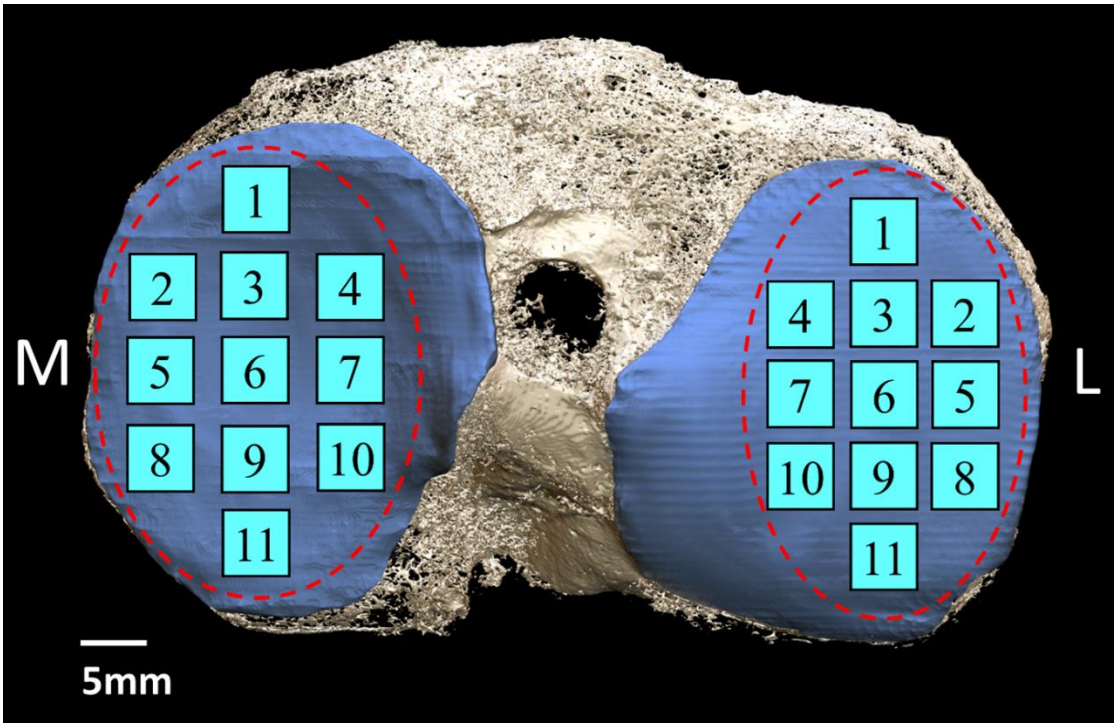

Figure 5.1: 3D representation of a right tibial plateau with the 22 cubic VOIs (5mm side length).

5.3.7 Morphometric analysis

From the micro-CT images, the following morphometric features were investigated in the 22 VOIs per tibial plateau using CTAnalyser: cartilage thickness (Cart.Th; mm), cortical SBP thickness (SBPl.Th; mm), cortical SBP porosity (SBPl.Po, %) and STB bone volume fraction (BV/TV, %). Cart.Th was an average measurement for each VOI, calculated by dividing the volume of voxels identified as non-calcified cartilage (mm^3) by the square cross-section area (5 x 5 mm^2) of each VOI (Chapters 3,4; Rapagna *et al.,* 2021a, Rapagna *et al*., 2021b). This approach was used instead of a 3D sphere-fitting thickness algorithm to prevent overestimations of cartilage thickness over the VOI in areas of partially denuded cartilage. The 3D SBPl.Th was computed using a sphere-fitting method to determine the average thickness of the corresponding SBP VOI, as done previously (Hildebrand *et al.*, 1997a, Perilli *et al.*, 2006, Roberts *et al.*, 2017b). The STB BV/TV was

calculated as the percentage voxels segmented as bone divided by the voxels constituting the examined STB VOI (Perilli *et al.*, 2012, Roberts *et al.*, 2017b).

5.3.8 Statistical Analysis

All morphometric parameters for each group (control, varus-OA, non-varus-OA) were tested for assumptions of normality (Shapiro-Wilk test of normality) and sphericity (Mauchly's test of sphericity). Where the assumption of sphericity was violated, the Greenhouse-Geisser correction was applied.

5.3.8.1 Regional comparisons

Differences in morphometric parameters among the 11 regions, the average value of these regions within each condyle, and between corresponding regions in the medial and lateral condyles, were assessed using two-way repeated measures ANOVA. If significant, the "between-condyle" and "within-condyle" differences were then investigated using one-way repeated measures ANOVA, followed by paired t-tests with Bonferroni adjustment for multiple comparisons. Statistical significance was set to $p < 0.05$. Statistical analyses were performed using SPSS Statistics 25 (IBM Corp, Armonk, NY).

5.3.8.2 Associations between cartilage and bone parameters

Region-specific relationships between Cart.Th, SBPl.Th and SBPl.Po and STB BV/TV for the control and OA group were examined using Pearson's correlations. Relationships between the average morphometric parameters per condyle were then investigated. Statistical significance was set to $p < 0.05$. Statistical analyses were performed using SPSS Statistics 25 (IBM Corp, Armonk, NY).

5.4 Results

The distribution of each investigated morphometric parameter among the 11 regions for each condyle for the control, varus-OA and non-varus-OA groups, is reported graphically in Figure 5.2 (colour map). Statistically significant differences among these 11 regions per condyle are reported in Supplementary Table 1 at the end of the chapter (Table S1).

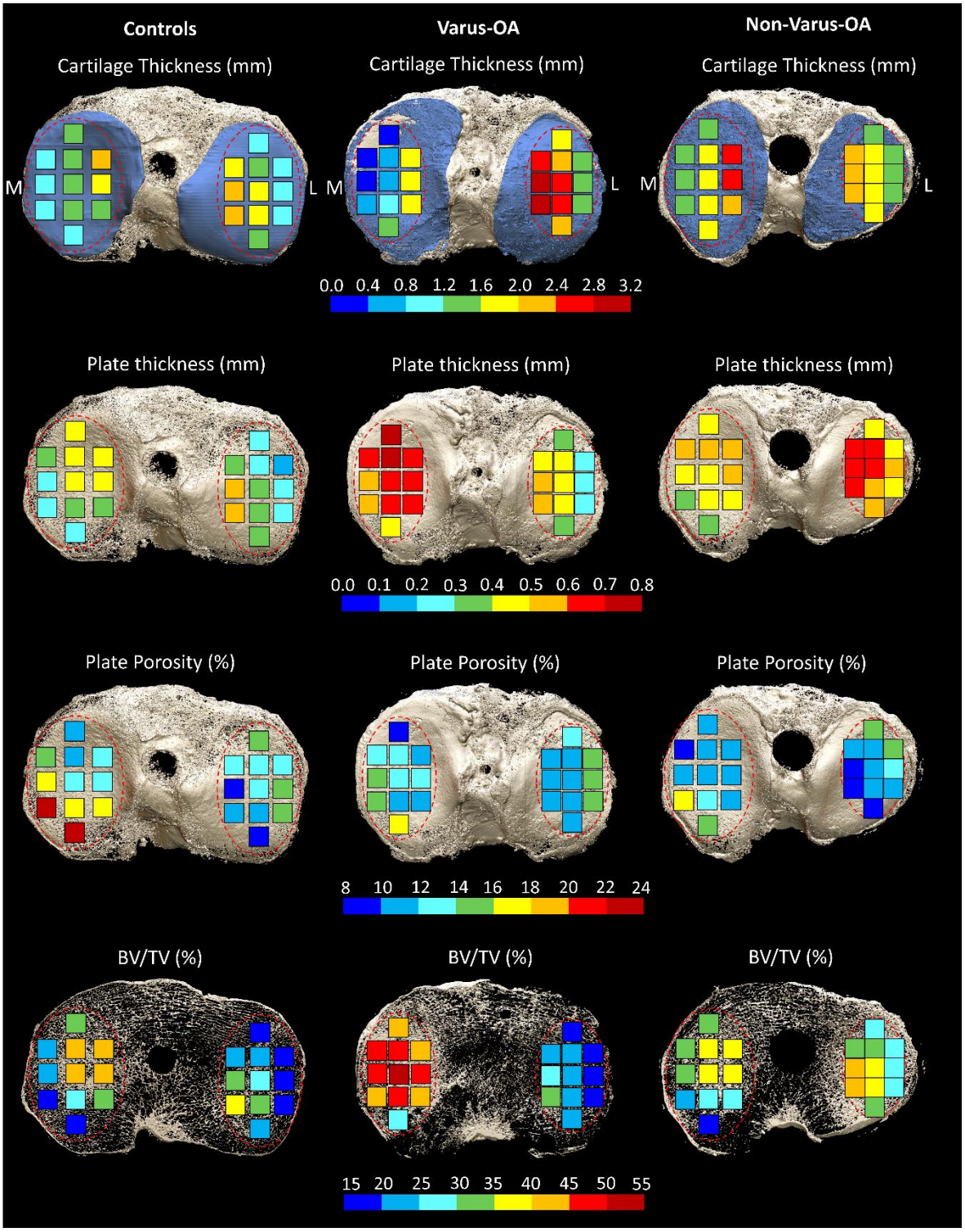

Figure 5.2: Colour heat map (11 regions per condyle), right tibial plateaus. Controls (left column), varus-OA (central column) and non-varus-OA (right column), regional distribution of: cartilage thickness (top row), subchondral bone plate thickness (second row), subchondral plate porosity (third row) and subchondral trabecular bone volume fraction (BV/TV, in %, bottom row). The values are averaged over the 15 controls, 16 varus-OA and 10 non-varus-OA tibial plateaus investigated.

5.4.1 Within-Condylar Differences in Cart.Th

In the control group (Cart.Th range 0.99-2.14 mm), in both the medial and lateral condyles, cartilage was significantly thinner in the external regions (ROIs 2,5,8) and thickest in the internal regions (ROIs 4,7,10), compared to the central condylar regions (ROIs 3,6,9; Figure 5.2; Table S1). In varus-OA (range 0.11-2.94 mm), medially, significantly thinner cartilage anteriorly and thicker internally (4,7,10,11) was found, compared to the rest of the condyle. In non-varus-OA (range 1.36-2.55 mm), laterally, no significant differences in cartilage thickness were found among the 11 ROIs. The medial condyle showed significantly thicker cartilage in the internal ROIs (4,7) compared to the majority of the other ROIs in the condyle.

5.4.2 Within-Condylar Differences in SBPl.Th

In the control group, the subchondral plate (range 0.20-0.48 mm) in the medial condyle was thinnest in the external regions (ROIs 5,8,9,11) and thickest anterior-centrally (ROIs 1,3,4,6,7; Figure 5.2; Table S1). In the lateral condyle, it was thickest in the inner regions (ROIs 7,10) and thinnest in the external regions (1,2,5,8). In varus-OA (range: 0.26-0.71 mm), medial condyle, the plate was significantly thicker anteriorly compared to the most posterior region (ROI 11); in the lateral condyle it was significantly thicker in the internal and central ROIs (2,4,6,7,9,10) compared to the external ROIs (1,2,5,8). In non-varus-OA (range 0.32-0.67 mm), medial condyle, the posterior ROIs 8 and 11 were significantly thinner than the central-interior ROIs 3,4,6,7.

5.4.3 Within-Condylar Differences in SBPl.Po

In controls, in the medial condyle, the plate porosity (range 8.81-23.1%) was significantly higher posteriorly (ROIs 8-11) than anteriorly (Figure 5.2; Table S1). In the lateral condyle it was significantly lower in ROIs 7 and 11 compared to the rest of the condyle. In varus-OA (range 9.04-16.0%), the medial condyle showed no significant differences among regions except for the most anterior (ROI 1, lowest porosity) and the most posterior region (ROI 11, highest porosity). Laterally, the external regions (2,5 and 8) showed highest porosity. In non-varus-OA (range 8.13-16.4%), no differences in porosity among regions were found, except ROI 8 showing higher porosity than 9 in the medial condyle, and ROI 5 higher than 11 in the lateral condyle.

5.4.4 Within-Condylar Differences in BV/TV

In the control group, the BV/TV (range 14.6-41.6%) in the medial condyle was significantly higher anterior-internally (ROIs 3,4,6,7; Figure 5.2; Table S1) and lower posterior-externally (ROIs 8,9). For the lateral condyle the BV/TV was highest posterior-internally (ROIs 7,10) and lowest externally (ROIs 1,2,5,8). In varus-OA (range 16.7-51.5%), medially, no significant differences among ROIs were found, except for ROI 11, which was significantly lower. Laterally, BV/TV was highest in ROI 10 and significantly lower in the external ROIs (1,2,5,8). In non-varus-OA (range 18.8-41.7%), medial condyle, significantly lower BV/TV in the posterior ROI 11 compared to the central-internal regions (ROIs 3,4,6,7,10) were found. In the lateral condyle no significant differences were found, aside from internal ROIs 7 and 10, which had higher BV/TV than ROIs 1 and 8, respectively.

5.4.5 Between-Condylar (Medial-to-Lateral) Differences in Cart.Th, SBPl.Th, SBPl.Po and BV/TV

The control group showed no significant differences in cartilage thickness between the medial and lateral condyles, apart from the posterior-internal ROIs (9,10) exhibiting thicker cartilage in the lateral condyle compared to medial (Figure 5.3). The SBPl.Th and BV/TV were significantly higher in the medial condyle compared to lateral anteriorly (ROIs 1-6), in the posterior ROI 11 and in the average per condyle. The SBPL.Po was significantly higher medially than laterally in the posterior ROIs 8-11 and in the average value per condyle.

In varus-OA, cartilage was significantly thinner in the medial condyle compared to lateral for all ROIs, except for the most posterior ROI (11, Figure 5.3). The SBPl.Th was significantly higher medially, except in internal posterior ROIs 6,7,10,11. The BV/TV was significantly higher for all ROIs medially than laterally. There were no significant differences in SBPl.Po between medial and lateral ROIs.

In non-varus-OA, no significant differences between medial and lateral condyles were found for Cart.Th, SBPl.Th, SBPl.Po or BV/TV, apart from ROIs 10 and 11 showing a higher SBPl.Th and ROI 2 higher SBPl.Po laterally than medially (Figure 5.3).

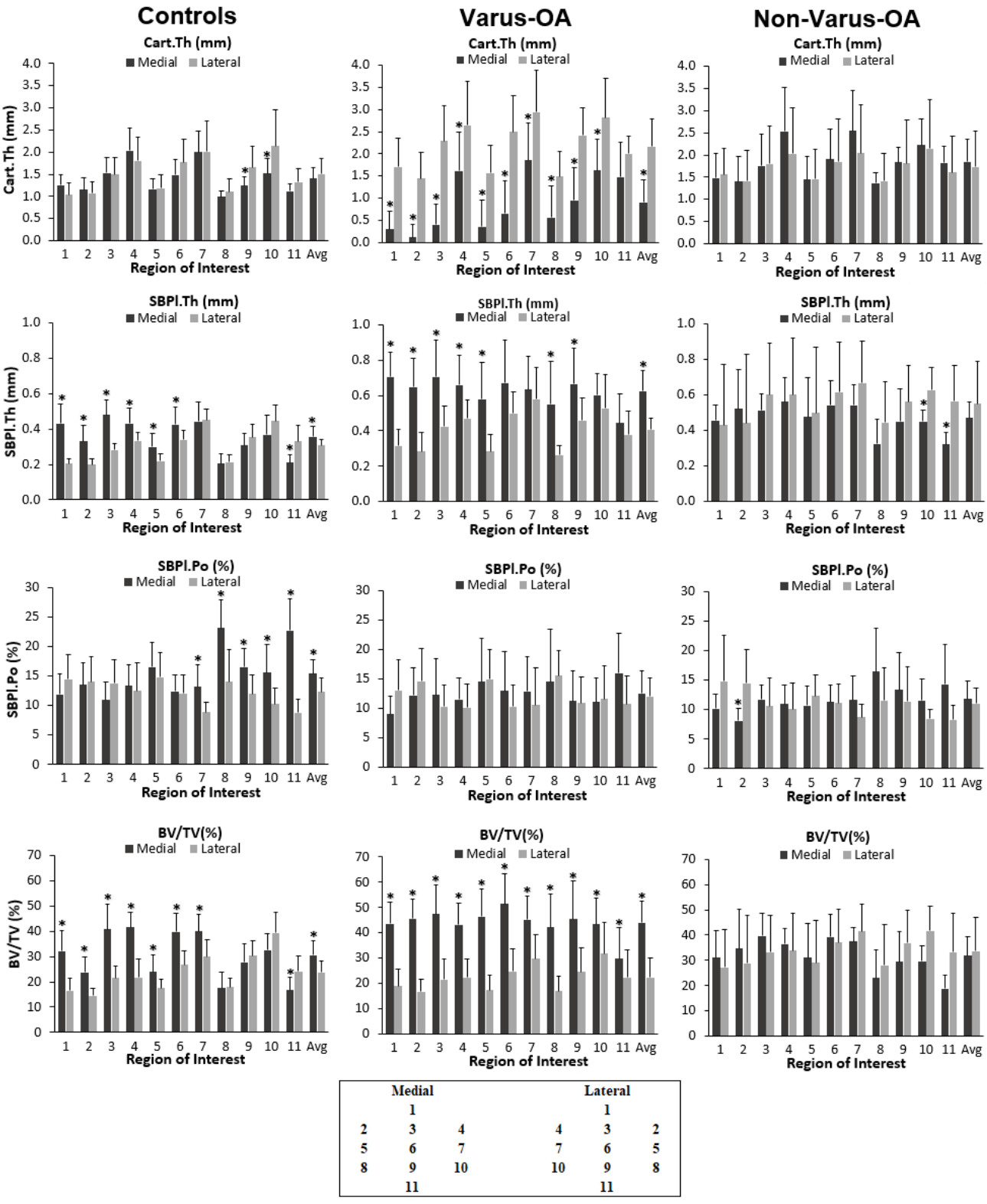

Medial			Lateral		
	1			1	
2	3	4	4	3	2
5	6	7	7	6	5
8	9	10	10	9	8
	11			11	

Figure 5.3: Bar graphs reporting average values and standard deviations (error bars) of Cartilage thickness (Cart.Th), subchondral bone plate thickness (SBPl.Th), plate porosity (SBPl.Po) and subchondral trabecular bone volume fraction (BV/TV) in the 11 subregions of interest within the medial and lateral tibial condyles of control, varus-OA and non-varus-OA groups.

5.4.6 Associations between Cart.Th and SBP and STB parameters

5.4.6.1 Associations between cartilage thickness and subchondral bone parameters

Region-specific associations between the investigated parameters were found, depending on the group (Table 5.2; Figure 5.4).

In the control group, cartilage thickness was not significantly associated with the underlying BV/TV, neither in the medial nor in the lateral condyle. In the OA group, however, significant negative associations were detected in several regions of the medial condyle (ROIs 1,2,5,6,8,9,11 and average value; Table 5.2) and lateral condyle (ROIs 3,4,6,9 and average value), being strongest in medial external ROIs (5,8,9; r= -0.67 to -0.78, $p<0.001$, Figure 5.4).

In controls, cartilage thickness was not correlated with the subchondral plate thickness, apart from one region medially (external, ROI 2) and one region laterally (anterior, ROI 3). In OA, several significant associations were found. These were all negative in sign and located predominately in the medial condyle (ROIs 1,2,5,6,8,10 and average value; Figure 5.4) compared to lateral (ROIs 3, 11 and average value).

In the control group, cartilage thickness was not correlated with plate porosity in any region, except for ROIs 2 and 11 of the medial condyle and the average value for the lateral condyle. In OA, cartilage thickness was not correlated with plate porosity in any region, apart from ROI 2 of the medial condyle.

5.4.6.2 Associations within the subchondral bone

The SBPl.Th and BV/TV were significantly positively correlated in the control and OA group, for most of the medial and lateral ROIs, as well as their average values (Table 5.2; Figure 5.4).

For controls and OA, the SBPl.Th and SBPL.Po were significantly negatively associated in several ROIs (11 and 15 regions, respectively), particularly so medially.

In controls, the SBPl.Po and BV/TV were negatively associated medially in ROIs 7 and 8, laterally in the external ROIs (2,5,8,9). In OA, the SBPl.Po and BV/TV were not correlated, apart from one single positive correlation in the lateral condyle anteriorly (ROI 4).

Table 5.2: Pearson's correlations for region-specific correlations between Cart.Th, SBPl.Th, SBPl.Po and BV/TV

CONTROLS (n=15)

Cart.Th vs. BV/TV

	Medial			Lateral	
	-.006			-.361	
.357	-.060	.374	.154	-.001	-.283
.402	.129	.014	.122	-.090	-.046
.346	.210	.155	-.229	-.143	-.135
	.193			.026	
Avg	.230		**Avg**	-.230	

Cart.Th vs. SBPl.Th

	Medial			Lateral	
	.198			-.109	
.746**	-.209	-.042	.455	**.555***	-.120
.284	.200	-.147	.230	.253	-.204
.479	.060	.193	-.003	.313	-.210
	.410			.256	
Avg	.010		**Avg**	.090	

Cart.Th vs. SBPl.Po

	Medial			Lateral	
	-.410			.353	
-.668*	-.074	-.266	.110	.273	.075
-.555	-.185	.110	.221	-.017	.322
-.217	.267	.319	.241	-.042	.122
	-.623*			-.032	
Avg	.080		**Avg**	**.544***	

SBPl.Th vs. BV/TV

	Medial			Lateral	
	.531			**.641***	
.541	.163	.490	.377	**.561***	**.668***
.714*	**.810****	**.588***	.457	**.708****	**.589***
.885*	**.704***	.465	**.731****	**.518***	.463
	.691*			.274	
Avg	**.677***		**Avg**	**.749****	

SBPl.Th vs. SBPl.Po

	Medial			Lateral	
	.721**			-.308	
-.617*	-.379	**-.669***	-.110	-.108	-.495
-.750**	-.445	**-.593***	-.117	-.336	**-.564***
-.767**	**-.525***	**-.616***	-.429	**-.579***	**-.674***
	-.646*			**-.601***	
Avg	**-.552***		**Avg**	-.089	

SBPl.Po vs. BV/TV

	Medial			Lateral	
	-.352			-.129	
-.331	-.259	-.184	.342	-.172	**-.471***
-.610*	-.427	-.359	.012	-.457	**-.590***
-.698*	-.001	-.160	-.404	**-.619***	**-.582***
	.010			-.412	
Avg	-.316		**Avg**	-.423	

OSTEOARTHRITIS (n=26)

Cart.Th vs. BV/TV

	Medial			Lateral	
	-.486*			-.388	
-.663**	-.371	-.287	**-.413***	**-.427***	-.319
-.669**	**-.506***	-.199	-.309	**-.420***	-.339
-.779**	**-.508***	-.389	-.217	**-.483***	-.338
	-.482*			-.483	
Avg	**-.605****		**Avg**	**-.450***	

Cart.Th vs. SBPl.Th

	Medial			Lateral	
	-.719**			-.377	
-.470*	-.370	-.040	-.319	**-.399***	-.339
-.416*	**-.434***	.312	-.222	-.247	-.355
-.715**	-.403	.006	.009	.086	-.345
	-.646**			**-.426***	
Avg	**-.464***		**Avg**	**-.471***	

Cart.Th vs. SBPl.Po

	Medial			Lateral	
	.264			.012	
-.502*	-.165	-.213	.118	.086	.021
-.389	-.101	-.290	.156	-.012	.100
.382	.026	-.053	-.018	-.222	.085
	.264			.155	
Avg	-.179		**Avg**	.282	

SBPl.Th vs. BV/TV

	Medial			Lateral	
	.513*			**.598****	
.520*	**.493***	-.013	.266	**.460***	**.750****
.578**	**.583****	.189	.360	**.450***	**.706****
.771**	**.485***	.208	**.500***	**.498***	**.767****
	.751**			**.777****	
Avg	**.499***		**Avg**	**.649****	

SBPl.Th vs. SBPl.Po

	Medial			Lateral	
	-.637**			**-.403***	
-.309	**-.726****	**-.669****	**-.414***	-.379	**-.413***
-.475*	**-.677****	**-.624****	**-.518***	**-.407***	-.369
-.740**	**-.700****	-.357	**-.669****	**-.470***	**-.393***
	-.491*			-.380	
Avg	**-.494***		**Avg**	-.256	

SBPl.Po vs. BV/TV

	Medial			Lateral	
	-.258			.072	
.279	-.290	.016	**.480***	.219	-.094
-.080	-.398	-.099	.291	.165	-.236
-.376	-.239	.159	-.089	.122	-.397
	-.207			-.239	
Avg	-.051		**Avg**	.044	

***p<0.05**

****p<0.005**

Medial			**Lateral**		
	1			**1**	
2	**3**	**4**	**4**	**3**	**2**
5	**6**	**7**	**7**	**6**	**5**
8	**9**	**10**	**10**	**9**	**8**
	11			**11**	

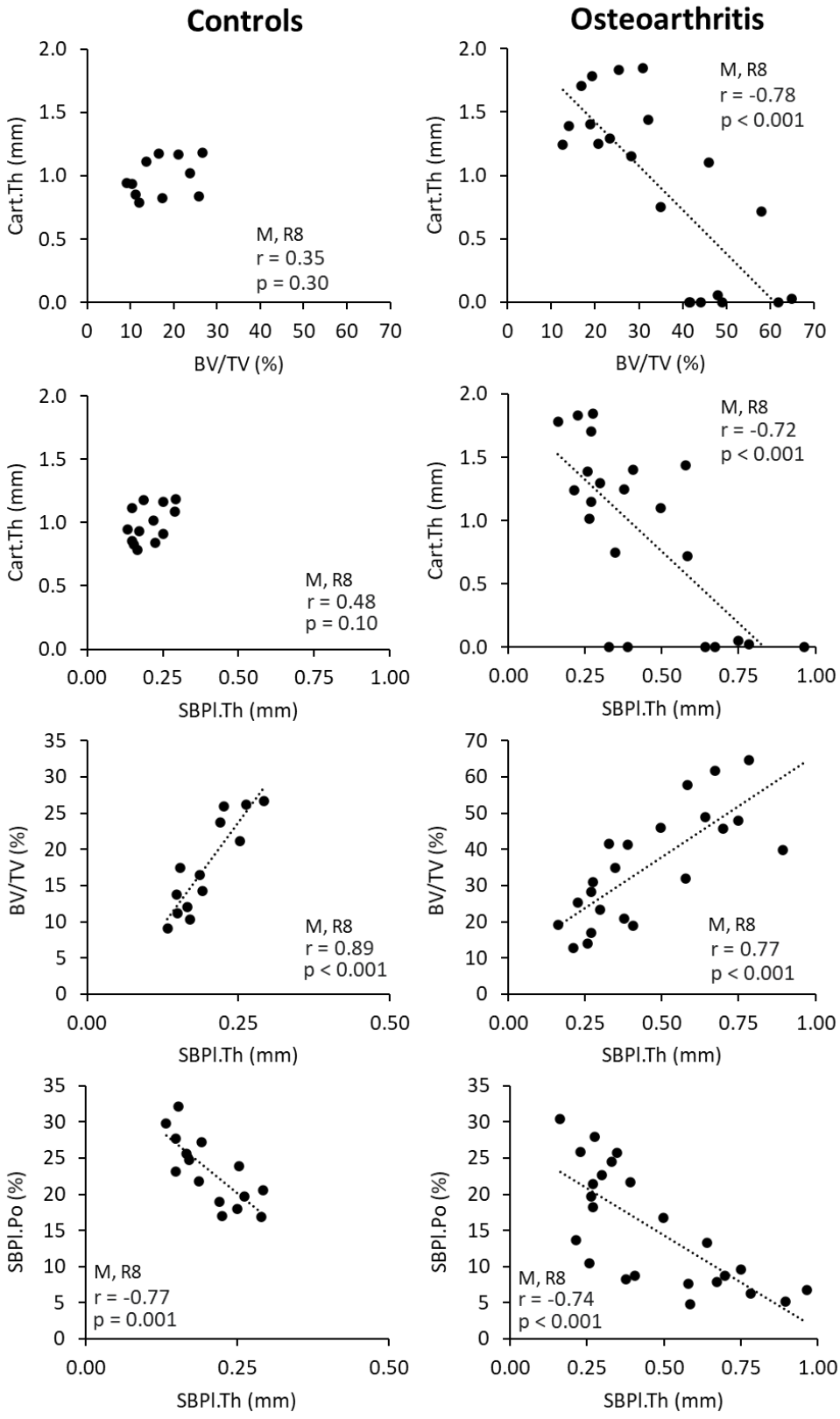

Figure 5.4: Scatter plots with line of best fit for region-specific correlations (medial condyle, ROI 8) between cartilage thickness (Cart.Th), subchondral bone plate thickness (SBPl.Th), subchondral bone plate porosity (SBPl.Po) and subchondral trabecular bone volume fraction (BV/TV), for control and OA group.

5.5 Discussion

In this study, a systematic spatial mapping over a dense grid of 22 sub-volumes for each tibia (11 per condyle), of the cartilage and underlying subchondral bone of entire human tibial plateaus was conducted, from micro-CT scans of 15 controls and 26 OA specimens. Region-specific differences were observed, in the within- and between- (medial-to-lateral) condyle comparisons, depending on the group. This mapping revealed significant negative region-specific relationships between the cartilage and bone tissues, which were present or not, depending on the group.

In controls, cartilage was thinnest in the external regions, thicker in the central regions and thickest internally. This pattern was consistent for both medial and lateral condyles and was similar in the underlying bone, where the SBPl.Th and BV/TV were lowest in the external regions, and highest in the central and internal regions. Similar patterns have been reported in non-OA subjects in MRI studies focussing on cartilage thickness (Favre *et al.*, 2017), and in the subchondral bone plate in a histological mapping study (Milz *et al.*, 1994). In varus-OA, the medial condyle tissue distribution differed the most to controls, showing thinner cartilage anteriorly and more bone throughout the condyle, consistent with the literature (Eckstein *et al.*, 2008, Han *et al.*, 2020, Renault *et al.*, 2020). In non-varus-OA, whereas the cartilage thickness followed a similar distribution pattern to the controls, the SBPl.Th and BV/TV were highest in the lateral condyle (Han *et al.*, 2020, Renault *et al.*, 2020).

In this study, cartilage thickness was found to be correlated with the subchondral bone plate and trabecular bone volume fraction in OA, but not in controls. In OA, these correlations had a negative sign (i.e. regions with less cartilage had higher SBPl.Th and BV/TV underneath) which is consistent with histology findings in OA specimens (Matsui *et al.*, 1997, Bobinac *et al.*, 2003). However, the negative correlations found here between the average values of the cartilage thickness, SBPl.Th and BV/TV differ from some other studies the literature (Bolbos *et al.*, 2008, Cao *et al.*, 2014). Cao et al. did not find any relationships, but this could be attributed to limitations in using DEXA (a 2D measure) for characterising bone microarchitecture. Whereas Bolbos et al. found positive relationships in patients with mild-OA; given that our specimens were from end-stage OA subjects, this could suggest different relationships between cartilage and bone during the progression of OA, although this would need further research.

Region-specific relationships found in OA between cartilage thickness, SBPl.Th and BV/TV were strongest in the external regions compared to the central weight-bearing regions of the medial condyle. This can be attributed to investigating end-stage OA, where the articular cartilage was completely denuded within these weight-bearing regions in some specimens. It is possible that these relationships would have been stronger earlier in the disease, when there was more cartilage present.

Interestingly, in controls, almost no correlations were found between cartilage thickness and the subchondral bone parameters (Table 5.2; Figure 5.3) in any region. Moreover, there were no medial-to-lateral differences in cartilage thickness. Whereas the SBPl.Th and BV/TV were significantly higher in the majority of medial regions compared to lateral, with significant correlations among them. This could be reflective of bone adaptation to higher habitual loading medially compared to laterally in controls. While we don't have the mechanical alignment of the control group, it can be expected based on a study of 5000 knees (Niu *et al.*, 2009), that the control group would have a neutral-to-slightly varus alignment, and thereby more medially loaded (Sharma *et al.*, 2010, Van Rossom *et al.*, 2019). The absence of correlations between cartilage and subchondral bone parameters, but presence of correlations within the subchondral bone, could also indicate that cartilage and bone respond differently to habitual loading in controls compared to OA; whereas cartilage might withstand (be accustomed) to a certain amount of everyday cyclic loading (Andriacchi *et al.*, 2009), the bone may adapt to the load by increasing BV/TV and SBPl.Th and reducing SBPl.Po. However, once OA is initiated, a cycle of degeneration starts, resulting in a localised cartilage degradation and increases in the underlying bone volume, in response to mechanical stimuli. This also suggests that for the monitoring of the onset and progression of OA, the subchondral bone could be a sensitive marker. Longitudinal studies on the alteration of subchondral trabecular bone in patients at-risk of OA, using high resolution peripheral quantitative CT (HR-pQCT), could provide valuable insights into the progression of the disease (Kroker *et al.*, 2017).

5.6 Conclusion

In this study, articular cartilage thickness, subchondral bone plate thickness, plate porosity and trabecular bone volume fraction were systematically mapped across the tibial condyles in controls and end-stage knee OA from micro-CT cross-section images.

This mapping revealed region-specific differences within and between condyles, depending on the group. Subchondral bone plate thickness and bone volume fraction were positively correlated in both controls and OA. Interestingly, cartilage thickness was found to negatively correlate with BV/TV in the medial and lateral condyles in OA, but not in controls. This suggests a cartilage and bone response in OA to habitual loading, which might be altered compared to controls. This systematic approach to mapping the tissues of the tibial plateau reveals patterns and region-specific relationships, which may be important in monitoring the progression of OA.

Table S1: Within-Condyle differences for the morphometric parameters in the 11 regions of interest in the medial and lateral condyle

Control

ROI	Cart.Th (mm)	Sig. diff. to ROI	SBPl.Th (mm)	Sig. diff. to ROI	SBPl.Po (%)	Sig. diff. to ROI	BV/TV (%)	Sig. diff. to ROI
Medial Condyle								
R1	1.26 ± 0.23 [0.75, 1.61]	3,4,6-8	0.43 ± 0.11 [0.25, 0.59]	5,8,9,11	11.9 ± 3.40 [6.92, 20.5]	8-11	32.2 ± 8.08 [22.3, 53.8]	2-8,11
R2	1.16 ± 0.27 [0.78, 1.73]	3,4,6,7,10	0.33 ± 0.09 [0.20, 0.54]	3,8,11	13.5 ± 3.69 [6.22, 22.2]	5,8,11	23.7 ± 6.22 [11.2, 34.4]	1,3,4,6-11
R3	1.53 ± 0.34 [0.91, 2.12]	1,2,4,5,7-9,11	0.48 ± 0.08 [0.36, 0.64]	2,5,8,9,11	10.9 ± 3.11 [7.98, 20.7]	5,8-11	40.8 ± 9.82 [28.5, 61.7]	1,2,5,8,9,11
R4	2.03 ± 0.51 [1.37, 3.05]	1-3,5,6,8-11	0.43 ± 0.09 [0.31, 0.56]	5,8,9,11	13.4 ± 3.52 [8.82, 21.5]	8-11	41.6 ± 5.77 [34.1, 53.4]	1,2,5,8-11
R5	1.16 ± 0.24 [0.81, 1.69]	3,4,6,7,10	0.30 ± 0.08 [0.19, 0.40]	1,3,4,6-8,11	16.5 ± 4.16 [10.8, 26.2]	2,3,6,8	23.9 ± 6.78 [10.4, 34.6]	1,3,4,6-11
R6	1.49 ± 0.34 [0.83, 2.02]	1,2,4,5,7-9,11	0.42 ± 0.10 [0.30, 0.65]	5,8,9,11	12.4 ± 2.87 [8.67, 19.3]	5,8,9,11	39.9 ± 7.20 [30.2, 56.8]	1,2,5,8-11
R7	1.99 ± 0.49 [1.25, 3.15]	1-3,5,6,8-11	0.44 ± 0.11 [0.26, 0.65]	5,8,9,11	13.1 ± 3.82 [8.82, 21.4]	8,9,11	40.0 ± 6.47 [26.6, 51.4]	1,2,5,8-11
R8	0.99 ± 0.14 [0.79, 1.18]	1,3,4,6,7,9-11	0.21 ± 0.05 [0.13, 0.29]	1-7,9,10	23.1 ± 4.73 [16.9, 32.1]	1-7,9,10	17.5 ± 6.47 [9.03, 26.7]	1-7,9,10
R9	1.25 ± 0.19 [0.94, 1.47]	3,4,6-8,10	0.31 ± 0.06 [0.21, 0.40]	1,3,4,6-8,11	16.5 ± 3.21 [10.9, 22.8]	1,3,4,6-8,11	27.8 ± 7.15 [17.9, 38.6]	2-8,10,11
R10	1.52 ± 0.32 [0.97, 2.13]	2,4,5,7-9,11	0.37 ± 0.11 [0.20, 0.65]	8,11	15.5 ± 4.79 [8.01, 23.3]	1,3,8,11	32.5 ± 6.44 [19.0, 42.8]	2,4-9,11
R11	1.12 ± 0.16 [0.87, 1.37]	3,4,6-8,10	0.21 ± 0.04 [0.13, 0.27]	1-7,9,10	22.7 ± 5.31 [15.8, 34.4]	1-4,6,7,9,10	16.7 ± 5.02 [8.56, 24.1]	1-7,9,10
Lateral Condyle								
R1	1.03 ± 0.28 [0.54, 1.57]	3,4,6,7,9,10	0.21 ± 0.03 [0.16, 0.24]	3,4,6,7,9-11	14.4 ± 4.16 [7.30, 20.9]	7,11	16.5 ± 4.69 [7.62, 23.8]	3,4,6,7,9-11
R2	1.07 ± 0.26 [0.75, 1.71]	3,4,6,7,9,10	0.20 ± 0.03 [0.14, 0.25]	3-7,9-11	14.0 ± 4.31 [8.09, 23.0]	7,11	14.6 ± 2.88 [7.41, 17.9]	3-11
R3	1.49 ± 0.39 [1.04, 2.22]	1,2,4,6,7,8,10	0.28 ± 0.04 [0.21, 0.34]	1,2,4-10	13.8 ± 4.00 [4.90, 19.7]	7,11	21.6 ± 4.85 [14.1, 29.8]	1,2,5,7,9,10
R4	1.81 ± 0.54 [0.72, 2.64]	1-3,5,8,11	0.33 ± 0.05 [0.25, 0.40]	1-3,5,7,8,10	12.5 ± 4.74 [3.92, 20.1]	7	21.8 ± 7.32 [12.8, 39.6]	1,2,6,7,9,10
R5	1.18 ± 0.31 [0.83, 1.89]	4,6,7,9,10	0.22 ± 0.04 [0.15, 0.29]	2-4,6,7,9-11	14.8 ± 4.27 [7.48, 24.9]	7,10,11	17.5 ± 3.32 [10.3, 21.5]	2,3,6,7,9-11
R6	1.77 ± 0.53 [1.14, 2.95]	1-3,5,7,8,10,11	0.34 ± 0.05 [0.24, 0.43]	1-3,5,7,8,10	12.0 ± 3.15 [4.21, 17.9]	7,11	26.7 ± 5.63 [16.8, 35.6]	1-5,8-10
R7	2.01 ± 0.70 [0.83, 3.38]	1-3,5,6,8,9,11	0.45 ± 0.06 [0.36, 0.56]	1-6,8,9,11	8.84 ± 1.66 [5.33, 11.4]	1-6,8,9	29.9 ± 6.89 [21.3, 48.6]	1-5,8,10
R8	1.10 ± 0.30 [0.72, 1.81]	3,4,6,7,9,10	0.21 ± 0.04 [0.14, 0.27]	3,4,6,7,9-11	14.0 ± 5.55 [6.84, 28.7]	7,11	18.0 ± 3.32 [10.5, 23.6]	2,6,7,9-11
R9	1.66 ± 0.47 [0.97, 2.66]	1,2,5,7,8,10,11	0.35 ± 0.07 [0.22, 0.45]	1-3,5,7,8,10	11.9 ± 3.31 [4.66, 17.4]	7,11	30.3 ± 5.89 [20.4, 39.1]	1-6,8,10,11
R10	2.14 ± 0.82 [0.79, 3.82]	1-3,5,6,8,9,11	0.44 ± 0.09 [0.31, 0.63]	1-6,8,9,11	10.3 ± 2.67 [5.87, 17.4]	5	39.3 ± 8.15 [28.3, 57.9]	1-9,11
R11	1.32 ± 0.31 [0.83, 1.97]	4,6,7,9,10	0.33 ± 0.09 [0.22, 0.53]	1,2,5,7,8,10	8.81 ± 2.27 [4.31, 13.7]	1-3,5,6,8,9	24.2 ± 6.18 [14.5, 36.7]	1,2,5,8-10

Varus-OA

ROI	Cart.Th (mm)	Sig. diff. to ROI	SBPl.Th (mm)	Sig. diff. to ROI	SBPl.Po (%)	Sig. diff. to ROI	BV/TV (%)	Sig. diff. to ROI
Medial Condyle								
R1	0.29 ± 0.40 [0.00, 1.06]	4,7,10,11	0.70 ± 0.14 [0.52, 0.99]	11	9.04 ± 3.00 [4.88, 14.3]	11	43.6 ± 8.69 [24.3, 59.3]	11
R2	0.11 ± 0.29 [0.00, 1.01]	3,4,6,7,9-11	0.65 ± 0.17 [0.46, 1.18]	11	12.2 ± 4.66 [5.08, 21.1]		45.7 ± 7.64 [36.8, 60.9]	11
R3	0.40 ± 0.46 [0.00, 1.53]	2,4,7,9-11	0.71 ± 0.21 [0.34, 0.99]	11	12.3 ± 6.16 [5.46, 23.5]		47.5 ± 11.5 [21.3, 69.3]	11
R4	1.61 ± 0.88 [0.01, 3.23]	1-3,5,6,8	0.66 ± 0.17 [0.43, 1.07]	11	11.5 ± 3.66 [5.36, 16.2]		43.2 ± 8.60 [23.5, 59.9]	6,11
R5	0.36 ± 0.60 [0.00, 1.71]	4,7,9-11	0.58 ± 0.21 [0.25, 0.98]		14.5 ± 7.30 [6.98, 29.8]		46.4 ± 10.9 [29.3, 62.4]	11
R6	0.65 ± 0.75 [0.00, 2.07]	2,4,7,9-11	0.67 ± 0.24 [0.24, 1.08]		13.0 ± 6.61 [3.84, 31.7]		51.5 ± 12.0 [28.3, 71.2]	4,10,11
R7	1.85 ± 0.83 [0.14, 3.17]	1-3,5,6,8,9	0.63 ± 0.19 [0.29, 0.94]		12.9 ± 5.91 [6.52, 29.9]		45.2 ± 9.20 [29.8, 60.7]	11
R8	0.56 ± 0.72 [0.00, 1.84]	4,7,9-11	0.55 ± 0.24 [0.23, 0.96]		14.7 ± 8.78 [4.75, 28.0]		42.2 ± 13.2 [19.0, 64.8]	11
R9	0.95 ± 0.73 [0.00, 1.99]	2,3,5-8,10,11	0.67 ± 0.20 [0.40, 1.08]	11	11.3 ± 5.13 [5.13, 23.2]		45.5 ± 15.0 [23.1, 74.9]	11
R10	1.62 ± 0.71 [0.29, 2.49]	1-3,5,6,8,9	0.60 ± 0.12 [0.35, 0.84]		11.1 ± 4.09 [6.94, 19.8]		43.5 ± 10.2 [29.3, 59.9]	6,11
R11	1.48 ± 0.78 [0.08, 2.50]	1-3,5,6,8,9	0.44 ± 0.17 [0.23, 0.84]	1,2,3,4,9	16.0 ± 6.71 [8.01, 31.6]	1	29.9 ± 12.1 [13.4, 50.8]	1-10
Lateral Condyle								
R1	1.70 ± 0.66 [0.00, 2.94]	2-4,6,7,9,10	0.31 ± 0.09 [0.18, 0.51]	3,4,6,7,9,10	13.1 ± 5.28 [6.01, 26.3]		18.9 ± 6.77 [7.15, 34.3]	4,6,7,9,10
R2	1.45 ± 0.59 [0.00, 2.42]	1,3,4,6,7,9-11	0.28 ± 0.11 [0.16, 0.57]	3,4,6,7,9,10	14.6 ± 5.49 [7.03, 23.5]	3,11	16.7 ± 4.96 [8.91, 26.6]	3,4,6,7,9,10
R3	2.29 ± 0.79 [0.00, 3.80]	1,2,5,7,8	0.42 ± 0.12 [0.27, 0.74]	1,2,5,7,8	10.3 ± 3.57 [5.55, 19.5]	2,5,8	21.5 ± 8.19 [10.2, 41.0]	2,5,6,7,8,9,10
R4	2.64 ± 0.98 [0.52, 4.75]	1,2,5,8	0.47 ± 0.10 [0.27, 0.68]	1,2,5,8	10.2 ± 3.94 [4.22, 22.5]	5,8	22.3 ± 7.37 [12.0, 40.5]	1,2,5,7,8,10
R5	1.57 ± 0.62 [0.00, 2.58]	3,4,6,7,9,10	0.28 ± 0.09 [0.20, 0.54]	3,4,6,7,9,10	15.0 ± 5.04 [9.34, 27.5]	3,4,6,11	17.3 ± 5.84 [9.98, 28.8]	3,4,6,7,9,10
R6	2.50 ± 0.81 [0.02, 4.05]	1,2,5,8	0.50 ± 0.12 [0.36, 0.74]	1,2,5,8	10.3 ± 3.70 [6.57, 21.8]	5,8	24.7 ± 9.10 [12.0, 46.9]	1,2,3,5,7,8,10
R7	2.94 ± 0.95 [1.09, 4.85]	1-3,5,8,11	0.58 ± 0.18 [0.21, 0.91]	1,2,3,5,8,11	10.5 ± 6.36 [5.33, 28.4]		29.8 ± 9.38 [16.6, 46.9]	1-6,8,9,11
R8	1.49 ± 0.57 [0.30, 2.32]	3,4,6,7,9-11	0.26 ± 0.06 [0.21, 0.41]	3,4,6,7,9,10,11	15.6 ± 4.30 [7.92, 22.5]	3,4,6,9,11	17.0 ± 5.93 [7.58, 27.8]	3,4,6,7,9,10,11
R9	2.42 ± 0.63 [0.96, 3.56]	1,2,5,8,11	0.46 ± 0.12 [0.32, 0.69]	1,2,5,8	10.9 ± 4.40 [5.04, 22.9]	8	24.6 ± 9.43 [12.9, 49.7]	1,2,3,5,7,8,10
R10	2.81 ± 0.89 [1.00, 4.74]	1,2,5,8,11	0.53 ± 0.19 [0.25, 0.80]	1,2,5,8	11.6 ± 5.57 [5.58, 23.0]		31.7 ± 12.6 [14.1, 51.3]	1-6,8,9,11
R11	2.00 ± 0.41 [1.26, 2.60]	2,7-10	0.38 ± 0.13 [0.23, 0.78]	7,8	10.7 ± 4.81 [4.55, 19.1]	2,5,8	22.4 ± 10.8 [9.97, 54.6]	7,8,10

Non-Varus-OA

ROI	Cart.Th (mm)	Sig. diff. to ROI	SBPl.Th (mm)	Sig. diff. to ROI	SBPl.Po (%)	Sig. diff. to ROI	BV/TV (%)	Sig. diff. to ROI
Medial Condyle								
R1	1.48 ± 0.56 [0.55, 2.25]	4,7,10	0.46 ± 0.09 [0.34, 0.59]		10.1 ± 2.51 [6.85, 13.6]		31.2 ± 10.6 [17.2, 52.1]	3
R2	1.40 ± 0.56 [0.23, 2.10]	4,6,7,9,10	0.52 ± 0.22 [0.28, 0.90]		8.13 ± 2.12 [5.54, 11.4]		34.6 ± 15.4 [15.5, 54.6]	
R3	1.76 ± 0.72 [0.03, 2.66]	4,7	0.51 ± 0.09 [0.41, 0.72]	8,11	11.8 ± 2.35 [8.28, 14.8]		39.8 ± 8.72 [27.7, 55.1]	1,8,11
R4	2.53 ± 0.99 [0.53, 3.85]	1-3,5,6,8	0.56 ± 0.13 [0.41, 0.79]	11	10.9 ± 3.16 [5.89, 15.7]		36.5 ± 6.16 [27.9, 47.2]	11
R5	1.44 ± 0.52 [0.13, 1.86]	4,6,7,10	0.47 ± 0.22 [0.27, 0.93]	8	10.7 ± 3.26 [7.65, 16.9]		31.2 ± 13.5 [18.7, 55.2]	8
R6	1.90 ± 0.68 [0.30, 2.65]	1,2,4,5,7	0.54 ± 0.14 [0.36, 0.75]	8,11	11.3 ± 2.93 [8.10, 17.6]		39.4 ± 8.90 [27.4, 53.6]	8,9,11
R7	2.55 ± 0.92 [0.70, 3.70]	1-3,5,6,8	0.54 ± 0.12 [0.36, 0.70]	8,10,11	11.6 ± 4.01 [7.92, 20.6]		37.5 ± 5.35 [28.2, 45.2]	10,11
R8	1.36 ± 0.24 [1.01, 1.78]	4,7,9-11	0.32 ± 0.14 [0.16, 0.58]	3,5-7,9	16.4 ± 7.37 [7.59, 30.4]	9	23.1 ± 11.1 [12.6, 46.1]	3,5,6,9
R9	1.84 ± 0.34 [1.29, 2.26]	2,8,10	0.45 ± 0.18 [0.23, 0.84]	8	13.4 ± 6.25 [6.63, 26.1]	8	29.4 ± 11.8 [16.2, 50.0]	6,8
R10	2.22 ± 0.59 [1.25, 2.86]	1,2,5,8,9	0.45 ± 0.07 [0.35, 0.53]	11	11.5 ± 3.73 [7.43, 17.8]		29.6 ± 6.10 [19.8, 36.5]	7,11
R11	1.83 ± 0.37 [1.20, 2.28]	8	0.32 ± 0.07 [0.22, 0.41]	3,4,6,7,10	14.3 ± 6.81 [7.16, 25.0]		18.8 ± 5.28 [12.2, 28.4]	3,4,6,7,10
Lateral Condyle								
R1	1.56 ± 0.58 [0.18, 2.23]		0.43 ± 0.34 [0.20, 1.32]	3,4,7	14.8 ± 7.82 [6.73, 31.7]		27.3 ± 14.9 [17.4, 56.8]	7
R2	1.41 ± 0.70 [0.01, 2.26]		0.44 ± 0.39 [0.18, 1.45]	5,7	14.5 ± 5.81 [6.66, 24.3]		28.8 ± 19.1 [10.9, 61.9]	
R3	1.80 ± 0.86 [0.00, 2.80]		0.60 ± 0.29 [0.32, 1.30]	1	10.6 ± 4.71 [5.85, 21.6]		33.2 ± 14.5 [17.1, 57.8]	
R4	2.04 ± 1.03 [0.18, 3.51]		0.60 ± 0.32 [0.37, 1.40]	1	10.1 ± 4.41 [5.70, 19.9]		33.9 ± 14.5 [17.7, 52.8]	
R5	1.45 ± 0.67 [0.02, 2.23]		0.50 ± 0.37 [0.27, 1.45]	2	12.3 ± 3.56 [8.19, 19.2]	11	29.1 ± 16.8 [14.6, 54.6]	
R6	1.84 ± 0.97 [0.00, 3.04]		0.62 ± 0.28 [0.42, 1.24]		11.1 ± 3.22 [5.56, 16.4]		37.1 ± 13.0 [17.9, 55.2]	
R7	2.04 ± 1.09 [0.00, 3.34]		0.67 ± 0.23 [0.41, 1.23]	1,2,8	8.72 ± 2.16 [6.86, 13.7]		41.5 ± 10.5 [27.3, 56.9]	1
R8	1.41 ± 0.63 [0.09, 2.13]		0.44 ± 0.23 [0.24, 0.97]	7,10,11	11.6 ± 5.46 [6.47, 23.6]		28.0 ± 16.0 [12.0, 54.0]	10
R9	1.81 ± 0.99 [0.00, 3.27]		0.56 ± 0.20 [0.35, 1.01]		11.3 ± 5.99 [5.05, 26.0]		36.8 ± 13.2 [18.4, 55.2]	
R10	2.14 ± 1.12 [0.09, 3.54]		0.63 ± 0.13 [0.47, 0.89]	8	8.48 ± 1.59 [6.33, 10.7]		41.7 ± 9.89 [29.1, 56.8]	8
R11	1.61 ± 0.82 [0.01, 2.63]		0.56 ± 0.20 [0.38, 0.97]	8	8.31 ± 2.50 [5.08, 13.9]	5	33.3 ± 15.3 [13.7, 54.8]	

The indicated values are average ± standard deviation [minimum, maximum].
Sig. diff to ROI' indicates ROIs within the same condyle showing statistically significant differences to the ROI considered paired t-test with Bonferroni adjustment, $p<0.05$).

Chapter 6
Discussion and Future Directions

The overarching aims of the research presented in this thesis were 1) to explore regional differences in, and relationships between, the tibial cartilage morphology and subchondral bone microarchitecture of human knees in OA and controls, using micro-CT imaging; and 2) to determine the association of *in vivo* joint loading indices, measured from pre-operative gait analysis (external joint moments) and radiographs (alignment), with these tissues.

More specifically, this included:

1. To quantify tibia cartilage thickness, cortical subchondral bone plate thickness and STB bone volume fraction in subjects diagnosed with end-stage knee OA with varus- or valgus-aligned joints and compare them to control (non-OA) knees.
2. To validate the human tibial cartilage thickness measured from micro-CT cross-sections against histology (gold standard).
3. To investigate in people with end-stage knee OA, relationships between knee joint external moments (peak knee adduction moments, flexion/extension moments and external/internal rotation moments), joint alignment (pre-operative gait analysis and radiographs) and cartilage thickness of their excised tibial plateaus quantified with 3D micro-CT.
4. To perform, in micro-CT scans of entire human tibial plateaus from controls and OA, a systematic spatial mapping (22 regions) of the cartilage and underlying bone; and to map the region-specific relationships in these parameters in control and OA groups.

6.1 Principal Findings

Tibial cartilage thickness, subchondral bone plate thickness and trabecular bone volume fraction in varus-OA and valgus-OA differ from controls

Varus- and valgus-aligned tibial plateaus from end-stage knee OA subjects (n=17 and 8 respectively) differed significantly from controls (n=15) in cartilage thickness, subchondral bone plate thickness and subchondral trabecular BV/TV, and their medial-to-lateral ratios, depending on joint alignment. Micro-CT cartilage thickness measurements had a strong linear relationship with histology thickness measurements (R^2 = 0.93, $p<0.001$), giving confidence that the here presented micro-CT analysis protocol allows to accurately quantify gross cartilage morphology. Cartilage thickness was significantly lower anteromedially in varus-OA compared to controls, whereas it was higher posteromedially in valgus-OA. Control medial-to-lateral cartilage thickness ratios were around unity (0.8–1.1), in varus-OA significantly below (0.2–0.6) and in valgus-OA slightly above (1.0–1.3) unity and controls. SBPl.Th and BV/TV were significantly higher medially in varus-OA and laterally in valgus-OA, compared to controls. In varus-OA, the medial-to-lateral SBPl.Th and BV/TV ratios were above unity (1.4–2.4) and controls (0.8–2.1); in valgus-OA they were closer to unity (0.8-1.1) and below controls. Overall, this suggests that structural changes in OA may reflect differences in medial-to-lateral load distribution upon the tibial plateau due to joint alignment. Compared to previous studies, the M:L cartilage thickness findings are consistent with those from MRI studies in OA, however, those did not consider the underlying bone (Eckstein *et al.*, 2008); our M:L BV/TV ratios findings are consistent with M:L BMD studies using DEXA, which, however, did not investigate the overlying cartilage (Christensen *et al.*, 1982, Hulet *et al.*, 2002). In this study, regions of lower cartilage thickness in OA corresponded to regions of thicker cortical subchondral bone plate and higher BV/TV underneath, and *vice versa.* This suggests an interplay between cartilage thickness and subchondral bone, and a whole-joint response in OA to daily stimuli. Moreover, cartilage thickness measurements from the presented micro-CT scanning protocol were validated against histology, enabling the concurrent imaging of cartilage morphology and bone microarchitecture to be performed within the same scan and without staining.

Joint loading indices correlated with regional cartilage thickness values and their medial-to-lateral ratios in end-stage knee OA subjects

In 25 end-stage OA subjects, relationships were found between tibial cartilage thickness (assessed from micro-CT scans), mechanical alignment and external knee joint moments (pre-operative gait analysis). Significant correlations were found between Cart.Th and joint loading indices, positive anteromedially with the first peak knee adduction moment ($r= 0.55$, $p<0.01$) and external rotation moment (ERM; $r= 0.52$, $p<0.01$), and negative with MAD ($r= -0.76$, $p<0.001$). In the lateral regions, these correlations had opposite signs. The medial-to-lateral Cart.Th ratio correlated strongly with ERM ($r= 0.63$, $p=0.001$) and MAD ($r= -0.75$, $p<0.001$). These relationships have the opposite sign compared to the subchondral bone microarchitecture found in a previous study by our group on the same specimens (Roberts *et al.*, 2018). This suggests a complementary bone-cartilage interplay in OA, in response to loading. The high spatial resolution of micro-CT (17 μm/voxel) may provide higher sensitivity compared to cartilage measurements from MRI, and, combined with the broad range of specimens in this study (mechanical axis alignment ranging from varus- to valgus-aligned), may explain the significant relationships found here (such as between medial and lateral cartilage thickness, ERM and KAM), and not found in other studies (Vanwanseele *et al.*, 2010, Erhart-Hledik *et al.*, 2015, Maly *et al.*, 2015).

In healthy and end-stage OA knees, regional differences exist in cartilage thickness and subchondral bone microarchitecture within- and between-condyles, depending on the group.

A systematic mapping of the cartilage and subchondral bone of the tibial plateau (22 sub-regions) in healthy and OA knees exhibited within-condyle and between-condyle (medial-to-lateral) regional differences in the tissues, depending on the group. In controls, Cart.Th, SBPl.Th and BV/TV were lowest in the external regions and thickest in the central and anterior regions. The cartilage thickness distribution is consistent with MRI studies (Favre *et al.*, 2017). In the varus-OA group, the cartilage was thinnest anteriorly in the medial condyle with high underlying SBPl.Th and BV/TV. In the non-varus-OA group, the cartilage distribution was similar to controls but with higher underlying SBPl.Th and BV/TV.

Region-specific relationships between cartilage and subchondral bone were found in end-stage OA, but not in controls.

The subchondral bone plate thickness and bone volume fraction were positively correlated in both controls and OA. However, interestingly, whereas in controls almost no relationships were found between cartilage thickness and the underlying subchondral bone, in OA, where significant, these relationships were negative in sign. Previous studies have reported conflicting relationships between cartilage and bone (as discussed in Chapter 5), but this may be attributed to pooling together regions and datasets (controls, mild OA and severe OA), whereas the region-specific analysis in this thesis was performed separately for end-stage OA and control cohorts. The negative relationships between cartilage and subchondral bone in end-stage OA were opposite in sign to an MRI study in early-stage OA (Bolbos *et al.*, 2008), which may also suggest that the relationship between cartilage and bone may change during the progression of the disease, warranting further investigation.

6.2 Significance to OA research

The research presented in this thesis builds on previously published findings on the influence of joint loading on tibial bone microarchitecture in end-stage OA (Roberts *et al.*, 2017a, Roberts *et al.*, 2017b, Roberts *et al.*, 2018). Regional heterogeneity in bone microarchitecture was found to differ with variations in static knee joint alignment and to be associated with external knee joint moments. However, it was not clear if these variations were unique to end-stage OA or also present in non-pathological joints, and if they were reflective in the overlying cartilage within the same regions. In fact, despite the consensus that the entire osteochondral unit is involved in OA, with abnormal alterations of one tissue affecting the other (Radin *et al.*, 1986, Burr *et al.*, 2012, Loeser *et al.*, 2012), the interaction between the tissues at high spatial resolutions, within the same subjects, and how they are influenced by known risk factors of OA such as joint loading, is not well understood. Thus, this was the focus of the research presented in this thesis.

The paucity of research in this area can be attributed to limitations in imaging the osteochondral unit. *In vivo* studies are restricted to using imaging modalities (MRI, DEXA, CT) with low spatial resolutions to typically visualise either cartilage (MRI) or bone (DEXA, CT). Advancements in micro-CT devices and computational power in the past

decade have improved the feasibility of *ex vivo* imaging of large human samples and processing of the sizable, generated datasets (Perilli *et al.*, 2012). Indeed, since the start of this PhD candidature, the use of micro-CT for imaging the entire tibial plateau has become a growing area of research (Chen *et al.*, 2017, Chen *et al.*, 2018, Gatenholm *et al.*, 2019, Muratovic *et al.*, 2019, Han *et al.*, 2020, Holzer *et al.*, 2020). However, of these studies, only a few have characterised the articular cartilage morphology in addition to bone microarchitecture, and of those studies, none considered the influence of joint loading. As has been shown in this thesis, joint loading indices were associated with the cartilage and bone distribution across the tibial plateau (Chapters 3, 4, 5; Rapagna *et al.,* 2021a, Rapagna *et al.,* 2021b).

In Study 2 it was revealed that the mechanical axis deviation was the joint loading indicator that most strongly correlated with end-stage OA cartilage thickness, and its medial-to-lateral ratio. When stratifying the OA cohort into varus- and valgus-aligned OA tibial plateaus, each group differed significantly from controls in cartilage thickness, SBPl.Th and BV/TV, depending on joint alignment. Not considering joint alignment diminishes regional differences among the tissues in OA compared to controls (as shown in Study 1 in this thesis), which may explain why Chen et. *al.* (2018) found no significant differences in some regions in OA compared to controls.

Similarly, in this thesis, differences in cartilage thickness, SBPl.Th, BV/TV between medial and lateral condyles in OA and against controls, were higher in subregions, rather than using an average measurement for the entire condyle. Moreover, cartilage thickness in OA was correlated with gait parameters anteromedially and posterolaterally, but not anterolaterally and posteromedially. In addition to the improved sensitivity of using a high spatial resolution (17 μm/pixel, currently unachievable with *in vivo* methods) this might explain relationships found in this study but not in the literature (Vanwanseele *et al.*, 2010, Erhart-Hledik *et al.*, 2015, Maly *et al.*, 2015). Relationships with KAM, KFM, ERM and MAD were found for regional cartilage thickness, whereas with ERM and MAD for the medial-to-lateral cartilage thickness ratio. The approach to investigate all external knee moments revealed relationships in OA otherwise underreported in the literature. This should be considered in the development of OA treatment options (e.g. orthotics) which have had mixed reported outcomes (Arnold *et al.*, 2016), potentially due to being designed to reduce the KAM only, where forces in all three principal directions should be considered.

Interestingly, examined relationships with joint loading indices and cartilage thickness were weaker compared to those involving bone, likely due to the presence of denuded cartilage in some areas of end-stage OA specimens. This affected the examined relationships between cartilage and joint loading indices (Study 2) and bone parameters (Study 3). OA is characterised by a loss of cartilage, and once this cartilage has worn away, it is unlikely to grow back naturally, nor can it further reduce in response to more load. As a result, while the external knee moments and BV/TV may have altered, regions of 0 mm cartilage would not similarly adapt, and hence would weaken statistical correlations. It is possible that these relationships would have been stronger earlier in the disease, where there was still cartilage left. This opens a prospect for using high resolution longitudinal joint imaging in future, to explore the disease progression *in vivo*. Moreover, in Study 3, controls did not differ in cartilage thickness between corresponding regions in the medial and lateral condyles, but did so in the underlying bone, likely in response to habitual joint loading. Hence, subchondral BV/TV, along with cartilage thickness, might be a sensitive marker for monitoring the progression of OA and reflecting the efficacy of treatment options aimed to reduce abnormal loading.

6.3 Recommendations for future research

Investigating the influence of joint loading on cartilage thickness and subchondral bone morphometry during the progression of OA

Micro-CT imaging, as used in this thesis, enables concurrent high resolution imaging of cartilage and bone in entire human tibial plateaus, but is restricted to *ex vivo* specimens. Thus, the specimens used in this study were either from end-stage OA subjects (with gait analysis and alignment determined pre-operatively) or from cadaveric controls with no such *in vivo* gait analysis or joint alignment measure. Relationships between regional articular cartilage thickness and joint loading indices in end-stage OA were found. However, it is unclear from this cross-sectional investigation, whether possible changes in joint loading indices were in response to the structural changes in OA and a compensatory strategy to reduce pain, or if pre-existing abnormal gait patterns altered the loads across the joint, causing structural alterations to the joint and progressing the disease. Moreover, while there were relationships between tibial articular cartilage thickness and underlying subchondral bone microarchitecture in end-stage OA, and

differences in these tissues from controls, it is still not known in what tissue the disease originated.

As currently micro-CT imaging on humans can only be performed *ex vivo*, future studies may use a combination of MRI, particularly if the spatial resolution might improve in the future, and high-resolution peripheral quantitative CT (HR-pQCT) (Bhatla *et al.*, 2018), or contrast-enhanced HR-pQCT (Michalak *et al.*, 2019), to monitor the tibial cartilage and subchondral bone morphology in non-OA subjects and during disease progression. This could be investigated alongside gait analysis and estimated joint loading. However, the use of HR-pQCT is currently subjected to joint size limitations due to gantry size as described in Chapter 2.4.2. Alternatively, vBMD measured with pQCT *in vivo*, although lower in spatial resolution (200x200 μm in-plane, with 2.3 mm slice thickness) compared to HR-pQCT (61 μm/pixel), may also be suitable. pQCT has a larger gantry, enabling scanning of bigger joints and has previously been used to reveal significant relationships between external knee moments and regional vBMD in controls (Thewlis *et al.*, 2021).

Improving estimations of *in vivo* habitual tissue loading

Measuring internal knee contact forces is currently not possible in clinical settings (Fregly *et al.*, 2012, Meyer *et al.*, 2013). Instead, both joint alignment and external knee moments (computed from gait analysis) have been used as surrogate markers for contact forces (Studies 1, 2 and 3, Andriacchi, 1994, Baliunas et al., 2002, Miyazaki et al., 2002, Adouni et al., 2014a, Roberts et al., 2017a, Roberts et al., 2017b, Roberts et al., 2018). However, this may not be appropriate, particularly in conditions (altered gait pattens) where the total contact force or muscle forces may change (Meyer *et al.*, 2013). Estimates may be slightly improved by monitoring muscle activation patterns using electromyographic (EMG) signals (Hafer *et al.*, 2020). Alternatively, due to recent advancements in musculoskeletal models, modelling knee contact forces during gait may result in improved predictions of variations in cartilage thickness and subchondral bone morphometry in OA, rather than using the external joint moments (Fregly *et al.*, 2012, Meyer *et al.*, 2013).

Improving understanding of the material properties of the osteochondral unit due to joint alignment

In Study 1 differences in cartilage thickness, subchondral plate thickness and trabecular bone volume fraction between OA and control joints were found to depend on joint

alignment. However, it is unknown if these relationships are also reflected in the material properties of each tissue. In previous studies published in the literature, cartilage and bone material properties have been reported to vary among regions of the tibial plateau (Thambyah *et al.*, 2006, Renault *et al.*, 2020, Li *et al.*, 2021). However, only one of these studies considered the influence of joint alignment on material properties of the bone. By using nanoindentation in the subchondral bone of OA tibial plateaus, Renault *et al.* (2020) found the hip-knee-ankle angle to be negatively correlated with the elastic modulus of trabeculae from the centre of the medial condyle (a more varus alignment corresponded with a higher elastic modulus medially) and positively with the central region of the lateral condyle. These relationships were weak-to-moderate, however, they can be expected to be stronger if considering specific load-bearing regions such as those presented in this thesis (Chapter 4; Rapagna *et al.* 2021b); for example, the anterior region of the medial condyle, which in this thesis was the region where cartilage thickness correlated the strongest with MAD in OA. Moreover, it is unclear if these tissues differ in material properties (e.g., elastic modulus) to age-matched controls within the same regions. Future studies may use nano- or micro-indentation to determine these properties. These material properties may in turn be used in the development and refinement of finite element models for predicting the mechanical behaviour of the joint in specific patient cohorts (e.g., varus-aligned OA patients) (Perillo-Marcone *et al.*, 2000).

6.4 Concluding statement

In this thesis, micro-CT was used for the non-destructive concurrent imaging of cartilage and bone microarchitecture at high spatial resolutions (17 μm/voxel) on entire human tibial plateaus. Such high resolution imaging is unattainable using clinical scans (e.g. MRI or peripheral quantitative CT). The non-contrast agent based micro-CT protocol for quantifying gross cartilage morphology was validated against histology. Detectable morphological differences in cartilage thickness and subchondral bone between control and OA joints depend on joint alignment and could become useful indicators of disease progression, warranting further exploration. Pre-operative joint loading indices (such as the knee adduction moment, external rotation moment and mechanical axis deviation) significantly correlated with regional cartilage thickness and the medial-to-lateral cartilage thickness ratios in OA. Subchondral bone plate thickness and bone volume

fraction were positively correlated in both controls and OA. However, negative relationships between cartilage thickness and underlying subchondral bone were identified in end-stage OA but not in controls, suggesting a whole-joint response in OA to daily stimuli, which is altered compared to controls. While this study was performed in controls and late-stage OA, further research is needed to determine whether the relationships between cartilage thickness, subchondral bone and joint loading indices are also present in earlier stages of the disease. This could, in the future, be performed *in vivo* by using a combination of high-resolution MRI and HR-pQCT, which may facilitate longitudinal monitoring of subjects at various stages of the disease over time.

References

Abulhasan JF, Grey MJ. Anatomy and Physiology of Knee Stability. J Funct Morphol Kinesiol. 2017;2(4):34.

Adouni M, Shirazi-Adl A. Evaluation of knee joint muscle forces and tissue stresses-strains during gait in severe OA versus normal subjects. J Orthop Res. 2014a;32(1):69-78.

Adouni M, Shirazi-Adl A. Partitioning of knee joint internal forces in gait is dictated by the knee adduction angle and not by the knee adduction moment. J Biomech. 2014b;47(7):1696-703.

Affatato S. Biomechanics of the knee. In: Affatato S, editor. Surgical Techniques in Total Knee Arthroplasty and Alternative Procedures. Oxford: Woodhead Publishing; 2015. p. 17-35.

Akizuki S, Mow VC, Müller F, Pita JC, Howell DS. Tensile properties of human knee joint cartilage. II. Correlations between weight bearing and tissue pathology and the kinetics of swelling. J Orthop Res. 1987;5(2):173-86.

Akizuki S, Mow VC, Müller F, Pita JC, Howell DS, Manicourt DH. Tensile properties of human knee joint cartilage: I. Influence of ionic conditions, weight bearing, and fibrillation on the tensile modulus. J Orthop Res. 1986;4(4):379-92.

American Joint Replacement Registry (AJRR). 2019 Annual Report Rosemont, IL American Academy of Orthopaedic Surgeons (AAOS). Available from: http://connect.ajrr.net/2019-ajrr-annual-report; 2019.

An YH, Martin KL. Handbook of histology methods for bone and cartilage: Springer; 2003.

Andriacchi TP. Dynamics of knee malalignment. Orthop Clin North Am. 1994;25(3):395-403.

Andriacchi TP, Favre J. The nature of in vivo mechanical signals that influence cartilage health and progression to knee osteoarthritis. Curr Rheumatol Rep. 2014;16(11):463.

Andriacchi TP, Koo S, Scanlan SF. Gait mechanics influence healthy cartilage morphology and osteoarthritis of the knee. J Bone Joint Surg Am. 2009;91 Suppl 1:95-101.

Andriacchi TP, Mündermann A. The role of ambulatory mechanics in the initiation and progression of knee osteoarthritis. Curr Opin Rheumatol. 2006;18(5):514-8.

Andriacchi TP, Mündermann A, Smith RL, Alexander EJ, Dyrby CO, Koo S. A framework for the in vivo pathomechanics of osteoarthritis at the knee. Ann Biomed Eng. 2004;32(3):447-57.

Arnold JB, Wong DX, Jones RK, Hill CL, Thewlis D. Lateral Wedge Insoles for Reducing Biomechanical Risk Factors for Medial Knee Osteoarthritis Progression: A Systematic Review and Meta-Analysis. Arthritis Care Res (Hoboken). 2016;68(7):936-51.

Astephen JL, Deluzio KJ, Caldwell GE, Dunbar MJ. Biomechanical changes at the hip, knee, and ankle joints during gait are associated with knee osteoarthritis severity. J Orthop Res. 2008;26(3):332-41.

Australian Institute of Health and Wealfare (AIHW). Osteoarthritis. . AIHW: Canberra. Available from: https://www.aihw.gov.au/reports/arthritis-other-musculoskeletal-conditions/osteoarthritis/data; 2017.

Aweid O, Osmani H, Melton J. Biomechanics of the knee. Orthop Trauma. 2019;33(4):224-30.

Baliunas AJ, Hurwitz DE, Ryals AB, Karrar A, Case JP, Block JA, Andriacchi TP. Increased knee joint loads during walking are present in subjects with knee osteoarthritis. Osteoarthritis Cartilage. 2002;10(7):573-9.

Benjamini Y, Hochberg Y. Controlling the False Discovery Rate - a Practical and Powerful Approach to Multiple Testing. J R Stat Soc B. 1995;57(1):289-300.

Bennell KL, Bowles KA, Wang Y, Cicuttini F, Davies-Tuck M, Hinman RS. Higher dynamic medial knee load predicts greater cartilage loss over 12 months in medial knee osteoarthritis. Ann Rheum Dis. 2011;70(10):1770-4.

Berry JL, Thaeler-Oberdoerster DA, Greenwald AS. Subchondral pathways to the superior surface of the human talus. Foot Ankle. 1986;7(1):2-9.

Bertuglia A, Lacourt M, Girard C, Beauchamp G, Richard H, Laverty S. Osteoclasts are recruited to the subchondral bone in naturally occurring post-traumatic equine carpal osteoarthritis and may contribute to cartilage degradation. Osteoarthritis Cartilage. 2016;24(3):555-66.

Bettica P, Cline G, Hart DJ, Meyer J, Spector TD. Evidence for increased bone resorption in patients with progressive knee osteoarthritis: longitudinal results from the Chingford study. Arthritis Rheum. 2002;46(12):3178-84.

Bhatla JL, Kroker A, Manske SL, Emery CA, Boyd SK. Differences in subchondral bone plate and cartilage thickness between women with anterior cruciate ligament reconstructions and uninjured controls. Osteoarthritis Cartilage. 2018;26(7):929-39.

Bobinac D, Spanjol J, Zoricic S, Maric I. Changes in articular cartilage and subchondral bone histomorphometry in osteoarthritic knee joints in humans. Bone. 2003;32(3):284-90.

Bolbos RI, Zuo J, Banerjee S, Link TM, Ma CB, Li X, Majumdar S. Relationship between trabecular bone structure and articular cartilage morphology and relaxation times in early OA of the knee joint using parallel MRI at 3 T. Osteoarthritis Cartilage. 2008;16(10):1150-9.

Brouwer GM, van Tol AW, Bergink AP, Belo JN, Bernsen RM, Reijman M, Pols HA, Bierma-Zeinstra SM. Association between valgus and varus alignment and the development and progression of radiographic osteoarthritis of the knee. Arthritis Rheum. 2007;56(4):1204-11.

Buckwalter JA, Mow VC, Ratcliffe A. Restoration of Injured or Degenerated Articular Cartilage. J Am Acad Orthop Surg. 1994;2(4):192-201.

Buie HR, Campbell GM, Klinck RJ, MacNeil JA, Boyd SK. Automatic segmentation of cortical and trabecular compartments based on a dual threshold technique for in vivo micro-CT bone analysis. Bone. 2007;41(4):505-15.

Burnett WD, Kontulainen SA, McLennan CE, Hazel D, Talmo C, Wilson DR, Hunter DJ, Johnston JD. Proximal tibial trabecular bone mineral density is related to pain in patients with osteoarthritis. Arthritis Res Ther. 2017;19(1):200.

Burr DB. Anatomy and physiology of the mineralized tissues: role in the pathogenesis of osteoarthrosis. Osteoarthritis Cartilage. 2004;12 Suppl A:S20-30.

Burr DB, Gallant MA. Bone remodelling in osteoarthritis. Nat Rev Rheumatol. 2012;8(11):665-73.

Burr DB, Schaffler MB. The involvement of subchondral mineralized tissues in osteoarthrosis: quantitative microscopic evidence. Microsc Res Tech. 1997;37(4):343-57.

Calvo E, Palacios I, Delgado E, Sánchez-Pernaute O, Largo R, Egido J, Herrero-Beaumont G. Histopathological correlation of cartilage swelling detected by magnetic resonance imaging in early experimental osteoarthritis. Osteoarthritis Cartilage. 2004;12(11):878-86.

Camomilla V, Cereatti A, Cutti AG, Fantozzi S, Stagni R, Vannozzi G. Methodological factors affecting joint moments estimation in clinical gait analysis: a systematic review. Biomed Eng Online. 2017;16(1):106-.

Campbell AB, Knopp MV, Kolovich GP, Wei W, Jia G, Siston RA, Flanigan DC. Preoperative MRI Underestimates Articular Cartilage Defect Size Compared With Findings at Arthroscopic Knee Surgery. Am J Sports Med. 2013;41(3):590-5.

Cao Y, Stannus OP, Aitken D, Cicuttini F, Antony B, Jones G, Ding C. Cross-sectional and longitudinal associations between systemic, subchondral bone mineral density and knee cartilage thickness in older adults with or without radiographic osteoarthritis. Ann Rheum Dis. 2014;73(11):2003-9.

Chang AH, Moisio KC, Chmiel JS, Eckstein F, Guermazi A, Prasad PV, Zhang Y, Almagor O, Belisle L, Hayes K, Sharma L. External knee adduction and flexion moments during gait and medial tibiofemoral disease progression in knee osteoarthritis. Osteoarthritis Cartilage. 2015;23(7):1099-106.

Chaudhari AM, Briant PL, Bevill SL, Koo S, Andriacchi TP. Knee kinematics, cartilage morphology, and osteoarthritis after ACL injury. Med Sci Sports Exerc. 2008;40(2):215-22.

Chehab EF, Favre J, Erhart-Hledik JC, Andriacchi TP. Baseline knee adduction and flexion moments during walking are both associated with 5 year cartilage changes in patients with medial knee osteoarthritis. Osteoarthritis Cartilage. 2014;22(11):1833-9.

Chen F, Su W, Bedenbaugh AV, Oruc A. Health care resource utilization and burden of disease in a U.S. Medicare population with a principal diagnosis of osteoarthritis of the knee. J Med Econ. 2020;23(10):1151-8.

Chen Y, Hu Y, Yu YE, Zhang X, Watts T, Zhou B, Wang J, Wang T, Zhao W, Chiu KY, Leung FK, Cao X, Macaulay W, Nishiyama KK, Shane E, Lu WW, Guo XE. Subchondral Trabecular Rod Loss and Plate Thickening in the Development of Osteoarthritis. J Bone Miner Res. 2018;33(2):316-27.

Chen Y, Huang Y-C, Yan CH, Chiu KY, Wei Q, Zhao J, Guo XE, Leung F, Lu WW. Abnormal subchondral bone remodeling and its association with articular cartilage degradation in knees of type 2 diabetes patients. Bone Res. 2017;5(1):17034.

Choi K, Kuhn JL, Ciarelli MJ, Goldstein SA. The elastic moduli of human subchondral, trabecular, and cortical bone tissue and the size-dependency of cortical bone modulus. J Biomech. 1990;23(11):1103-13.

Christensen P, Kjaer J, Melsen F, Nielsen HE, Sneppen O, Vang PS. The subchondral bone of the proximal tibial epiphysis in osteoarthritis of the knee. Acta Orthop Scand. 1982;53(6):889-95.

Cohen ZA, McCarthy DM, Kwak SD, Legrand P, Fogarasi F, Ciaccio EJ, Ateshian GA. Knee cartilage topography, thickness, and contact areas from MRI: in-vitro calibration and in-vivo measurements. Osteoarthritis Cartilage. 1999;7(1):95-109.

Creaby MW, Wang Y, Bennell KL, Hinman RS, Metcalf BR, Bowles KA, Cicuttini FM. Dynamic knee loading is related to cartilage defects and tibial plateau bone area in medial knee osteoarthritis. Osteoarthritis Cartilage. 2010;18(11):1380-5.

Crema MD, Roemer FW, Marra MD, Burstein D, Gold GE, Eckstein F, Baum T, Mosher TJ, Carrino JA, Guermazi A. Articular Cartilage in the Knee: Current MR Imaging Techniques and Applications in Clinical Practice and Research. RadioGraphics. 2011;31(1):37-61.

Cross M, Smith E, Hoy D, Nolte S, Ackerman I, Fransen M, Bridgett L, Williams S, Guillemin F, Hill CL, Laslett LL, Jones G, Cicuttini F, Osborne R, Vos T, Buchbinder R, Woolf A, March L. The global burden of hip and knee osteoarthritis: estimates from the global burden of disease 2010 study. Ann Rheum Dis. 2014;73(7):1323-30.

Cui A, Li H, Wang D, Zhong J, Chen Y, Lu H. Global, regional prevalence, incidence and risk factors of knee osteoarthritis in population-based studies. EClinicalMedicine. 2020;29-30:100587.

Cummings SR, Bates D, Black DM. Clinical use of bone densitometry: scientific review. Jama. 2002;288(15):1889-97.

Day JS, Ding M, van der Linden JC, Hvid I, Sumner DR, Weinans H. A decreased subchondral trabecular bone tissue elastic modulus is associated with pre-arthritic cartilage damage. J Orthop Res. 2001;19(5):914-8.

Delecourt C, Relier M, Touraine S, Bouhadoun H, Engelke K, Laredo JD, Chappard C. Cartilage morphology assessed by high resolution micro-computed tomography in non OA knees. Osteoarthritis Cartilage. 2016;24(3):567-71.

Deshpande BR, Katz JN, Solomon DH, Yelin EH, Hunter DJ, Messier SP, Suter LG, Losina E. Number of Persons With Symptomatic Knee Osteoarthritis in the US: Impact of Race and Ethnicity, Age, Sex, and Obesity. Arthritis Care Res (Hoboken). 2016;68(12):1743-50.

Ding M. Microarchitectural adaptations in aging and osteoarthrotic subchondral bone issues. Acta Orthop Suppl. 2010;81(340):1-53.

Ding M, Dalstra M, Linde F, Hvid I. Mechanical properties of the normal human tibial cartilage-bone complex in relation to age. Clin Biomech (Bristol, Avon). 1998;13(4-5):351-8.

Ding M, Odgaard A, Hvid I. Changes in the three-dimensional microstructure of human tibial cancellous bone in early osteoarthritis. J Bone Joint Surg Br. 2003;85(6):906-12.

Doriot N, Cheze L. A three-dimensional kinematic and dynamic study of the lower limb during the stance phase of gait using an homogeneous matrix approach. IEEE Trans Biomed Eng. 2004;51(1):21-7.

Driban JB, Tassinari A, Lo GH, Price LL, Schneider E, Lynch JA, Eaton CB, McAlindon TE. Bone Marrow Lesions are Associated with Altered Trabecular Morphometry. Osteoarthritis Cartilage. 2012;20(12):1519-26.

Duthon VB, Barea C, Abrassart S, Fasel JH, Fritschy D, Ménétrey J. Anatomy of the anterior cruciate ligament. Knee Surg Sports Traumatol Arthrosc. 2006;14(3):204-13.

Eckstein F, Cicuttini F, Raynauld JP, Waterton JC, Peterfy C. Magnetic resonance imaging (MRI) of articular cartilage in knee osteoarthritis (OA): morphological assessment. Osteoarthritis Cartilage. 2006;14:46-75.

Eckstein F, Guermazi A, Gold G, Duryea J, Le Graverand MPH, Wirth W, Miller CG. Imaging of cartilage and bone: promises and pitfalls in clinical trials of osteoarthritis. Osteoarthritis Cartilage. 2014;22(10):1516-32.

Eckstein F, Wirth W. Quantitative cartilage imaging in knee osteoarthritis. Arthritis. 2011;2011:475684.

Eckstein F, Wirth W, Hudelmaier M, Stein V, Lengfelder V, Cahue S, Marshall M, Prasad P, Sharma L. Patterns of femorotibial cartilage loss in knees with neutral, varus, and valgus alignment. Arthritis Rheum. 2008;59(11):1563-70.

Edd SN, Omoumi P, Andriacchi TP, Jolles BM, Favre J. Modeling knee osteoarthritis pathophysiology using an integrated joint system (IJS): a systematic review of relationships among cartilage thickness, gait mechanics, and subchondral bone mineral density. Osteoarthritis Cartilage. 2018;26(11):1425-37.

Erhart-Hledik JC, Favre J, Andriacchi TP. New insight in the relationship between regional patterns of knee cartilage thickness, osteoarthritis disease severity, and gait mechanics. J Biomech. 2015;48(14):3868-75.

Evans JT, Walker RW, Evans JP, Blom AW, Sayers A, Whitehouse MR. How long does a knee replacement last? A systematic review and meta-analysis of case series and national registry reports with more than 15 years of follow-up. The Lancet. 2019;393(10172):655-63.

Favre J, Babel H, Cavinato A, Blazek K, Jolles BM, Andriacchi TP. Analyzing Femorotibial Cartilage Thickness Using Anatomically Standardized Maps: Reproducibility and Reference Data. J Clin Med. 2021;10(3):461.

Favre J, Erhart-Hledik JC, Blazek K, Fasel B, Gold GE, Andriacchi TP. Anatomically Standardized Maps Reveal Distinct Patterns of Cartilage Thickness With Increasing Severity of Medial Compartment Knee Osteoarthritis. J Orthop Res. 2017;35(11):2442-51.

Favre J, Erhart-Hledik JC, Chehab EF, Andriacchi TP. Baseline ambulatory knee kinematics are associated with changes in cartilage thickness in osteoarthritic patients over 5 years. J Biomech. 2016;49(9):1859-64.

Fazzalari NL, Parkinson IH. Fractal properties of subchondral cancellous bone in severe osteoarthritis of the hip. J Bone Miner Res. 1997;12(4):632-40.

Feldkamp LA, Goldstein SA, Parfitt AM, Jesion G, Kleerekoper M. The direct examination of three-dimensional bone architecture in vitro by computed tomography. J Bone Miner Res. 1989;4(1):3-11.

Findlay DM, Kuliwaba JS. Bone-cartilage crosstalk: a conversation for understanding osteoarthritis. Bone Res. 2016;4(1):16028.

Fox AJ, Bedi A, Rodeo SA. The basic science of human knee menisci: structure, composition, and function. Sports health. 2012;4(4):340-51.

Fox AJS, Bedi A, Rodeo SA. The basic science of articular cartilage: structure, composition, and function. Sports health. 2009;1(6):461-8.

Fregly BJ, Besier TF, Lloyd DG, Delp SL, Banks SA, Pandy MG, D'Lima DD. Grand challenge competition to predict in vivo knee loads. J Orthop Res. 2012;30(4):503-13.

Frost HM. From Wolff's law to the Utah paradigm: insights about bone physiology and its clinical applications. Anat Rec. 2001;262(4):398-419.

Gatenholm B, Lindahl C, Brittberg M, Stadelmann VA. Spatially matching morphometric assessment of cartilage and subchondral bone in osteoarthritic human knee joint with micro-computed tomography. Bone. 2019;120:393-402.

Gold GE, Chen CA, Koo S, Hargreaves BA, Bangerter NK. Recent advances in MRI of articular cartilage. Am J Roentgenol. 2009;193(3):628-38.

Goldring MB, Goldring SR. Articular cartilage and subchondral bone in the pathogenesis of osteoarthritis. Ann N Y Acad Sci. 2010;1192:230-7.

Goldring SR. Alterations in periarticular bone and cross talk between subchondral bone and articular cartilage in osteoarthritis. Ther Adv Musculoskelet Dis. 2012;4(4):249-58.

Goldring SR, Goldring MB. Changes in the osteochondral unit during osteoarthritis: structure, function and cartilage-bone crosstalk. Nat Rev Rheumatol. 2016;12(11):632-44.

Gollehon DL, Torzilli PA, Warren RF. The role of the posterolateral and cruciate ligaments in the stability of the human knee. A biomechanical study. JBJS. 1987;69(2).

Gomoll AH, Yoshioka H, Watanabe A, Dunn JC, Minas T. Preoperative Measurement of Cartilage Defects by MRI Underestimates Lesion Size. Cartilage. 2011;2(4):389-93.

Griffin TM, Guilak F. The role of mechanical loading in the onset and progression of osteoarthritis. Exerc Sport Sci Rev. 2005;33(4):195-200.

Guilak F. Biomechanical factors in osteoarthritis. Best Pract Res Clin Rheumatol. 2011;25(6):815-23.

Guo H, Maher SA, Torzilli PA. A biphasic finite element study on the role of the articular cartilage superficial zone in confined compression. J Biomech. 2015;48(1):166-70.

Gupta S, Hawker GA, Laporte A, Croxford R, Coyte PC. The economic burden of disabling hip and knee osteoarthritis (OA) from the perspective of individuals living with this condition. Rheumatology (Oxford). 2005;44(12):1531-7.

Gwynne-Jones JH, Wilson RA, Wong JMY, Abbott JH, Gwynne-Jones DP. The Outcomes of Nonoperative Management of Patients With Hip and Knee Osteoarthritis Triaged to a Physiotherapy-Led Clinic at Minimum 5-Year Follow-Up and Factors Associated With Progression to Surgery. J Arthroplasty. 2020;35(6):1497-503.

Hafer JF, Boyer KA. Muscle activation patterns differ with knee osteoarthritis status but not with physical activity level. Osteoarthritis Cartilage. 2020;28:S239.

Hair JF, Black WC, Babin BJ, Anderson RE. Multivariate data analysis. 7th ed: Harlow, England: Pearson.; 2014.

Han X, Cui J, Xie K, Jiang X, He Z, Du J, Chu L, Qu X, Ai S, Sun Q, Wang L, Wu H, Zhang W, Yu Z, Yan M. Association between knee alignment, osteoarthritis disease severity, and subchondral trabecular bone microarchitecture in patients with knee osteoarthritis: a cross-sectional study. Arthritis Res Ther. 2020;22(1):203.

Hannan MT, Anderson JJ, Zhang Y, Levy D, Felson DT. Bone mineral density and knee osteoarthritis in elderly men and women. The Framingham Study. Arthritis Rheum. 1993;36(12):1671-80.

Hara T, Tanck E, Homminga J, Huiskes R. The influence of microcomputed tomography threshold variations on the assessment of structural and mechanical trabecular bone properties. Bone. 2002;31(1):107-9.

Hardisty MR, Whyne CM. Whole bone strain quantification by image registration: a validation study. J Biomech Eng. 2009;131(6):064502.

Harrigan TP, Mann RW. Characterization of microstructural anisotropy in orthotropic materials using a second rank tensor. J Mater Sci. 1984;19(3):761-7.

Hatfield GL, Hubley-Kozey CL, Astephen Wilson JL, Dunbar MJ. The effect of total knee arthroplasty on knee joint kinematics and kinetics during gait. J Arthroplasty. 2011;26(2):309-18.

Hellio Le Graverand MP, Buck RJ, Wyman BT, Vignon E, Mazzuca SA, Brandt KD, Piperno M, Charles HC, Hudelmaier M, Hunter DJ, Jackson C, Kraus VB, Link TM, Majumdar S, Prasad PV, Schnitzer TJ, Vaz A, Wirth W, Eckstein F. Subregional femorotibial cartilage morphology in women--comparison between healthy controls and participants with different grades of radiographic knee osteoarthritis. Osteoarthritis Cartilage. 2009;17(9):1177-85.

Hendee WR, Ritenour ER, Hoffmann KR. Medical imaging physics. Medical Physics. 2003;30(4):730-.

Hildebrand T, Rüegsegger P. A new method for the model-independent assessment of thickness in three-dimensional images. J Microsc-Oxford. 1997a;185(1):67-75.

Hildebrand T, Rüegsegger P. Quantification of Bone Microarchitecture with the Structure Model Index. Comput Methods Biomech Biomed Engin. 1997b;1(1):15-23.

Hirschmann MT, Müller W. Complex function of the knee joint: the current understanding of the knee. Knee Surg Sports Traumatol Arthrosc. 2015;23(10):2780-8.

Holzer LA, Kraiger M, Talakic E, Fritz GA, Avian A, Hofmeister A, Leithner A, Holzer G. Microstructural analysis of subchondral bone in knee osteoarthritis. Osteoporos Int. 2020;31(10):2037-45.

Huebner JL, Hanes MA, Beekman B, TeKoppele JM, Kraus VB. A comparative analysis of bone and cartilage metabolism in two strains of guinea-pig with varying degrees of naturally occurring osteoarthritis. Osteoarthritis Cartilage. 2002;10(10):758-67.

Hulet C, Sabatier JP, Souquet D, Locker B, Marcelli C, Vielpeau C. Distribution of bone mineral density at the proximal tibia in knee osteoarthritis. Calcif Tissue Int. 2002;71(4):315-22.

Hunter DJ, Bierma-Zeinstra S. Osteoarthritis. The Lancet. 2019;393(10182):1745-59.

Hunter DJ, McDougall JJ, Keefe FJ. The symptoms of osteoarthritis and the genesis of pain. Rheum Dis Clin North Am. 2008;34(3):623-43.

Imhof H, Breitenseher M, Kainberger F, Rand T, Trattnig S. Importance of subchondral bone to articular cartilage in health and disease. Top Magn Reson Imaging. 1999;10(3):180-92.

Imhof H, Sulzbacher I, Grampp S, Czerny C, Youssefzadeh S, Kainberger F. Subchondral bone and cartilage disease: a rediscovered functional unit. Invest Radiol. 2000;35(10):581-8.

Jerban S, Chang EY, Du J. Magnetic resonance imaging (MRI) studies of knee joint under mechanical loading: Review. Magn Reson Imaging. 2020;65:27-36.

Johnson VL, Hunter DJ. The epidemiology of osteoarthritis. Best Pract Res Clin Rheumatol. 2014;28(1):5-15.

Johnston JD, Kontulainen SA, Masri BA, Wilson DR. A comparison of conventional maximum intensity projection with a new depth-specific topographic mapping technique in the CT analysis of proximal tibial subchondral bone density. Skeletal Radiol. 2010;39(9):867-76.

Keen CE, Whittier DE, Firminger CR, Edwards WB, Boyd SK. Validation of Bone Density and Microarchitecture Measurements of the Load-Bearing Femur in the Human Knee Obtained Using In Vivo HR-pQCT Protocol. J Clin Densitom. 2021.

Kohn D, Moreno B. Meniscus insertion anatomy as a basis for meniscus replacement: A morphological cadaveric study. Arthroscopy. 1995;11(1):96-103.

Koo S, Andriacchi TP. A comparison of the influence of global functional loads vs. local contact anatomy on articular cartilage thickness at the knee. J Biomech. 2007;40(13):2961-6.

Koo S, Giori NJ, Gold GE, Dyrby CO, Andriacchi TP. Accuracy of 3D cartilage models generated from MR images is dependent on cartilage thickness: laser scanner based validation of in vivo cartilage. J Biomech Eng. 2009;131(12):121004.

Koo S, Gold GE, Andriacchi TP. Considerations in measuring cartilage thickness using MRI: factors influencing reproducibility and accuracy. Osteoarthritis Cartilage. 2005;13(9):782-9.

Kopydlowski NJ, Weber AE, Sekiya JK. Functional Anatomy of the Hamstrings and Quadriceps. In: Kaeding CC, Borchers JR, editors. Hamstring and Quadriceps Injuries in Athletes: A Clinical Guide. Boston, MA: Springer US; 2014. p. 1-14.

Kroker A, Zhu Y, Manske SL, Barber R, Mohtadi N, Boyd SK. Quantitative in vivo assessment of bone microarchitecture in the human knee using HR-pQCT. Bone. 2017;97:43-8.

Krug R, Banerjee S, Han ET, Newitt DC, Link TM, Majumdar S. Feasibility of in vivo structural analysis of high-resolution magnetic resonance images of the proximal femur. Osteoporosis Int. 2005;16(11):1307-14.

Kuhn JL, Goldstein SA, Feldkamp LA, Goulet RW, Jesion G. Evaluation of a microcomputed tomography system to study trabecular bone structure. J Orthop Res. 1990;8(6):833-42.

Kutzner I, Trepczynski A, Heller MO, Bergmann G. Knee adduction moment and medial contact force--facts about their correlation during gait. PLoS One. 2013;8(12):e81036.

Landrigan MD, Li J, Turnbull TL, Burr DB, Niebur GL, Roeder RK. Contrast-enhanced micro-computed tomography of fatigue microdamage accumulation in human cortical bone. Bone. 2011;48(3):443-50.

Lane LB, Villacin A, Bullough PG. The vascularity and remodelling of subchondrial bone and calcified cartilage in adult human femoral and humeral heads. An age- and stress-related phenomenon. J Bone Joint Surg Br. 1977;59-B(3):272-8.

Lee JY, Harvey WF, Price LL, Paulus JK, Dawson-Hughes B, McAlindon TE. Relationship of bone mineral density to progression of knee osteoarthritis. Arthritis Rheum. 2013;65(6):1541-6.

Leng H, Wang X, Ross RD, Niebur GL, Roeder RK. Micro-computed tomography of fatigue microdamage in cortical bone using a barium sulfate contrast agent. J Mech Behav Biomed Mater. 2008;1(1):68-75.

Lepage SIM, Robson N, Gilmore H, Davis O, Hooper A, St John S, Kamesan V, Gelis P, Carvajal D, Hurtig M, Koch TG. Beyond Cartilage Repair: The Role of the Osteochondral Unit in Joint Health and Disease. Tissue engineering Part B, Reviews. 2019;25(2):114-25.

Li B, Aspden RM. Composition and mechanical properties of cancellous bone from the femoral head of patients with osteoporosis or osteoarthritis. J Bone Miner Res. 1997;12(4):641-51.

Li G, Park SE, DeFrate LE, Schutzer ME, Ji L, Gill TJ, Rubash HE. The cartilage thickness distribution in the tibiofemoral joint and its correlation with cartilage-to-cartilage contact. Clin Biomech (Bristol, Avon). 2005;20(7):736-44.

Li G, Yin J, Gao J, Cheng TS, Pavlos NJ, Zhang C, Zheng MH. Subchondral bone in osteoarthritis: insight into risk factors and microstructural changes. Arthritis Res Ther. 2013;15(6):223.

Li H, Li J, Yu S, Wu C, Zhang W. The mechanical properties of tibiofemoral and patellofemoral articular cartilage in compression depend on anatomical regions. Sci Rep. 2021;11(1):6128.

Lindsey CT, Narasimhan A, Adolfo JM, Jin H, Steinbach LS, Link T, Ries M, Majumdar S. Magnetic resonance evaluation of the interrelationship between articular cartilage and trabecular bone of the osteoarthritic knee. Osteoarthritis Cartilage. 2004;12(2):86-96.

Litwic A, Edwards MH, Dennison EM, Cooper C. Epidemiology and burden of osteoarthritis. Br Med Bull. 2013;105(1):185-99.

Liu C, Liu C, Si L, Shen H, Wang Q, Yao W. Relationship between subchondral bone microstructure and articular cartilage in the osteoarthritic knee using 3T MRI. J Magn Reson Imaging. 2018;48(3):669-79.

Loeser RF, Goldring SR, Scanzello CR, Goldring MB. Osteoarthritis: a disease of the joint as an organ. Arthritis Rheum. 2012;64(6):1697-707.

Lu TW, O'Connor JJ. Bone position estimation from skin marker co-ordinates using global optimisation with joint constraints. J Biomech. 1999;32(2):129-34.

Madry H, van Dijk CN, Mueller-Gerbl M. The basic science of the subchondral bone. Knee Surg Sports Traumatol Arthrosc. 2010;18(4):419-33.

Mahjoub M, Berenbaum F, Houard X. Why subchondral bone in osteoarthritis? The importance of the cartilage bone interface in osteoarthritis. Osteoporos Int. 2012;23 Suppl 8:S841-6.

Maly MR, Acker SM, Totterman S, Tamez-Peña J, Stratford PW, Callaghan JP, Adachi JD, Beattie KA. Knee adduction moment relates to medial femoral and tibial cartilage morphology in clinical knee osteoarthritis. J Biomech. 2015;48(12):3495-501.

Mancuso ME, Troy KL. Relating Bone Strain to Local Changes in Radius Microstructure Following 12 Months of Axial Forearm Loading in Women. J Biomech Eng. 2020;142(11).

Mankin HJ. Biochemical and metabolic aspects of osteoarthritis. Orthop Clin North Am. 1971;2(1):19-31.

Mankin HJ, Dorfman H, Lippiello L, Zarins A. Biochemical and metabolic abnormalities in articular cartilage from osteo-arthritic human hips. II. Correlation of morphology with biochemical and metabolic data. J Bone Joint Surg Am. 1971;53(3):523-37.

Mansfield PJ, Neumann DA. Chapter 10 - Structure and Function of the Knee. In: Mansfield PJ, Neumann DA, editors. Essentials of Kinesiology for the Physical Therapist Assistant (Third Edition). St. Louis (MO): Mosby; 2019. p. 278-310.

Manske SL, Zhu Y, Sandino C, Boyd SK. Human trabecular bone microarchitecture can be assessed independently of density with second generation HR-pQCT. Bone. 2015;79:213-21.

Matsui H, Shimizu M, Tsuji H. Cartilage and subchondral bone interaction in osteoarthrosis of human knee joint: a histological and histomorphometric study. Microsc Res Tech. 1997;37(4):333-42.

McKinley TO, English DK, Bay BK. Trabecular bone strain changes resulting from partial and complete meniscectomy. Clin Orthop Relat Res. 2003(407):259-67.

Mente PL, Lewis JL. Elastic modulus of calcified cartilage is an order of magnitude less than that of subchondral bone. J Orthop Res. 1994;12(5):637-47.

Meyer AJ, D'Lima DD, Besier TF, Lloyd DG, Colwell Jr CW, Fregly BJ. Are external knee load and EMG measures accurate indicators of internal knee contact forces during gait? J Orthop Res. 2013;31(6):921-9.

Michalak GJ, Walker R, Boyd SK. Concurrent Assessment of Cartilage Morphology and Bone Microarchitecture in the Human Knee Using Contrast-Enhanced HR-pQCT Imaging. J Clin Densitom. 2019;22(1):74-85.

Milz S, Putz R. Quantitative morphology of the subchondral plate of the tibial plateau. J Anat. 1994;185(Pt 1):103-10.

Mirahmadi F, Koolstra JH, Lobbezoo F, van Lenthe GH, Everts V. Ex vivo thickness measurement of cartilage covering the temporomandibular joint. J Biomech. 2017;52:165-8.

Miyazaki T, Wada M, Kawahara H, Sato M, Baba H, Shimada S. Dynamic load at baseline can predict radiographic disease progression in medial compartment knee osteoarthritis. Ann Rheum Dis. 2002;61(7):617-22.

Müller R, Van Campenhout H, Van Damme B, Van Der Perre G, Dequeker J, Hildebrand T, Rüegsegger P. Morphometric analysis of human bone biopsies: a quantitative structural comparison of histological sections and micro-computed tomography. Bone. 1998;23(1):59-66.

Mündermann A, Dyrby CO, Andriacchi TP. Secondary gait changes in patients with medial compartment knee osteoarthritis: increased load at the ankle, knee, and hip during walking. Arthritis Rheum. 2005;52(9):2835-44.

Muratovic D, Cicuttini F, Wluka A, Findlay D, Wang Y, Otto S, Taylor D, Humphries J, Lee Y, Labrinidis A, Williams R, Kuliwaba J. Bone marrow lesions detected by specific combination of MRI sequences are associated with severity of osteochondral degeneration. Arthritis Res Ther. 2016;18:54.

Muratovic D, Findlay DM, Cicuttini FM, Wluka AE, Lee YR, Edwards S, Kuliwaba JS. Bone marrow lesions in knee osteoarthritis: regional differences in tibial subchondral bone microstructure and their association with cartilage degeneration. Osteoarthritis Cartilage. 2019;27(11):1653-62.

Muratovic D, Findlay DM, Cicuttini FM, Wluka AE, Lee YR, Kuliwaba JS. Bone matrix microdamage and vascular changes characterize bone marrow lesions in the subchondral bone of knee osteoarthritis. Bone. 2018;108:193-201.

Nakagawa Y, Mukai S, Yabumoto H, Tarumi E, Nakamura T. Cartilage Degeneration and Alignment in Severe Varus Knee Osteoarthritis. Cartilage. 2015;6(4):208-15.

National Joint Registry. 16th Annual Report 2019: National Joint Registry for England, Wales, Northern Ireland and the Isle of Man. Available from: https://reports.njrcentre.org.uk/; 2019.

Nelson AE, Conaghan PG. Fast Facts: Osteoarthritis. First Edition ed: Health Press; 2009.

Nickmanesh R, Stewart RC, Snyder BD, Grinstaff MW, Masri BA, Wilson DR. Contrast-enhanced computed tomography (CECT) attenuation is associated with stiffness of intact knee cartilage. J Orthop Res. 2018;36(10):2641-7.

Nieminen HJ, Gahunia HK, Pritzker KPH, Ylitalo T, Rieppo L, Karhula SS, Lehenkari P, Hæggström E, Saarakkala S. 3D histopathological grading of osteochondral tissue using contrast-enhanced micro-computed tomography. Osteoarthritis Cartilage. 2017;25(10):1680-9.

Nieminen HJ, Ylitalo T, Karhula S, Suuronen JP, Kauppinen S, Serimaa R, Hæggström E, Pritzker KP, Valkealahti M, Lehenkari P, Finnila M, Saarakkala S. Determining collagen distribution in articular cartilage using contrast-enhanced micro-computed tomography. Osteoarthritis Cartilage. 2015;23(9):1613-21.

Nishiyama KK, Shane E. Clinical imaging of bone microarchitecture with HR-pQCT. Curr Osteoporos Rep. 2013;11(2):147-55.

Niu J, Zhang YQ, Torner J, Nevitt M, Lewis CE, Aliabadi P, Sack B, Clancy M, Sharma L, Felson DT. Is obesity a risk factor for progressive radiographic knee osteoarthritis? Arthritis Rheum. 2009;61(3):329-35.

Odgaard A. Three-dimensional methods for quantification of cancellous bone architecture. Bone. 1997;20(4):315-28.

Odgaard A, Kabel J, van Rietbergen B, Dalstra M, Huiskes R. Fabric and elastic principal directions of cancellous bone are closely related. J Biomech. 1997;30(5):487-95.

Oláh T, Madry H. The Osteochondral Unit: The Importance of the Underlying Subchondral Bone. In: Farr J, Gomoll AH, editors. Cartilage Restoration: Practical Clinical Applications. Cham: Springer International Publishing; 2018. p. 13-22.

Oldendorf W. Basics of Magnetic Resonance Imaging. Oldendorf W, editor: Boston, MA : Springer US; 1988.

Ombregt L. Applied anatomy of the knee. In: Ombregt L, editor. A System of Orthopaedic Medicine (Third Edition): Churchill Livingstone; 2013. p. e262-e9.

Paley D. Principles of Deformity Correction. 1st ed. Berlin, Heidelberg: Springer; 2002. 805 p.

Palmer AW, Guldberg RE, Levenston ME. Analysis of cartilage matrix fixed charge density and three-dimensional morphology via contrast-enhanced microcomputed tomography. Proc Natl Acad Sci USA. 2006;103(51):19255-60.

Pan J, Zhou X, Li W, Novotny JE, Doty SB, Wang L. In situ measurement of transport between subchondral bone and articular cartilage. J Orthop Res. 2009;27(10):1347-52.

Patel V, Issever AS, Burghardt A, Laib A, Ries M, Majumdar S. MicroCT evaluation of normal and osteoarthritic bone structure in human knee specimens. J Orthop Res. 2003;21(1):6-13.

Perilli E, Bala Y, Zebaze R, Reynolds KJ, Seeman E. Regional Heterogeneity in the Configuration of the Intracortical Canals of the Femoral Shaft. Calcif Tissue Int. 2015;97(4):327-35.

Perilli E, Baruffaldi F, Bisi MC, Cristofolini L, Cappello A. A physical phantom for the calibration of three-dimensional X-ray microtomography examination. J Microsc. 2006;222(Pt 2):124-34.

Perilli E, Baruffaldi F, Visentin M, Bordini B, Traina F, Cappello A, Viceconti M. MicroCT examination of human bone specimens: effects of polymethylmethacrylate embedding on structural parameters. J Microsc. 2007;225(Pt 2):192-200.

Perilli E, Parkinson IH, Reynolds KJ. Micro-CT examination of human bone: from biopsies towards the entire organ. Ann Ist Super Sanita. 2012;48(1):75-82.

Perillo-Marcone A, Barrett DS, Taylor M. The importance of tibial alignment: Finite element analysis of tibial malalignment. J Arthroplasty. 2000;15(8):1020-7.

Phan CM, Matsuura M, Bauer JS, Dunn TC, Newitt D, Lochmueller EM, Eckstein F, Majumdar S, Link TM. Trabecular Bone Structure of the Calcaneus: Comparison of MR Imaging at 3.0 and 1.5 T with Micro-CT as the Standard of Reference. Radiology. 2006;239(2):488-96.

Potter HG, Linklater JM, Allen AA, Hannafin JA, Haas SB. Magnetic resonance imaging of articular cartilage in the knee. An evaluation with use of fast-spin-echo imaging. JBJS. 1998;80(9):1276-84.

Pritzker KP, Gay S, Jimenez SA, Ostergaard K, Pelletier JP, Revell PA, Salter D, van den Berg WB. Osteoarthritis cartilage histopathology: grading and staging. Osteoarthritis Cartilage. 2006;14(1):13-29.

Radin EL, Burr DB, Caterson B, Fyhrie D, Brown TD, Boyd RD. Mechanical determinants of osteoarthrosis. Semin Arthritis Rheum. 1991;21(3 Suppl 2):12-21.

Radin EL, Rose RM. Role of subchondral bone in the initiation and progression of cartilage damage. Clin Orthop Relat Res. 1986;213(213):34-40.

Rapagna S, Roberts BC, Solomon LB, Reynolds KJ, Thewlis D, Perilli E. Tibial cartilage, subchondral bone plate and trabecular bone microarchitecture in varus- and valgus-osteoarthritis versus controls. J Orthop Res. 2021a;39(9):1988-99.

Rapagna S, Roberts BC, Solomon LB, Reynolds KJ, Thewlis D, Perilli E. Relationships between tibial articular cartilage, in vivo external joint moments and static alignment in end-stage knee osteoarthritis: A micro-CT study. Journal of Orthopaedic Research. 2021b; In Press.

Reichenbach S, Guermazi A, Niu J, Neogi T, Hunter DJ, Roemer FW, McLennan CE, Hernandez-Molina G, Felson DT. Prevalence of bone attrition on knee radiographs and MRI in a community-based cohort. Osteoarthritis Cartilage. 2008;16(9):1005-10.

Renault JB, Carmona M, Tzioupis C, Ollivier M, Argenson JN, Parratte S, Chabrand P. Tibial subchondral trabecular bone micromechanical and microarchitectural properties are affected by alignment and osteoarthritis stage. Sci Rep. 2020;10(1):3975.

Rieppo L, Karhula S, Thevenot J, Hadjab I, Quenneville E, Garon M, Buschmann MD, Nieminen HJ, Saarakkala S. Determination of Extracellular Matrix Orientation of Articular Cartilage in 3d Using Micro-Computed Tomography. Osteoarthritis Cartilage. 2017;25:S254-S.

Roberts BC, Solomon LB, Mercer G, Reynolds KJ, Thewlis D, Perilli E. Joint loading and proximal tibia subchondral trabecular bone microarchitecture differ with walking gait patterns in end-stage knee osteoarthritis. Osteoarthritis Cartilage. 2017a;25(10):1623-32.

Roberts BC, Solomon LB, Mercer G, Reynolds KJ, Thewlis D, Perilli E. Relationships between in vivo dynamic knee joint loading, static alignment and tibial subchondral bone microarchitecture in end-stage knee osteoarthritis. Osteoarthritis Cartilage. 2018;26(4):547-56.

Roberts BC, Thewlis D, Solomon LB, Mercer G, Reynolds KJ, Perilli E. Systematic mapping of the subchondral bone 3D microarchitecture in the human tibial plateau: Variations with joint alignment. J Orthop Res. 2017b;35(9):1927-41.

Ross MH, Pawlina W. Histology: Lippincott Williams & Wilkins; 2006.

Rüegsegger P, Koller B, Müller R. A microtomographic system for the nondestructive evaluation of bone architecture. Calcif Tissue Int. 1996;58(1):24-9.

Safiri S, Kolahi AA, Smith E, Hill C, Bettampadi D, Mansournia MA, Hoy D, Ashrafi-Asgarabad A, Sepidarkish M, Almasi-Hashiani A, Collins G, Kaufman J, Qorbani M, Moradi-Lakeh M, Woolf AD, Guillemin F, March L, Cross M. Global, regional and national burden of osteoarthritis 1990-2017: a systematic analysis of the Global Burden of Disease Study 2017. Ann Rheum Dis. 2020;79(6):819-28.

Schipplein OD, Andriacchi TP. Interaction between active and passive knee stabilizers during level walking. J Orthop Res. 1991;9(1):113-9.

Schmitz N, Laverty S, Kraus VB, Aigner T. Basic methods in histopathology of joint tissues. Osteoarthritis Cartilage. 2010;18 Suppl 3:S113-6.

Sell CA, Masi JN, Burghardt A, Newitt D, Link TM, Majumdar S. Quantification of Trabecular Bone Structure Using Magnetic Resonance Imaging at 3 Tesla—Calibration Studies Using Microcomputed Tomography as a Standard of Reference. Calcif Tissue Int. 2005;76(5):355-64.

Sharma L, Chmiel JS, Almagor O, Felson D, Guermazi A, Roemer F, Lewis CE, Segal N, Torner J, Cooke TD, Hietpas J, Lynch J, Nevitt M. The role of varus and valgus alignment in the initial development of knee cartilage damage by MRI: the MOST study. Ann Rheum Dis. 2013;72(2):235-40.

Sharma L, Hurwitz DE, Thonar EJ, Sum JA, Lenz ME, Dunlop DD, Schnitzer TJ, Kirwan-Mellis G, Andriacchi TP. Knee adduction moment, serum hyaluronan level, and disease severity in medial tibiofemoral osteoarthritis. Arthritis Rheum. 1998;41(7):1233-40.

Sharma L, Song J, Dunlop D, Felson D, Lewis CE, Segal N, Torner J, Cooke TDV, Hietpas J, Lynch J, Nevitt M. Varus and valgus alignment and incident and progressive knee osteoarthritis. Ann Rheum Dis. 2010;69(11):1940.

Sharma L, Song J, Felson DT, Cahue S, Shamiyeh E, Dunlop DD. The role of knee alignment in disease progression and functional decline in knee osteoarthritis. Jama. 2001;286(2):188-95.

Shenoy R, Pastides PS, Nathwani D. (iii) Biomechanics of the knee and TKR. Orthop Trauma. 2013;27(6):364-71.

Shepherd DE, Seedhom BB. Thickness of human articular cartilage in joints of the lower limb. Ann Rheum Dis. 1999;58(1):27-34.

Shiraishi K, Chiba K, Okazaki N, Yokota K, Nakazoe Y, Kidera K, Yonekura A, Tomita M, Osaki M. In vivo analysis of subchondral trabecular bone in patients with osteoarthritis of the knee using second-generation high-resolution peripheral quantitative computed tomography (HR-pQCT). Bone. 2020;132:115155.

Sniekers YH, Intema F, Lafeber FP, van Osch GJ, van Leeuwen JP, Weinans H, Mastbergen SC. A role for subchondral bone changes in the process of osteoarthritis; a micro-CT study of two canine models. BMC Musculoskelet Disord. 2008;9:20.

Suri S, Walsh DA. Osteochondral alterations in osteoarthritis. Bone. 2012;51(2):204-11.

Taqi SA, Sami SA, Sami LB, Zaki SA. A review of artifacts in histopathology. Journal of oral and maxillofacial pathology : JOMFP. 2018;22(2):279.

Tassani S, Perilli E. On local micro-architecture analysis of trabecular bone in three dimensions. Int Orthop. 2013;37(8):1645-6.

Teichtahl AJ, Wang Y, Wluka AE, Strauss BJ, Proietto J, Dixon JB, Jones G, Cicuttini FM. Associations between systemic bone mineral density and early knee cartilage changes in middle-aged adults without clinical knee disease: a prospective cohort study. Arthritis Res Ther. 2017;19(1):98.

Thambyah A, Nather A, Goh J. Mechanical properties of articular cartilage covered by the meniscus. Osteoarthritis Cartilage. 2006;14(6):580-8.

Thambyah A, Shim VP, Chong LM, Lee VS. Impact-induced osteochondral fracture in the tibial plateau. J Biomech. 2008;41(6):1236-42.

Thewlis D, Callary SA, Fraysse F, Solomon LB. Peak loading during walking is not associated with fracture migration following tibial plateau fracture: A preliminary case series. J Orthop Res. 2015;33(9):1398-406.

Thewlis D, Richards J, Bower J. Discrepancies in knee joint moments using common anatomical frames defined by different palpable landmarks. J Appl Biomech. 2008;24(2):185-90.

Thewlis D, Waters A, Solomon LB, Perilli E. Investigating in vivo knee volumetric bone mineral density and walking gait mechanics in healthy people. Bone. 2021;143:115662.

Thorp LE, Wimmer MA, Block JA, Moisio KC, Shott S, Goker B, Sumner DR. Bone mineral density in the proximal tibia varies as a function of static alignment and knee adduction

angular momentum in individuals with medial knee osteoarthritis. Bone. 2006;39(5):1116-22.

Tortora GJ, Derrickson BH. Principles of Anatomy and Physiology, 14th Edition. New York: New York: Wiley; 2014.

Touraine S, Bouhadoun H, Engelke K, Laredo JD, Chappard C. Influence of meniscus on cartilage and subchondral bone features of knees from older individuals: A cadaver study. PLoS One. 2017;12(8):e0181956.

Turner CH. Three rules for bone adaptation to mechanical stimuli. Bone. 1998;23(5):399-407.

van den Bergh JP, Szulc P, Cheung AM, Bouxsein M, Engelke K, Chapurlat R. The clinical application of high-resolution peripheral computed tomography (HR-pQCT) in adults: state of the art and future directions. Osteoporosis International. 2021.

Van Rossom S, Wesseling M, Smith CR, Thelen DG, Vanwanseele B, Dieter VA, Jonkers I. The influence of knee joint geometry and alignment on the tibiofemoral load distribution: A computational study. The Knee. 2019;26(4):813-23.

van Tiel J, Siebelt M, Reijman M, Bos PK, Waarsing JH, Zuurmond AM, Nasserinejad K, van Osch GJ, Verhaar JA, Krestin GP, Weinans H, Oei EH. Quantitative in vivo CT arthrography of the human osteoarthritic knee to estimate cartilage sulphated glycosaminoglycan content: correlation with ex-vivo reference standards. Osteoarthritis Cartilage. 2016;24(6):1012-20.

Vanwanseele B, Eckstein F, Smith RM, Lange AK, Foroughi N, Baker MK, Shnier R, Singh MA. The relationship between knee adduction moment and cartilage and meniscus morphology in women with osteoarthritis. Osteoarthritis Cartilage. 2010;18(7):894-901.

Vina ER, Kwoh CK. Epidemiology of osteoarthritis: literature update. Curr Opin Rheumatol. 2018;30(2):160-7.

Wada M, Maezawa Y, Baba H, Shimada S, Sasaki S, Nose Y. Relationships among bone mineral densities, static alignment and dynamic load in patients with medial compartment knee osteoarthritis. Rheumatology (Oxford). 2001;40(5):499-505.

Wilson JP, Mulligan K, Fan B, Sherman JL, Murphy EJ, Tai VW, Powers CL, Marquez L, Ruiz-Barros V, Shepherd JA. Dual-energy X-ray absorptiometry-based body volume measurement for 4-compartment body composition. Am J Clin Nutr. 2012;95(1):25-31.

Xie L, Lin AS, Levenston ME, Guldberg RE. Quantitative assessment of articular cartilage morphology via EPIC-microCT. Osteoarthritis Cartilage. 2009;17(3):313-20.

Ylitalo T, Finnilä MAJ, Gahunia HK, Karhula SS, Suhonen H, Valkealahti M, Lehenkari P, Haeggström E, Pritzker KPH, Saarakkala S, Nieminen HJ. Quantifying Complex Micro-

Topography of Degenerated Articular Cartilage Surface by Contrast-Enhanced Micro-Computed Tomography and Parametric Analyses. J Orthop Res. 2019;37(4):855-66.

Zhang J, Liao L, Zhu J, Wan X, Xie M, Zhang H, Zhang M, Lu L, Yang H, Jing D, Liu X, Yu S, Lu XL, Chen C, Shan Z, Wang M. Osteochondral Interface Stiffening in Mandibular Condylar Osteoarthritis. J Dent Res. 2018;97(5):563-70.

Zhang L, Liu G, Han B, Wang Z, Yan Y, Ma J, Wei P. Knee Joint Biomechanics in Physiological Conditions and How Pathologies Can Affect It: A Systematic Review. Appl Bionics Biomech. 2020;2020:7451683.

Zhang Y, Wang F, Tan H, Chen G, Guo L, Yang L. Analysis of the mineral composition of the human calcified cartilage zone. Int J Med Sci. 2012;9(5):353-60.

Zhao D, Banks SA, Mitchell KH, D'Lima DD, Colwell CW, Jr., Fregly BJ. Correlation between the knee adduction torque and medial contact force for a variety of gait patterns. J Orthop Res. 2007;25(6):789-97.

Appendix: Statements of contribution

Full publication details:

Rapagna S, Roberts BC, Solomon LB, Reynolds KJ, Thewlis D, Perilli E. Tibial cartilage, subchondral bone plate and trabecular bone microarchitecture in varus- and valgus-osteoarthritis versus controls. *Journal of* Or*thopaedic Research*. 2021; 39(9):1988-99. doi 10.1002/jor.24914.

Section of the thesis where the publication is referred to: Chapter 3: Study 1.

Outline of the authors' contribution to the publication:

In this paper, S Rapagna was the main contributor to the study design, data acquisition, data analysis and interpretation, graphical representation, manuscript formulation and subsequent manuscript drafting. S Rapagna developed the cartilage segmentation protocol and segmented the articular cartilage in all tibial plateaus from previously generated micro-CT cross-section image stacks. S Rapagna also segmented the subchondral bone plate and trabecular bone regions of interest for the non-OA tibial plateaus and performed all data analyses and interpretation of results. S Rapagna wrote the draft manuscript which was edited with feedback from primary supervisor (E Perilli), followed by feedback from co-authors.

Full publication details:

Rapagna S, Roberts BC, Solomon LB, Reynolds KJ, Thewlis D, Perilli E. Relationships between tibial articular cartilage, *in vivo* external joint moments and static alignment in end-stage knee osteoarthritis: a micro-CT study. *Journal of Orthopaedic Research*. 2021. doi: 10.1002/jor.25140. *In Press*.

Section of the thesis where the publication is referred to: Chapter 4: Study 2.

Outline of the authors' contribution to the publication:

In this paper, S Rapagna was the main contributor to the study design, data acquisition, data analysis and interpretation, graphical representation, manuscript formulation and subsequent manuscript drafting. S Rapagna segmented the articular cartilage in all tibial plateaus and generated the cartilage thickness measurements from the micro-CT cross-section image stacks. S Rapagna designed and performed the cartilage segmentation sensitivity analysis. Pre-operative gait analysis and micro-CT scanning of specimens were performed by BC Roberts (Roberts *et al.,* 2018). S Rapagna performed all subsequent data analyses and interpretation of results. She also wrote the draft manuscript which was edited with feedback from primary supervisor (E Perilli), followed by feedback from co-authors.

Full publication details:

Rapagna S, Roberts BC, Muratovic D, Solomon LB, Reynolds KJ, Thewlis D, Perilli E. Systematic mapping of cartilage and subchondral bone in human tibial controls and osteoarthritis using micro-computed tomography. 2021. *In Preparation.*

Section of the thesis where the publication is referred to: Chapter 5: Study 3 and part of Chapter 3: Study 1 (validation using histology)

Outline of the authors' contribution to the publication:

In this paper (presented in Chapter 5: Study 3), S Rapagna was the main contributor to the study design, data acquisition, data analysis and interpretation, graphical representation, manuscript formulation and subsequent manuscript drafting. S Rapagna segmented the articular cartilage in all tibial plateaus from previously generated micro-CT cross-section image stacks. S Rapagna also segmented the subchondral bone plate and trabecular bone for the non-OA controls and 5 OA specimens. S Rapagna performed the spatial mapping of the cartilage in all specimens and of the bone in the non-OA and 5 OA specimens. BC Roberts performed the spatial mapping of the bone in 21 OA specimens (Roberts *et al.* 2017b). S Rapagna performed all data analyses and interpretation of results.

In the validation study part of chapter 3: Study 1, S Rapagna planned the regions for histological processing. Processing was performed together with D Muratovic. Subsequent validation analysis was performed by S Rapagna.

S Rapagna wrote the draft manuscript which was edited with feedback from primary supervisor (E Perilli), followed by feedback from co-authors.